CHAPTER 5

In-vitro anticancer activity of the mixed ligand Ruthenium(II) complexes.

The synthesized mixed ligand ruthenium complexes have been evaluated for their bio-applicability as anticancer agenst, employing various assays and techniques mainly targeting apoptosis.

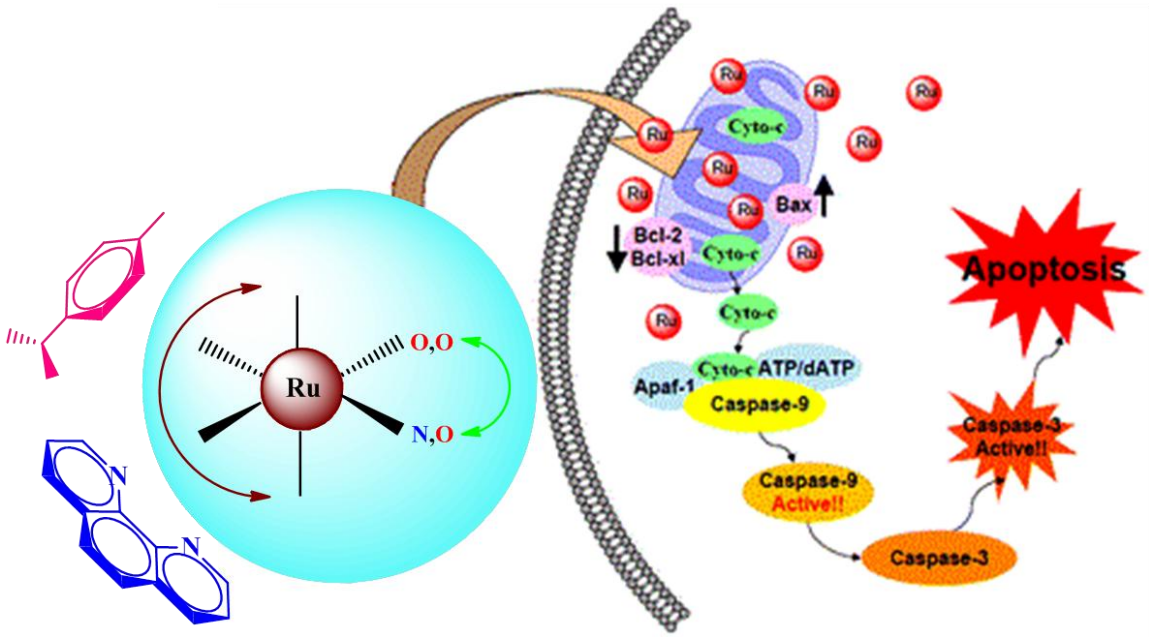

In-Vitro assays

In-Cellulo assays

5.1 Cancer: A worldwide epidemic- Research towards its cure:

5.1.1 Introduction to Cancer, types of cancer and its worldwide statistics:

❖ **Cancer- a fatal disease:**

Cancer (malignant tumour or malignant neoplasm) is the name given to a collection of related diseases. In all types of cancer, some of the body's cells begin to divide without stopping and spread into surrounding tissues. Cancer can start almost anywhere in the human body, which is made up of trillions of cells. Normally, human cells grow and divide to form new cells as the body needs them. When cells grow old or become damaged, they die, and new cells take their place. When cancer develops, however, this orderly process breaks down. As cells become more and more abnormal, old or damaged cells survive when they should die, and new cells form when they are not needed. These extra cells can divide without stopping and may form growths called tumors. Many cancers form solid tumors, which are masses of tissue. Cancers of the blood, such as leukemia, generally do not form solid tumors. Cancerous tumors are malignant, which means they can spread into, or invade, nearby tissues. In addition, as these tumors grow, some cancer cells can break off and travel to distant places in the body through the blood or the lymph system and form new tumors far from the original tumor (metastasis). Unlike malignant tumors, benign tumors do not spread into, or invade, nearby tissues. Benign tumors can sometimes be quite large, however. When removed, they usually don't grow back, whereas malignant tumors sometimes do. Unlike most benign tumors elsewhere in the body, benign brain tumors can be life threatening.

❖ **Causes of cancer:**

Cancer is a genetic disease, that is, it is caused by changes in genes that control the way our cells function, especially how they grow and divide. Genetic changes that cause cancer can be inherited from the previous generations (parents, grandparents, forefathers). They can also arise during a person's lifetime as a result of errors that occur as cells divide or because of damage to DNA caused by certain environmental exposures. Cancer-causing environmental exposures include substances, such as the chemicals in tobacco smoke, and radiation, such as ultraviolet rays from the sun. The genetic changes that contribute to cancer tend to affect three main types of genes: proto-oncogenes, tumor suppressor genes, and DNA repair genes. These changes are sometimes called "drivers" of cancer.

❖ **Types of cancer:**

There are more than 100 types of cancer. Types of cancer are usually named for the organs or tissues where the cancers form. For example, lung cancer starts in cells of the

lung, and brain cancer starts in cells of the brain. Cancers also may be described by the type of cell that formed them, such as an epithelial cell or a squamous cell.

- **Worldwide scenario of this epidemic:**[1]
  - Lung cancer remains the most common and deadliest cancer in the world, with an estimated 1.8 million new cases and 1.59 million deaths in 2012. It affects and kills more men than women around the globe.
  - Breast cancer is the most common cancer in women, with an estimated 1.7 million new cases in 2012 and 522,000 deaths around the world. Those figures have risen 20% and 14%, respectively, since 2008. *[Source: Globocan 2012 (International Agency for Research on Cancer)]*

5.1.2 Need for novel anticancer drugs:

Around the world, tremendous resources are being invested in prevention, diagnosis, and treatment of cancer. Discovery and development of anticancer agents are the key focus of several pharmaceutical companies as well as nonprofit government and non-government organizations. Identification of cytotoxic compounds led the development of anticancer therapeutics for several decades. Although the estimated incidence rates show rising trends for both sexes, the age-standardized cancer mortality rate has been falling continuously among women since 1970 and among men since 1985 [2]. The increase of the survival rates is due to better cancer treatment, in particular thanks to the introduction of efficient anticancer drugs which largely contributed to this improvement.

Advances in cancer treatment, however, continued to be limited by the identification of unique biochemical aspects of malignancies that could be exploited to selectively target tumor cells. Schwartsmann *et al.* noted in 1988 that of over 600,000 compounds screened by then, less than 40 agents were routinely used in the clinic [3]. Conventional anticancer drug discovery and development have focused on the cytotoxic agents. The drug discovery paradigms selected agents that had significant cytostatic or cytotoxic activity on tumor cell lines. The anticancer agents were discovered mainly by serendipity or inhibiting metabolic pathways crucial to cell division. Their exact mechanisms of action were often a subject of retrospective investigation. The recent developments in molecular biology and an understanding of the pharmacology of cancer at a molecular level have challenged researchers to come up with target-based drugs. Several target-based compounds have emerged in recent years [4]. For example Imatinib mesylate, Gefitinib, Bortezomib, Rituximab and Trastuzumab [5].

The landmark discovery of the antitumoural properties of *cis*-diamminedichloroplatinum(II) (cisplatin) by Rosenberg in 1965 heralded a new area of

anticancer research based on metallopharmaceuticals [6]. Platinum-based drugs have been in clinical use for cancer treatment for more than 30 years. The quest for alternative drugs to the well-known cisplatin and its derivatives, which are still used in more than 50% of the treatment regimes for patients suffering from cancer, is highly needed [7,8] Despite their tremendous success, these platinum compounds suffer from two main disadvantages:

1. They are inefficient against platinum-resistant tumors, and
2. They have severe side effects such as nephrotoxicity.

The latter drawback is the consequence of the fact that the ultimate target of these drugs is ubiquitous: It is generally accepted that Pt anticancer drugs target DNA, which is present in all cells [9,10]. Furthermore, as a consequence of its particular chemical structure, cisplatin in particular offers little possibility for rational improvements to increase its tumor specificity and thereby reduce undesired side effects and also the lack of activity of platinum compounds against several types of cancer, are the problems which need to be overcome [11]. This provides the impetus for the search for anticancer activity amongst complexes of other metals.

5.1.3 Target-based investigations towards anticancer property of a compound:

Conventional cancer chemotherapy is highly inadequate as a result of the lack of selectivity between cancer cells and normal cells. This calls for novel cancer therapies for selectively targeting cancers without toxicity to normal tissues. The discovery of novel anticancer agents that will hopefully provide the desired degree of selectivity for cancer cells versus normal tissues has been fueled by the unveiling of a host of novel potential molecular targets through the application of molecular biology methods to cancer biology. These novel targets include genes involved in malignant transformation, cancer progression and metastasis. In addition to the identification of many novel anticancer targets, molecular biology methods have facilitated the investigation of the potential of these targets for drug discovery, by allowing functional expression or production of the targets for use in high-throughput screening assays of natural and synthetic molecule libraries. Most of the potential novel molecular targets for anticancer drug discovery can be grouped into the following categories: growth factor receptor tyrosine kinases (RTKs) and serine/threonine kinase signal transduction pathway targets; cell cycle targets; apoptosis-related targets; extracellular matrix targets, tumor angiogenesis and metastasis targets; and cell life-span targets. [12].

❖ **Cancer cells *vs.* Normal cells – What's the difference?**

In order to develop drugs for selectively targeting cancers without toxicity to normal tissues and provide the desired degree of selectivity, it is important to understand the basic differences between a normal cell and a cancer cell. There are characteristic differences with respect to cell morphology and other cell behavior between a normal cell and a cancer cell. Today lot of targeted drug discovery is being done by and large harnessing the characteristics of a cancer cell. These basic differences have been tabulated in *table 5.1*.

Table 5.1: *Basic differences between a normal cell and a cancer cell.*

Normal cell		***Cancer cell***
Compare and contrast with regards to….		
Normal cells are uniform and orderly. They have less transferrin receptors on their surface.	**Morphology**	Cancer cells have large variations in cell size and shape. Often, they have a large irregularly shaped nucleus and a relatively small cytoplasm. They have increased numbers of transferrin receptors.
Normal cells grow, divide and die in a controlled way and with a predictable lifespan. Normal cells destroy themselves if they become damaged (through a process called apoptosis).	**Cell division and death**	Cancer cells exhibit uncontrolled growth as they have lost their normal control mechanisms. They grow and divide at a rapid rate and they outlive their normal lifespan (i.e. become immortal). They may also be able to prevent self-destruction when damaged.
Normal cells become specialised or ‘mature’. They start out as immature cells (stem cells) and acquire specific functions when they mature.	**Specialisation**	Cancer cells do not carry on maturing once they have become cancerous. In fact, the cancer cells can become less mature over time. Cancer cells can lose specialised functions and become more and more primitive.
Normal cell growth and healing is very orderly and precise. The cells know when there are enough new cells to mend the body. They send chemical messages to each other so that they stop growing and reproducing.	**Signal recognition**	Something in the cancer cells overrides the normal signalling system. This may be because the genes that tell the cell to reproduce keep on sending signals or because the genes that normally tell the cell to stop reproducing have been damaged or lost.
Cells have a natural ability to stick together in the right place. Scientists call this cell adhesion. Molecules on the surface of the cell match those on its neighbours.	**Adhesion and invasion**	Cancer cells can lose the molecules on their surface that keep normal cells in the right place so they can become detached from their neighbours.

❖ **Targeting Apoptosis:**

Apoptosis is a very tightly programmed cell death with distinct biochemical and genetic pathways that play a critical role in the development and homeostasis in normal tissues [13]. It contributes to elimination of unnecessary and unwanted cells to maintain the healthy balance between cell survival and cell death in metazoan [14,15]. It is critical to animals, especially long-lived mammals that must integrate multiple physiological as well as pathological death signals. Evidence indicates that insufficient apoptosis can manifest as cancer or autoimmunity, while accelerated cell death is evident in acute and chronic degenerative diseases, immunodeficiency, and infertility [16].

The structural changes take place in two discrete stages. The first comprises nuclear and cytoplasmic condensation and breaking up of the cell into a number of membrane-bound, ultrastructurally well-preserved fragments called apoptotic bodies. In the second stage these apoptotic bodies are shed from epithelial-lined surfaces or are taken up by other cells, where they undergo a series of changes resembling in vitro autolysis within phagosomes, and are rapidly degraded by lysosomal enzymes derived from the ingesting cells. Whereas in case of necrosis the cell swells up and ruptures releasing its contents out leading to inflammation (*Fig. 5.1*). There is essentially no inflammatory reaction associated neither with the process of apoptosis nor with the removal of apoptotic cells because: (1) apoptotic cells do not release their cellular constituents into the surrounding interstitial tissue; (2) they are quickly phagocytosed by surrounding cells thus likely preventing secondary necrosis; and, (3) the engulfing cells do not produce anti-inflammatory cytokines.

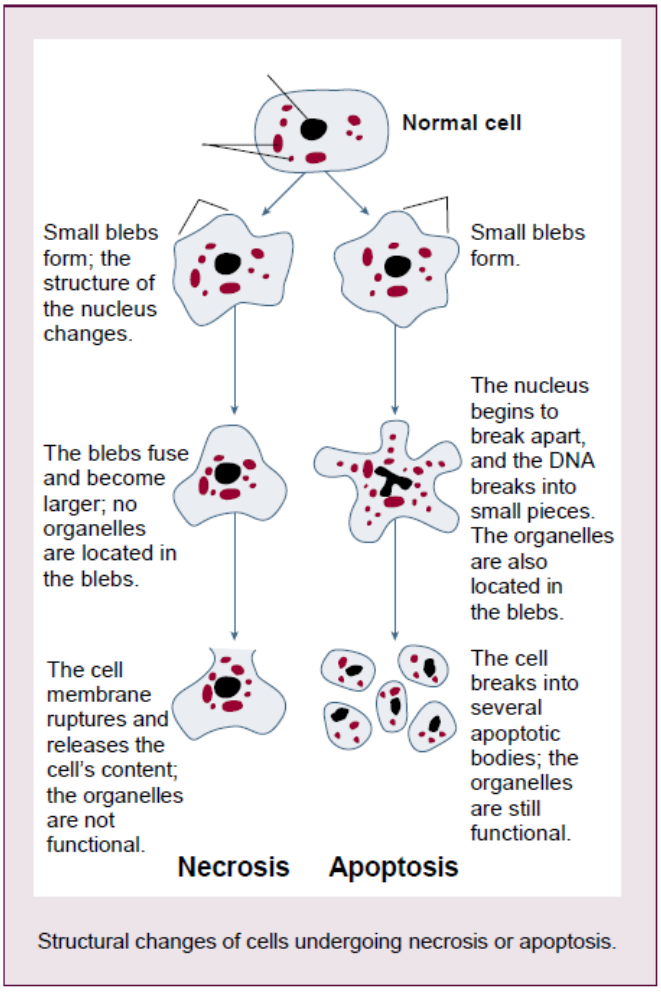

Fig. 5.1: *Figure summarizing the basic differences between the apoptotic cell death and the necrotic cell death.*

Apoptosis represents a universal and exquisitely efficient cellular suicide pathway. Most of the key players in cellular apoptosis regulation have been identified and can be targeted by therapeutic strategies. These include death receptors triggering apoptosis from the cell surface, Bcl-2 proteins as the gatekeepers of the mitochondrial pathway, caspases as the executioner enzymes, endogenous caspase inhibitors, and various transcriptional regulators. Because of this convergence between cancer biology and cell death regulation in development, cancer biologists now frequently find themselves focusing on molecular pathways whose endpoint (death) coincides with the goal of successful treatment. [16]

Induced Apoptosis: The success of each therapeutic strategy depends mainly on the ability of the therapeutic tool to induce apoptosis either by targeting the overexpressed anti-apoptotic molecules or by stimulating the expression of the pro-apoptotic molecules. Apoptosis as a therapeutic goal offers preferential advantages over non-apoptotic death mechanisms.

5.1.4 Brief about the investigations in the present work:

The work presented in this chapter envisages the anticancer property of the various mixed ligand Ru(II) complexes synthesised as the aim of this thesis. The as-synthesized ruthenium complexes have been investigated upon for their anticancer properties in a step-wise manner starting from the preliminary *in vitro* evaluations on interactions with the basic biomolecules like DNA and Serum albumin which were carried out outside cellular environment employing spectroscopic titration method within the cuvette. The results so obtained in these studies further prompted us to indulge in *in cellulo* studies comprising of the basic cytotoxicity evaluation on two different cancer cell lines followed by cell staining assays to get an insight into the type of the cell death (apoptosis / necrosis) and finally targeted apoptosis gene expression study to confirm apoptotic pathway.

In-Vitro assays

In-vitro studies are performed with micro-organisms, cells or biomolecules outside their normal biological context. Colloquially called "test tube experiments", these studies in biology and its sub-disciplines have traditionally been done in test-tubes, flasks, petri dishes etc. Studies that are conducted using components of an organism that have been isolated from their usual biological surroundings permit a more detailed or more convenient analysis than can be done with whole organisms. In the present context the *in vitro* assays solely involve the quantitative interactions of the compounds under study with the two most important biomolecules DNA and serum albumin outside the cellular environment. That is the studies have been carried out in cuvette using spectroscopic detection method.

5.2 Drug-DNA interactions:

5.2.1 DNA as an important cellular target:

The biopolymer DNA is the primary carrier of all genetic information. The central dogma of molecular biology underlines its central role in the storage and replication of genes. Through the RNA mediated processes of transcription and translation, DNA provides the ‘‘master genetic blueprint’’ for the construction of each protein required by individual cells. All these processes are initiated, regulated, and terminated by small molecules and/or proteins that bind to nucleic acids in site-specific ways. Consequently, synthetic molecules that interact with nucleic acids or modulate their function have found a variety of uses as biophysical and therapeutic agents [17].

DNA activation would produce more quantities of the required protein, or could induce DNA replication; depending on which site the drug is targeted. DNA inhibition would restrict protein synthesis, or replication, and could induce cell death. Though both these actions are possible, mostly DNA is targeted in an inhibitory mode, to destroy cells for antitumor and antibiotic action.

❖ **Metal complexes as DNA binders:**

In many ways, coordination complexes are ideal templates for the design of DNA-interactive systems, and the interaction of these structurally complex three-dimensional architectures with DNA is becoming increasingly studied. In addition to a variety of binding modes, metal complexes also offer distinctive chemical activities: they can coordinate directly to DNA Lewis base sites; they can undergo redox reactions with DNA or generate reactive oxygen containing species. The ability to bind to and cleave DNA,

and thus interfere with the essential cellular processes of transcription and translation, means that these systems could also be developed as potential therapeutics.

After briefly outlining the principal interactions generally used to target DNA, the following sub sections (*5.2.3.1 and 5.2.3.2*) of this chapter will focus on common spectroscopic assays to determine the basic interactions between metal complexes and DNA. The implication of these approaches, quantification of the extent of interaction with DNA and comparative evaluation between Ru(II) polypyridyl and Ru(II) arene complexes with respect to their binding constants have been discussed at length.

❖ **Different modes of drug-DNA interactions:**

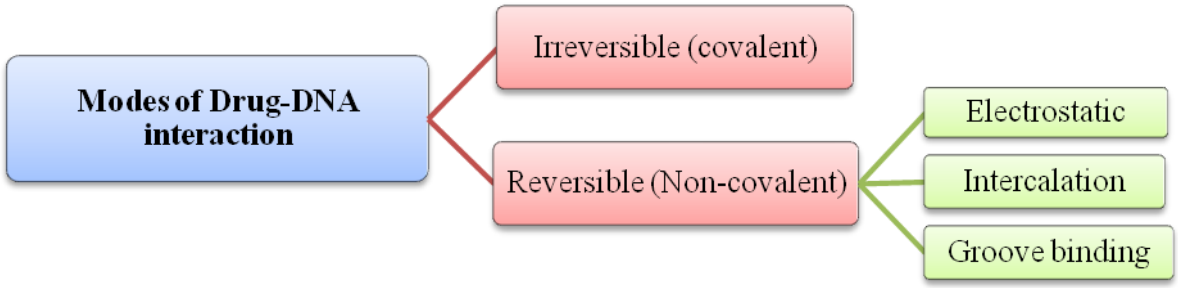

The structure and chemical composition of DNA leads to several mechanisms by which molecular substrates can bind to DNA and such interactions can be irreversible (covalent binding) or reversible (non-covalent binding).

Irreversible (covalent) binding to DNA

Molecules can form covalent bonds to the phosphodiester backbone, sugar residues or bases of the DNA molecule. The induction of DNA damage by a drug molecule forms the basis of ‘‘classical chemotherapy’’, where, as a result of genetic instability caused by this binding event, cancer cells are unable to effect the correct cell cycle checkpoint responses to induced damage and consequently undergo cell cycle arrest, ultimately leading to apoptosis, or ‘‘programmed cell death’’. Rapidly dividing cells, such as cancer cells, are preferentially targeted by such a therapeutic regime [18]. Cisplatin and its derivatives offer the paradigm of this approach: They interact with DNA through coordination bonds formed between the Pt(II) centres and available nitrogen atoms on nucleotides, commonly N7 atoms on adjacent purine bases (*Fig. 5.2 A*). The generation of intrastrand cross-links has the effect of kinking the structure of the DNA molecule; it is thought that this is the key event in the therapeutic action of these drugs. Based on the success of cisplatin and its derivatives, numerous metal complexes, including ruthenium-based systems, have

been designed to display a similar function. Further information on such systems is available in a number of excellent reviews on this fascinating area of research [19-21].

Reversible (non-covalent) binding to DNA

Coordination complexes that reversibly bind to DNA are becoming of increasing interest. In such systems the three dimensional arrangement of ligands provides a means by which binding to DNA can be achieved. Since ligands can be easily interchanged or modified, this provides a mechanism to control hydrophobicity, binding affinity and selectivity, in addition to cellular uptake. Judicious selection of ligands and the metal centre also allows for tuning of the photophysical properties of the complex as a whole. Research in this area has been dominated by octahedral d^6 metal complexes (specifically Ru(II) complexes) as they have well-developed substitution chemistry and possess attractive photophysical properties for these purposes [22]. These systems can exploit several reversible-binding motifs:

I. **Electrostatic interactions:** The negative charge of DNA means that cationic molecules are able to associate with the biopolymer. Ubiquitous naturally occurring polyamines such as spermine bind to DNA through polyvalent electrostatic interactions. As the majority of coordination complexes are charged, electrostatic binding effects often contribute to the binding affinity of complexes, which predominantly recognize DNA through binding modes described below. However, simple metal complexes, such as $[Ru(bpy)_3]^{2+}$ (bpy = 2,2'-bipyridine), that interact with DNA solely through electrostatic effects usually possess very low binding affinities.

II. **Intercalation** (*Fig. 5.2 B*)**:** By far the most widely studied group of metal complexes that reversibly interact with DNA is metallo-intercalators. Intercalation occurs when planar aromatic compounds are inserted between adjacent base pairs in the DNA double helix. Intercalation, which involves significant π system overlap between DNA bases and the intercalated molecule, as well as van der Waals, hydrophobic and electrostatic interactions, has the effect of unwinding and lengthening the DNA double helix. Intercalation preferentially occurs at G/C-rich sequences, because these sequences get unstacked easily [23]. The archetypical ruthenium-based metallo-intercalators are the much studied $[Ru(phen)_2(dppz)]^{2+}$ cation (where phen = 1,10-phenanthroline, and dppz = dipyridophenazine), bind to DNA with a high affinity (*sec.3.1.1*). Due to the vast range of auxiliary ligands available for coordination, metallo-intercalating platforms have been viewed as ideal candidates for the design of DNA sequence selective binding systems.

III. **Groove binding** (*Fig. 5.2 C*)**:** Another mode of reversible binding to DNA is by association within the minor or major grooves that run down the double helix. Molecules that bind in DNA grooves can span many base pairs and hence they can exhibit very high levels of DNA sequence-specific recognition. Molecules approach within van der Waals contact distances of the groove walls and then occupy the DNA grooves. Recognition and sequence-selective binding is dependent on a combination of hydrogen bonding, van der Waals, hydrophobic contacts and electrostatic interactions. Classical groove binders are usually cationic and composed of aromatic rings connected by bonds with torsional freedom so that they are able to twist and become isohelical with the DNA groove. Such systems tend to reside in the minor groove of B-DNA and selectively bind to narrower and more electronegative A/T rich sequences where electrostatic and van der Waals contacts are maximized. Any additional hydrogen bonding sites in the groove binder enhance binding affinities and largely drive more specific sequence preferences. It is somewhat surprising that only relatively few metal complexes based groove binders have been reported. Keene, Collins and co-workers have investigated the potential of dinuclear Ru(II)-based systems for DNA binding. One of their initial studies involved the interaction of stereoisomers of $[(Ru(Me_2bpy)_2)_2(\mu\text{-bpm})]^{4+}$ (where Me_2bpy=4,4-dimethyl-bpy; bpm=2,2-bipyrimidine) with duplex DNA, where NMR data indicated that these systems bind to more accessible sequences within the minor groove of the duplex [24].

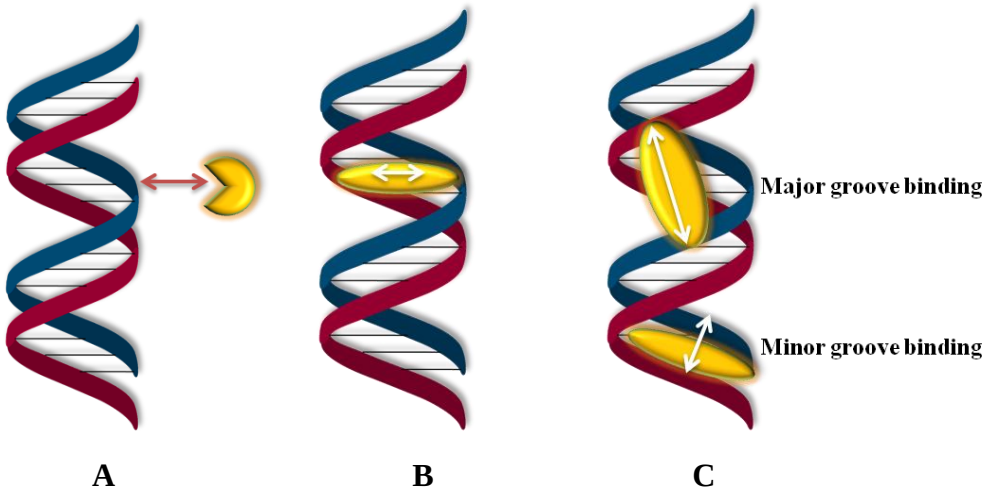

Fig. 5.2: *Schematic representation of the three major modes of drug-DNA interactions – (**A**) Covalent binding, (**B**) Intercalation binding and (**C**) Groove binding.*

❖ **Outlook:**

DNA-binding compounds have proven their utility and will continue to be a staple of anticancer regimes. Thus, the discovery of new DNA-targeting drugs that have improved toxicity and pharmacokinetic profiles is of great importance.

5.2.2 Materials and instrumentation:

The DNA binding studies were carried out solely in tris buffer (containing 15 mM tri-sodium citrate and 150 mM NaCl at pH 7.0) prepared in double distilled water. CT-DNA (calf thymus DNA) stock solution was prepared by dissolving a strand of CT-DNA in double distilled water at 4°C. The aqueous solution of CT-DNA gave a ratio of UV absorbance ~1.8-1.9:1 at 260 and 280 nm, indicating that the DNA was sufficiently free of protein [25]. The DNA concentration per nucleotide was determined by electronic absorption spectroscopy using the known molar extinction coefficient value of 6600 M^{-1} cm^{-1} at 260 nm [26]. The DNA-binding experiments were performed at ~30.0°C. Stock solution of EB (ethidium bromide) was prepared in double distilled water with a concentration of 10^{-3} M. The stock solutions of all the compounds under study were prepared in neat DMSO with a stock concentration of 10^{-3} M. CT-DNA, Tri-sodium citrate (tris), and EB (ethidium bromide) were purchased from SRL (Sisco research laboratory, Mumbai, India.). Conc. HCl used for adjusting the pH to 7.0 while preparing the buffer and DMSO used to prepare stock solutions were of analytical grade and were purchased from Merck.

UV spectra were recorded in tris buffer solution at concentrations of 10^{-6} M on Perkin Elmer Lambda-35 dual beam UV-*Vis* spectrophotometer. Fluorescence spectra were also recorded in tris buffer solution at concentrations of 10^{-6} M on JASCO FP-6300 fluorescence spectrophotometer.

The data generated from the titration experiments were analyzed and plotted with the help of the software OriginPro 8.

5.2.3 Experimental:

If a compound is suspected of targeting cellular DNA, a battery of simple *in vitro* experiments can be performed to readily determine whether the compound physically interacts with DNA. Together, these assays are powerful tools to determine the mechanism of previously discovered molecules, and will be crucial to the discovery of the next generation of DNA-binding anticancer drugs. Two such techniques: (i) UV-Vis absorption studies and (ii) Competitive binding studies with EB using fluorescence

spectroscopy; have been exploited the most for studying DNA binding with synthesized molecules. These are spectroscopy based titration methods.

5.2.3.1 UV absorption studies:

The presence of ground state interactions between the biological macromolecule DNA and compounds under study have been detected using absorption spectroscopy. The binding efficiency of a metal complex to DNA can be effectively investigated employing electronic spectroscopy since the observed changes in the spectra may give evidence of the existing interaction mode [27]. Any interaction between the compounds and DNA is expected to perturb the ligand or metal centred transitions of the compounds. Binding with DNA via non-intercalative binding modes, such as electrostatic forces, van der Waals interactions, dative bonds, hydrogen bonds and hydrophobic interactions generally results in increase in absorption intensity (hyperchromism) upon increasing the concentration of CT-DNA. Since DNA possesses several hydrogen bonding sites which are accessible both in minor and major grooves, it is likely that the amine or hydroxyl group of the compound form hydrogen bonds with N-3 of adenine or O-2 of thymine in the DNA, which may contribute to the hyperchormism observed in the absorption spectra. The hyperchromic effect may also be due to the electrostatic interaction between positively charged compound and the negatively charged phosphate backbone at the periphery of the double helix CT DNA [28]. If the binding mode is intercalation, the π^* orbital of the intercalated ligand can couple with the π orbital of the DNA base pairs, thus, decreasing the $\pi \rightarrow \pi^*$ transition energy and resulting in the bathochromism. On the other hand, the coupling π orbital is partially filled by electrons, thus, decreasing the transition probabilities and concomitantly resulting in hypochromism. It is a general observation that the binding of an intercalative molecule to DNA is accompanied by hypochromism and significant redshift (bathochromism) in the absorption spectra due to strong stacking interaction between the aromatic chromophore of the ligand and DNA base pairs with the extent of hypochromism and red-shift commonly consistent with the strength of intercalative interaction. [29,30].

The interaction of compounds (under study) with CT-DNA has been studied with UV spectroscopy in order to investigate the possible binding modes to CT DNA and to evaluate the extent of binding by calculating the binding constant ($\boldsymbol{K_b}$). Absorption studies were performed with fixed compound concentrations while varying the CT-DNA concentration within. Stock solution of the compound was diluted with tris

buffer to get the desired concentration. While measuring the absorption of the compound, equal increments of CT-DNA were added at different ratios to both the sample cell and the reference cell to eliminate the absorbance of CT-DNA itself. The titration curve so generated has been representatively shown for each series in *Fig. 5.3*.

The magnitude of binding strength to CT-DNA may be determined through the calculation of binding constant $\boldsymbol{K_b}$ which is obtained by monitoring the changes in the absorbance of the compounds with increasing concentrations of CT-DNA. The data so generated from the spectroscopic titration experiment is fitted in eq. **(5.1)** wherein $\boldsymbol{K_b}$ (binding constant) is given by the ratio of slope to the *y* intercept in plots [DNA]/(ε_A-ε_f) *versus* [DNA] according to eq. **(5.1)** [31]

$$\mathbf{[DNA] / (\varepsilon_A-\varepsilon_f) = [DNA]/(\varepsilon_b-\varepsilon_f)+1/K_b(\varepsilon_b-\varepsilon_f)} \qquad \mathbf{(5.1)}$$

where [DNA] is the concentration of DNA in base pairs, $\varepsilon_A = A_{obsd}/$ [compound], ε_f is the extinction coefficient for the unbound compound and ε_b is the extinction coefficient for the compound in the fully bound form.

The $\boldsymbol{K_b}$ plots for all the synthesized ligands and their corresponding Ru(II) complexes have been shown in *Fig. 5.4*. The $\boldsymbol{K_b}$ values obtained from these plots have been tabulated and discussed with significance to their structures in section *5.2.4*.

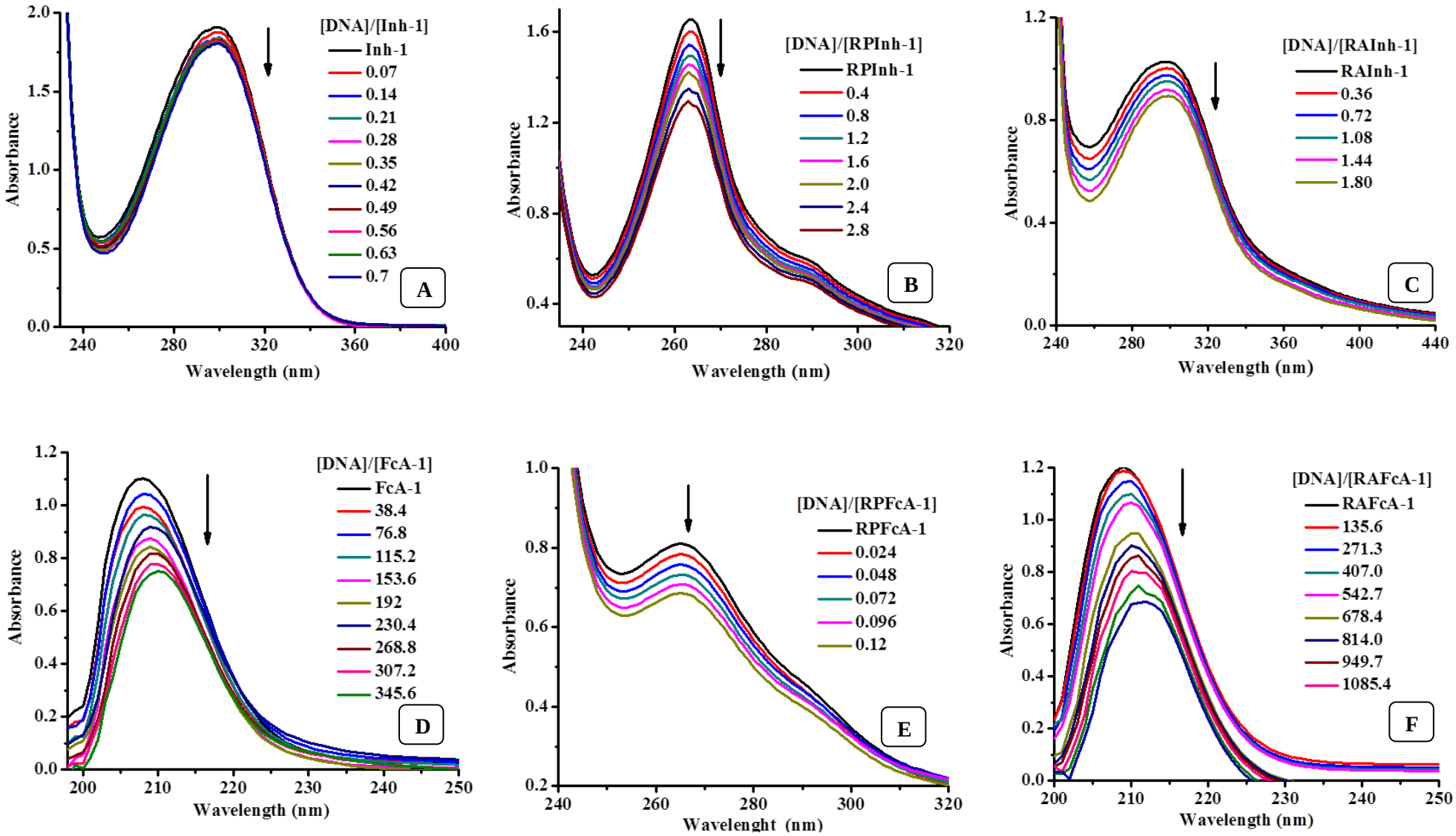

Fig. 5.3: *UV absorption spectra of (A)* ***Inh-1*** *(B)* ***RPInh-1*** *(C)* ***RAInh-1*** *(D)* ***FcA-1*** *(E)* ***RPFcA-1*** *(F)* ***RAFcA-1*** *at increasing concentrations of CT-DNA, the arrow shows decrease in intensity upon increasing concentration of the DNA.*

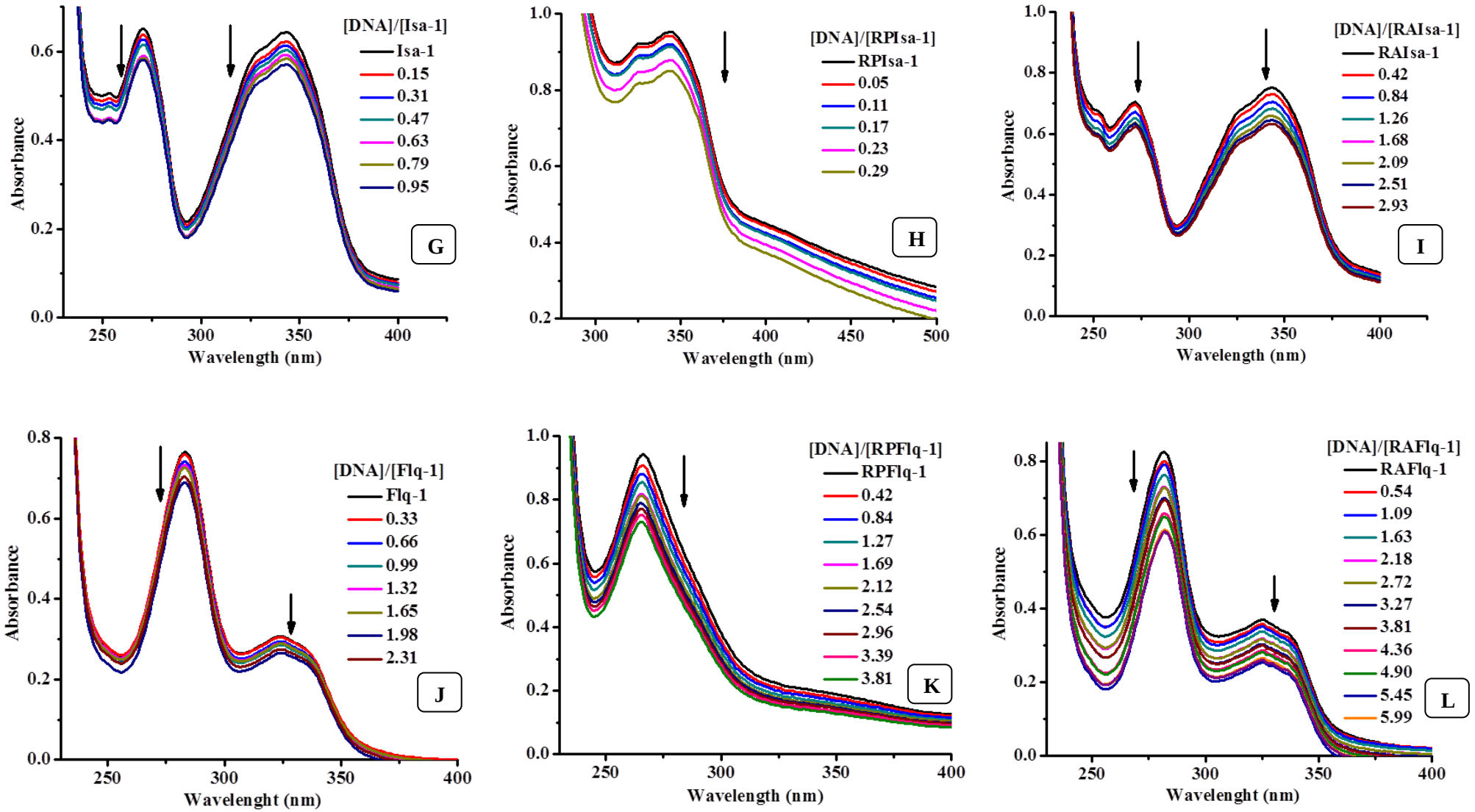

Fig. 5.3(Cont...): *UV absorption spectra of (G)* ***Isa-1*** *(H)* ***RPIsa-1*** *(I)* ***RAIsa-1*** *(J)* ***RAFlq-1*** *(K)* ***RPFlq 1-3*** *(L)* ***RAFlq-1*** *at increasing concentrations of CT-DNA, the arrow shows decrease in intensity upon increasing concentration of the DNA.*

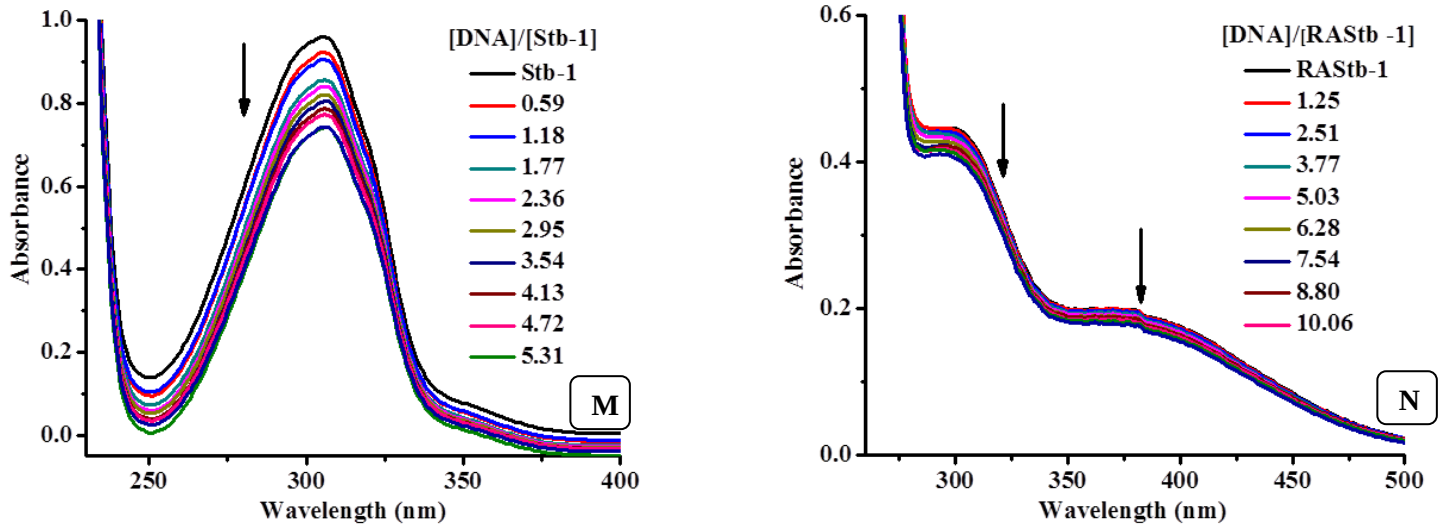

Fig. 5.3(Cont...): *UV absorption spectra of (M)* ***Stb-2*** *(N)* ***RAStb-2*** *at increasing concentrations of CT-DNA, the arrow shows decrease in intensity upon increasing concentration of the DNA.*

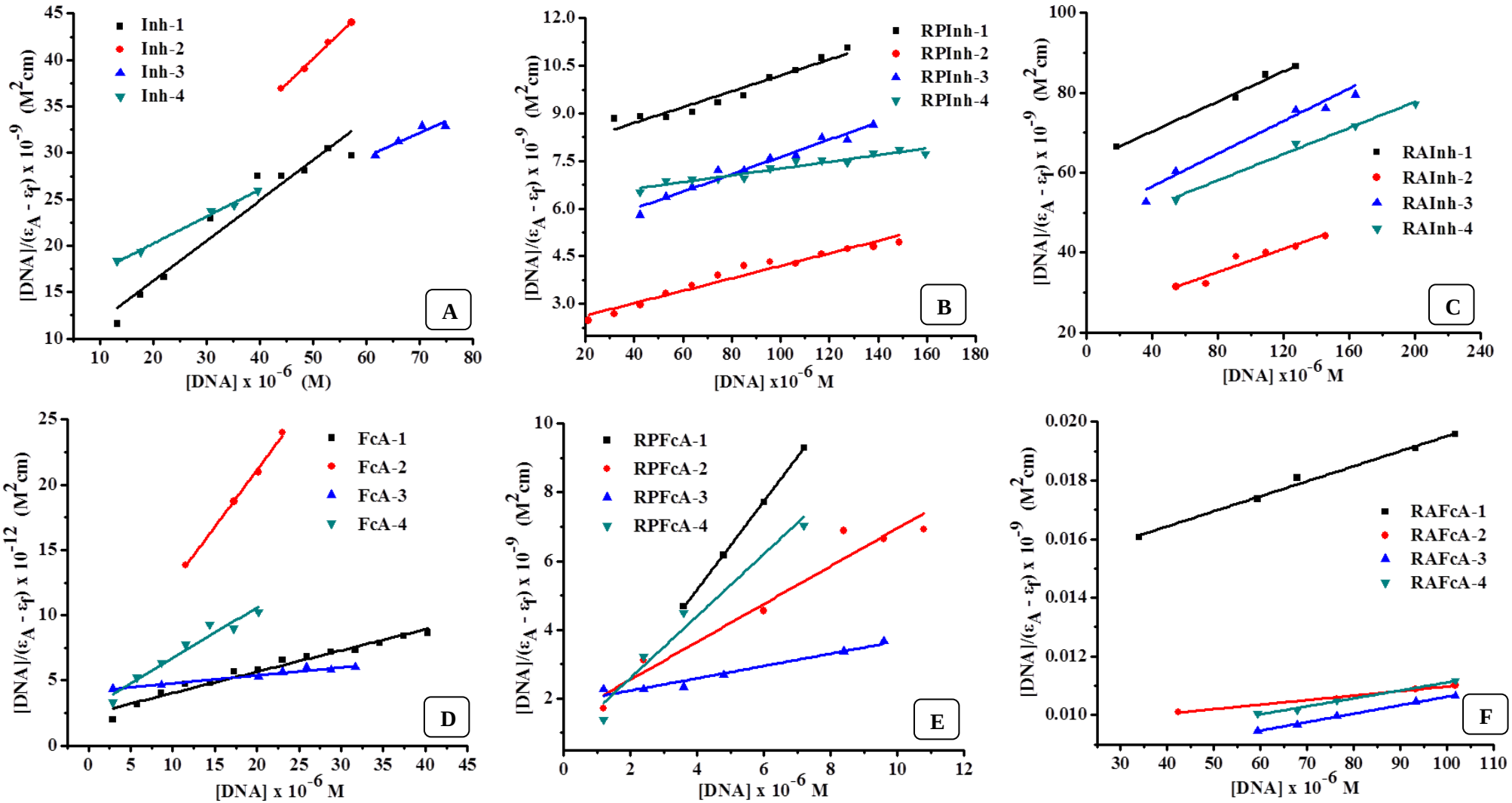

Fig. 5.4: *Plot of [DNA]/(ε_A -ε_f) versus [DNA] for (A)* ***Inh 1-4*** *(B)* ***RPInh 1-4*** *(C)* ***RAInh 1-4*** *(D)* ***FcA 1-4*** *(E)* ***RPFcA 1-4*** *(F)* ***RAFcA 1-4***

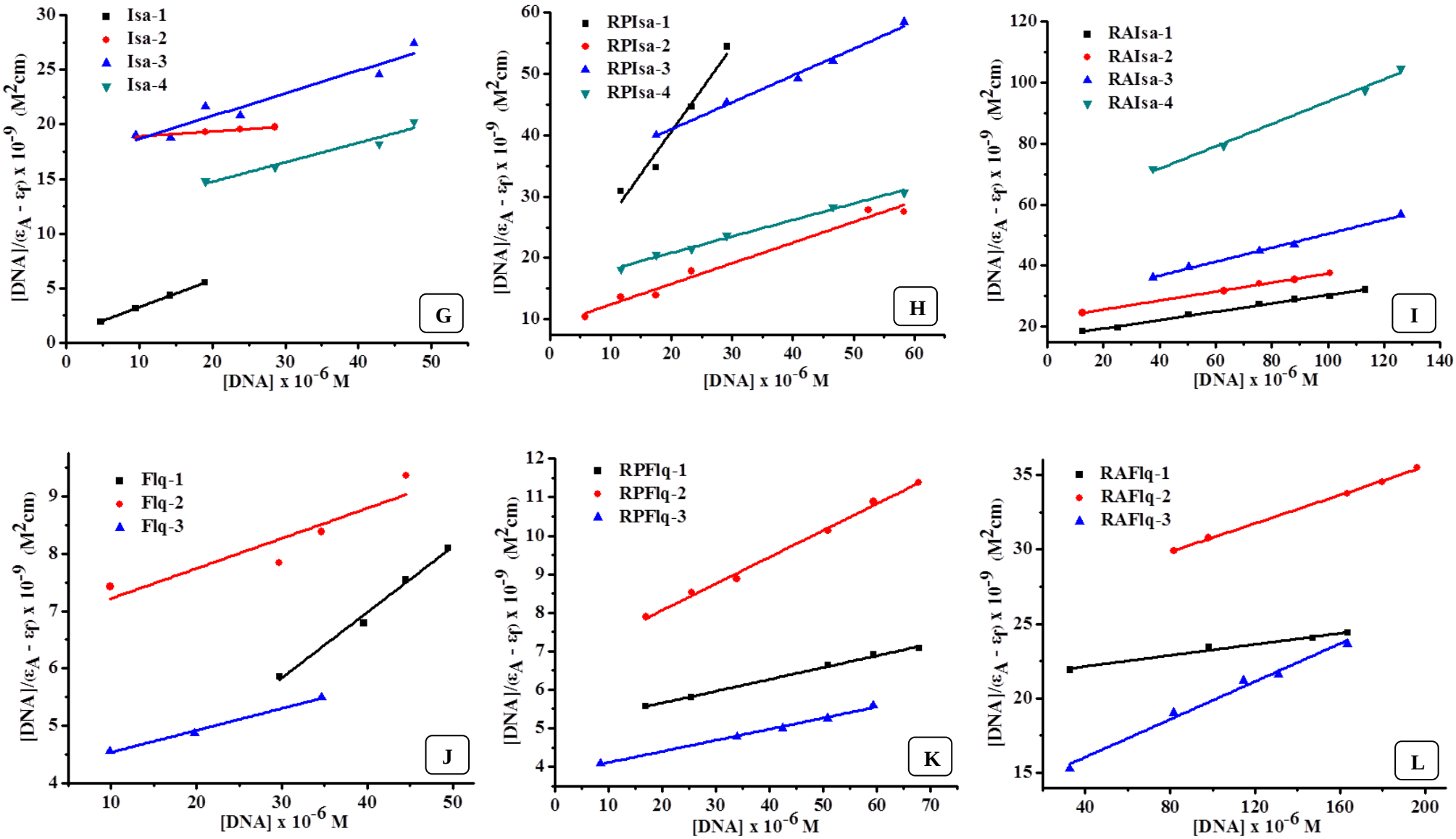

Fig. 5.4(Cont...): *Plot of [DNA]/(ε_A -ε_f) versus [DNA] for (G)* ***Isa 1-4*** *(H)* ***RPIsa 1-4*** *(I)* ***RAIsa 1-4*** *(J)* ***RAFlq 1-3*** *(K)* ***RPFlq 1-3*** *(L)* ***RAFlq 1-3***

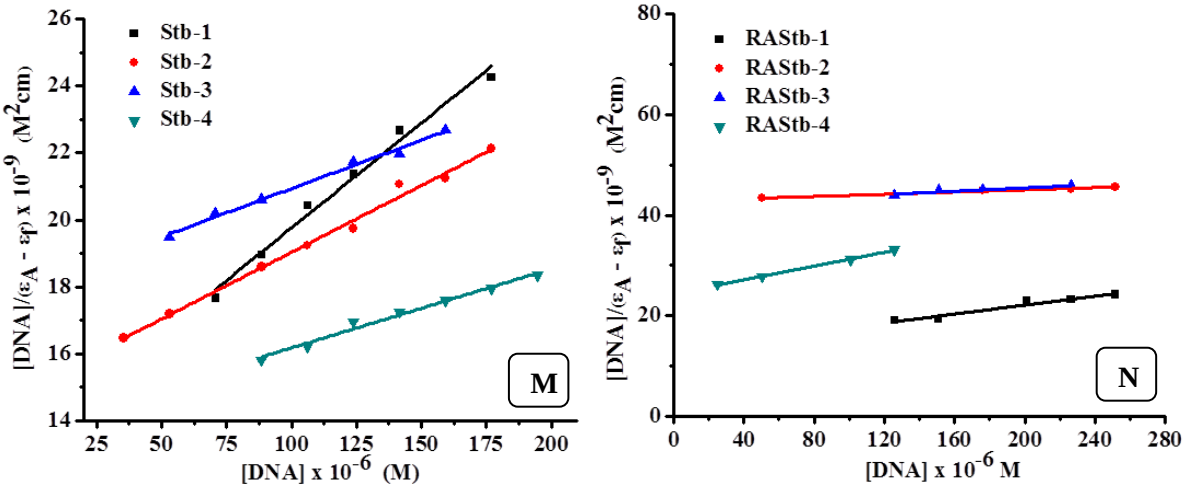

Fig. 5.4(Cont...): *Plot of [DNA]/(ε_A -ε_f) versus [DNA] for (M)* ***Stb 1-4*** *(N)* ***RAStb 1-4***

5.2.3.2 Competitive binding studies with EB using fluorescence spectroscopy:

In order to examine the ability of the compounds to displace EB from its DNA-EB complex, a competitive EB binding study has been undertaken employing fluorescence experiments [32].

Ethidium Bromide (EB = 3,8-diamino-5-ethyl-6-phenyl-phenanthridinium bromide) a phenanthridine fluorescent dye is a typical indicator of intercalation, forming soluble complexes with nucleic acids and emitting intense fluorescence in the presence of DNA due to the intercalation of the planar phenanthridinium ring between adjacent base pairs on the double helix [33,34]. The displacement of EB (quantified by fluorescence) by the addition of a compound is suggestive of an intercalative binding [35,36]. Addition of a second molecule (compound under study), which may replace EB from the DNA-EB complex results in a decrease of the DNA-induced EB emission due to displacement of EB from the intercalation sites of DNA [37].

The competitive binding study of each compound with EB has been investigated with fluorescence spectroscopy in order to examine whether the compound can displace EB from DNA–EB complex. The DNA–EB complex was prepared by adding EB (33.3 µM) and CT-DNA (20 µM) in tris buffer in the cuvette. The titration experiment was carried out by keeping the DNA-EB complex concentration constant and varying the compound concentration by adding increasing amount of solution step by step into the DNA–EB complex. The influence of the addition of each aliquot of the compound was obtained by recording the variation in the fluorescence emission spectra of the DNA-EB complex. The fluorescence intensities of EB bound to CT-DNA were measured at 609 nm (524 nm excitation) after addition of different

concentrations of the compound at different ratios. The titration curve so generated has been representatively shown for each series in *Fig. 5.5*.

The relative binding of complexes to CT-DNA was determined by calculating the quenching constant (K_{SV}) from the slopes of straight lines obtained from the Stern-Volmer equation **(5.2)** [38]:

$$Io/I = 1 + K_{SV}[Q] \qquad (5.2)$$

where Io and I are the emission intensities in the absence and the presence of the quencher (Q = compound) respectively, [Q] is the concentration of the quencher and K_{SV} is the Stern–Volmer constant which can be obtained from the slope of the plot of Io/I *versus* [Q] and is often used to evaluate the quenching efficiency of each compound.

The K_{SV} plots for all the synthesized ligands and their corresponding Ru(II) complexes have been shown in *Fig. 5.6.* The K_{SV} values obtained from these plots have been tabulated and discussed in section *5.2.4.*

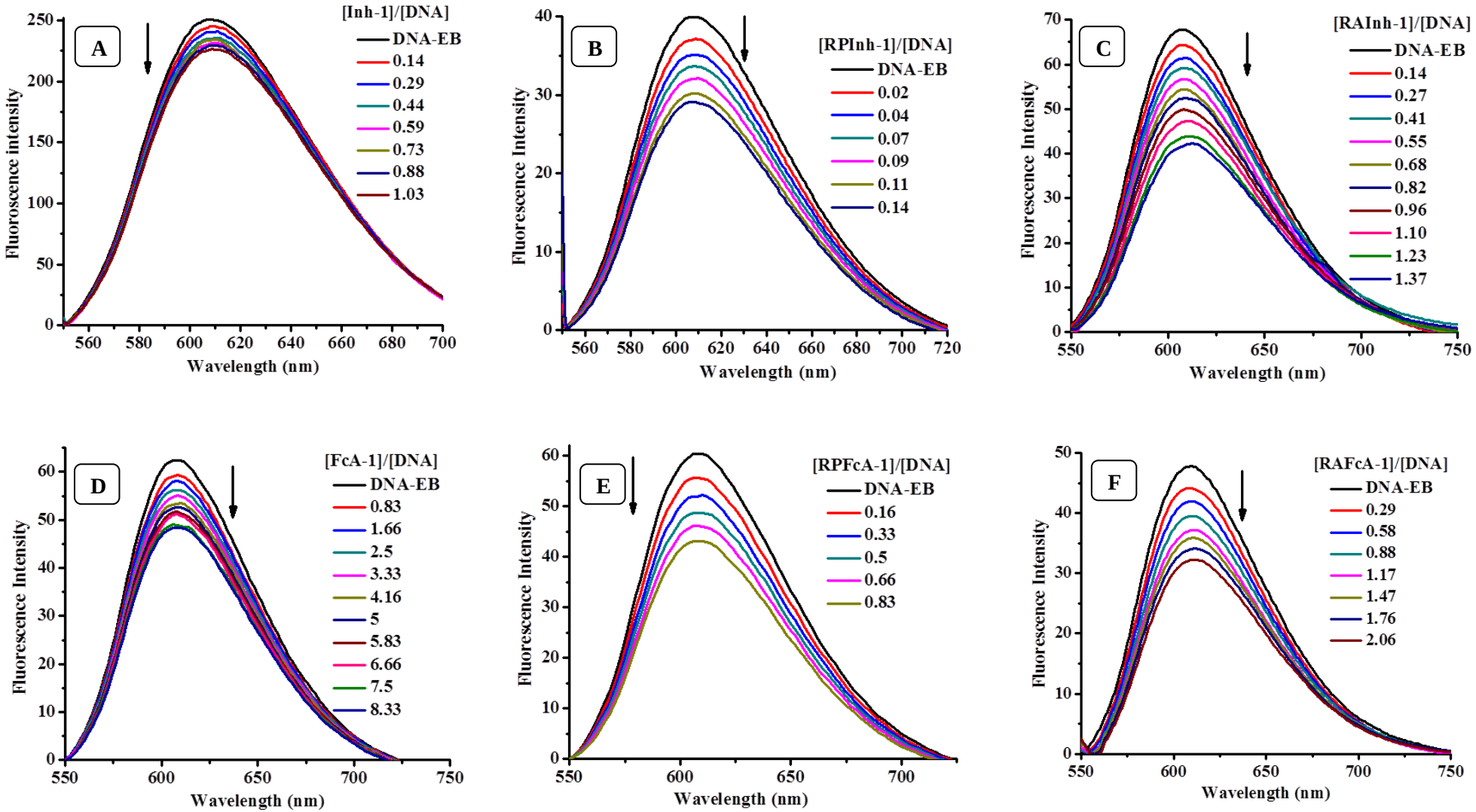

Fig. 5.5: *Fluorescence emission spectra of DNA-EB complex at increasing concentrations of (A)* ***Inh-1*** *(B)* ***RPInh-1*** *(C)* ***RAInh-1*** *(D)* ***FcA-1*** *(E)* ***RPFcA-1*** *(F)* ***RAFcA-1****, the arrow shows decrease in intensity (quenching of DNA-EB fluorescence) upon increasing concentration of the complex.*

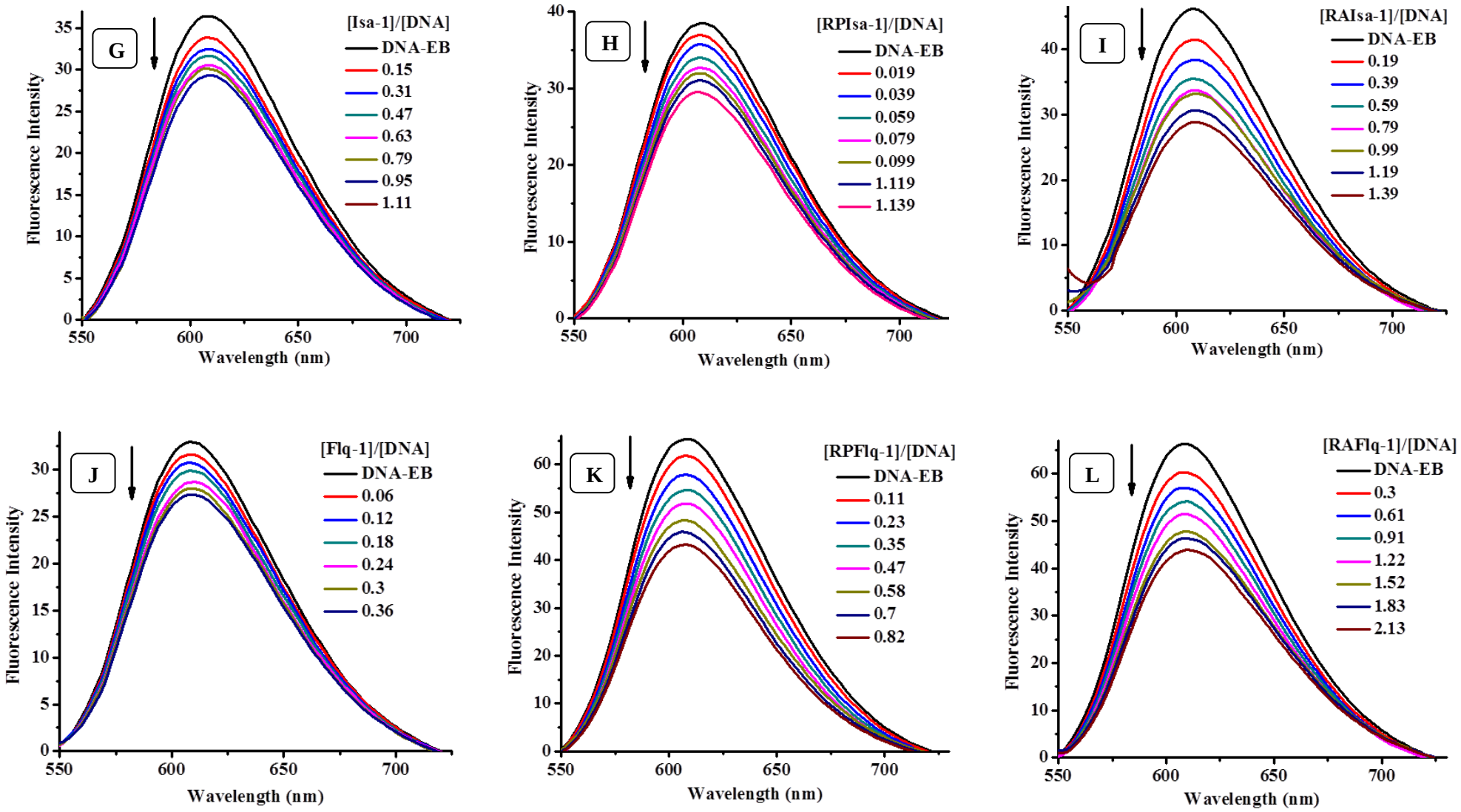

Fig. 5.5(Cont...): *Fluorescence emission spectra of DNA-EB complex at increasing concentrations of (G)* ***Isa-1*** *(H)* ***RPIsa-1*** *(I)* ***RAIsa-1*** *(J)* ***RAFlq-1*** *(K)* ***RPFlq 1-3*** *(L)* ***RAFlq-1****, the arrow shows decrease in intensity (quenching of DNA-EB fluorescence) upon increasing concentration of the complex.*

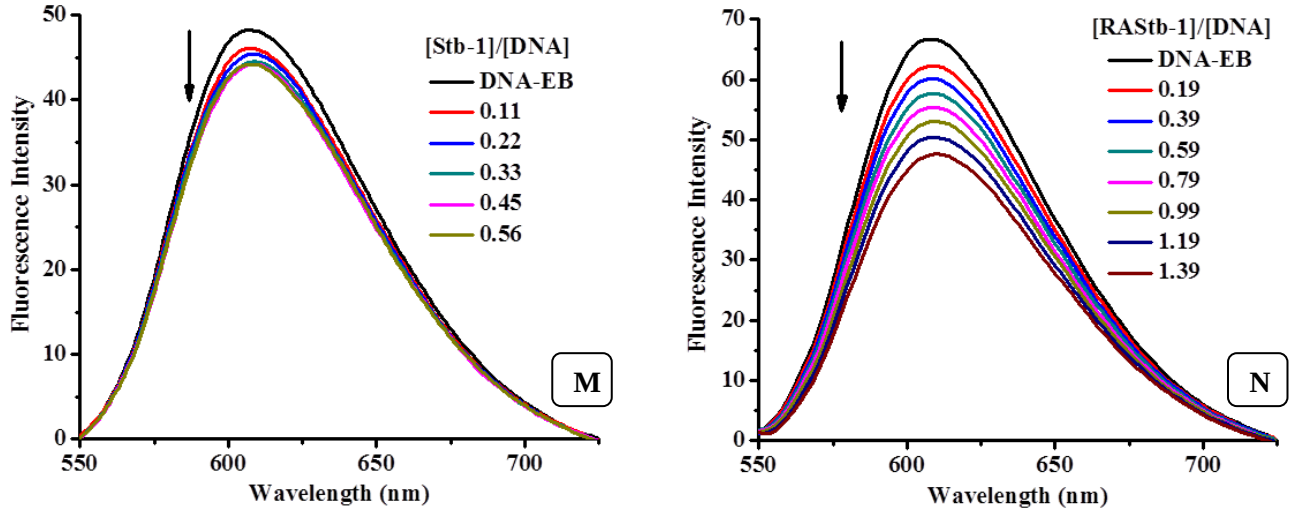

Fig. 5.5(Cont...): *Fluorescence emission spectra of DNA-EB complex at increasing concentrations of (M)* ***Stb-2*** *(N)* ***RAStb-2*** *the arrow shows decrease in intensity (quenching of DNA-EB fluorescence) upon increasing concentration of the complex.*

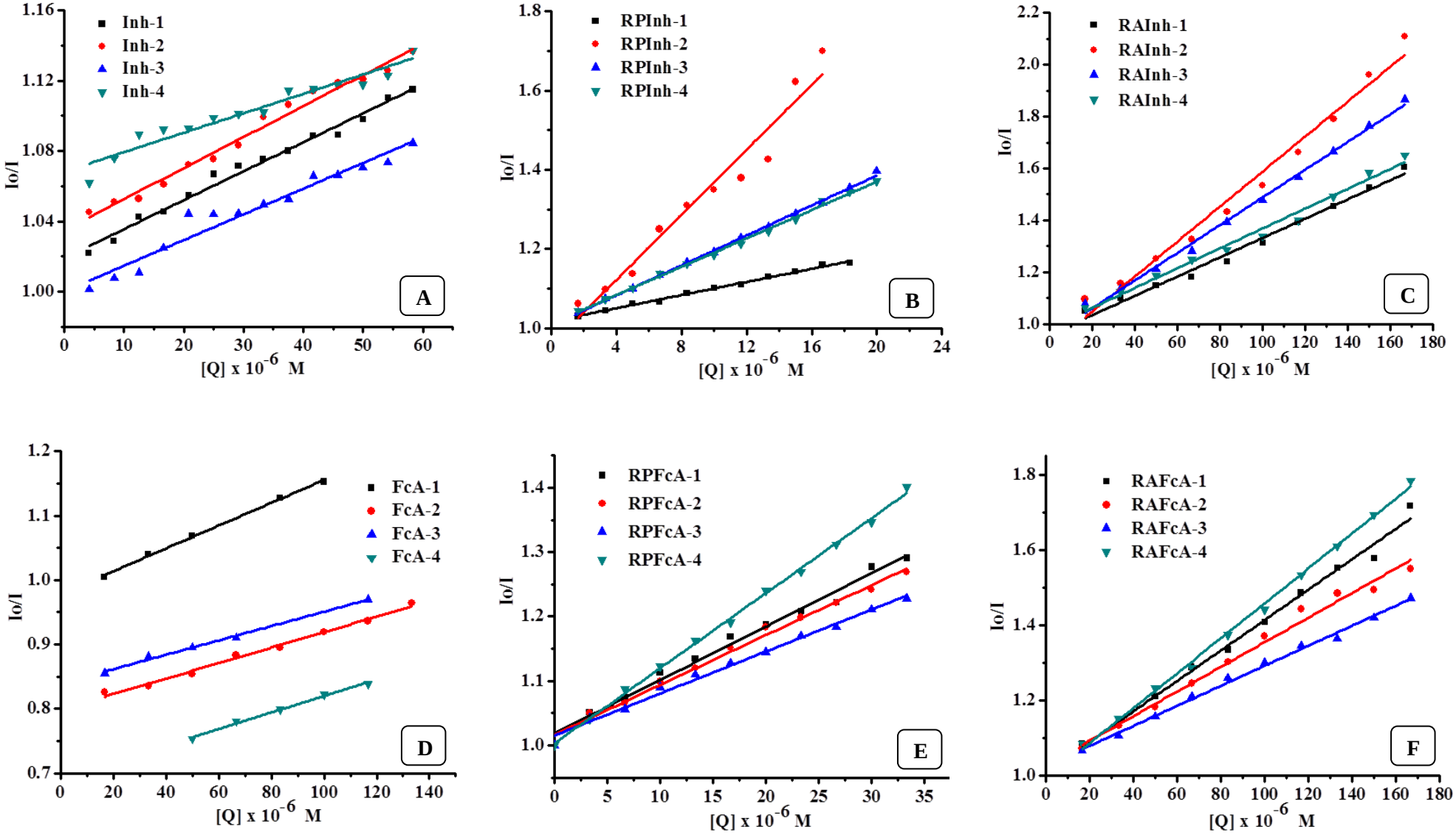

Fig. 5.6: *Stern-Volmer quenching plot Io/I versus [Q] of DNA-EB for (A)* ***Inh 1-4*** *(B)* ***RPInh 1-4*** *(C)* ***RAInh 1-4*** *(D)* ***FcA 1-4*** *(E)* ***RPFcA 1-4*** *(F)* ***RAFcA 1-4***

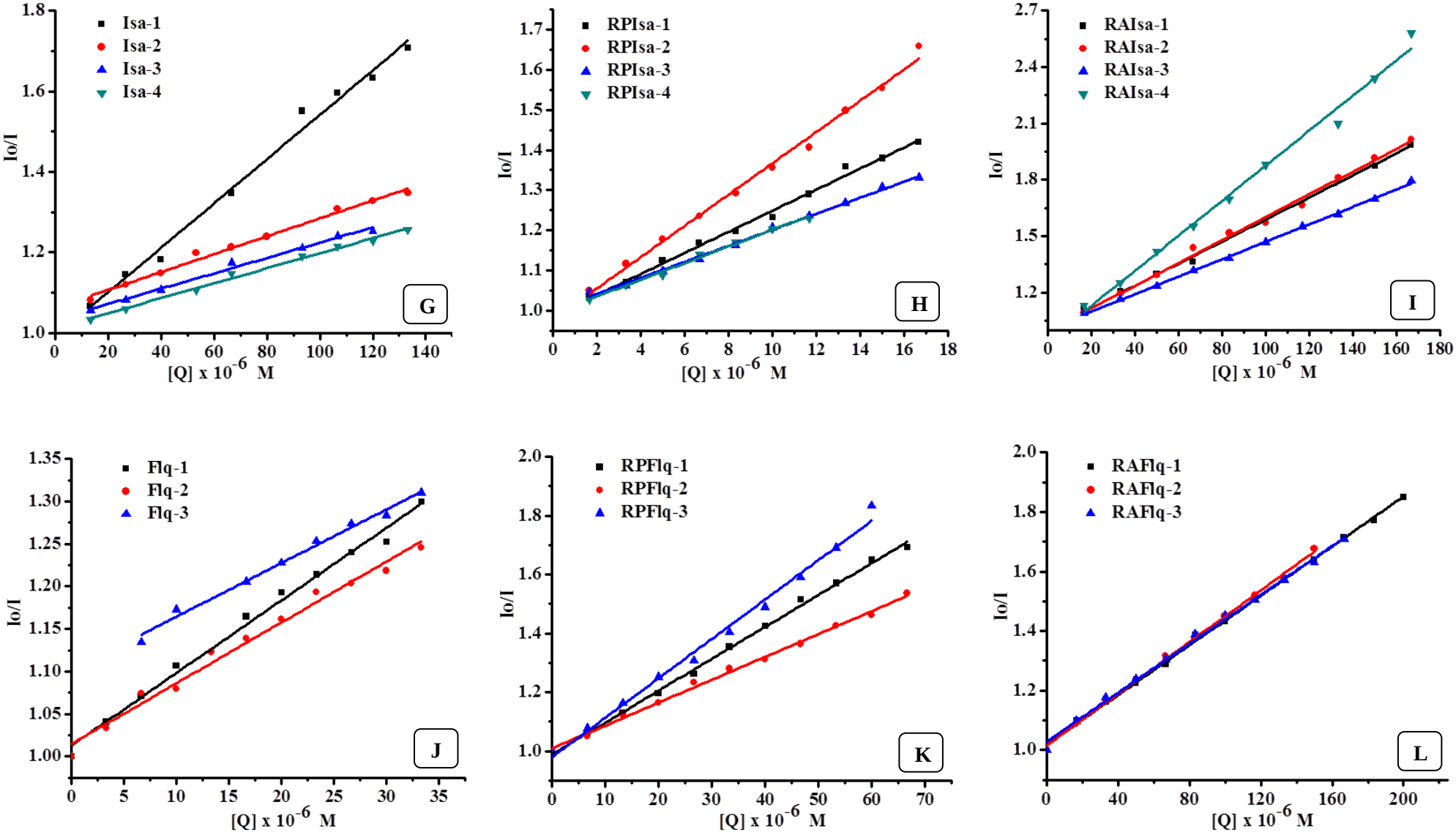

Fig. 5.6 (Cont...): *Stern-Volmer quenching plot Io/I versus [Q] of DNA-EB for (G)* ***Isa 1-4*** *(H)* ***RPIsa 1-4*** *(I)* ***RAIsa 1-4*** *(J)* ***Flq 1-3*** *(K)* ***RPFlq 1-3*** *(L)* ***RAFlq 1-3***

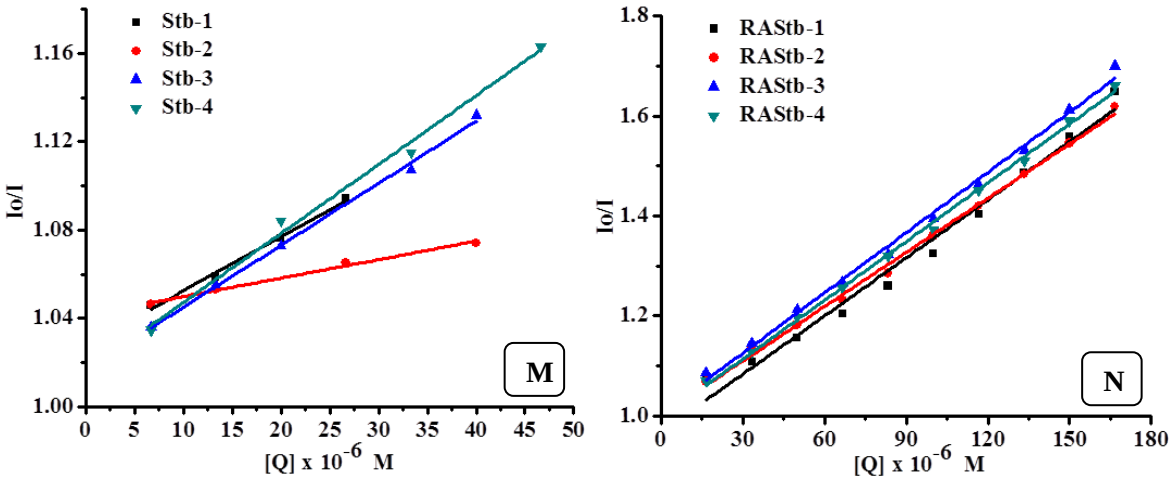

Fig. 5.6 (Cont...): *Plot of [DNA]/(ε_A -ε_f) versus [DNA] for (M)* ***Stb 1-4*** *(N)* ***RAStb 1-4***

5.2.3.3 Viscosity measurements:

The viscosity of DNA is sensitive to length changes and is regarded as the least ambiguous and the most critical clues of a DNA binding mode in solution [39]. In general, intercalating agents are expected to elongate the double helix to accommodate the ligands in between the base pairs, leading to an increase in the viscosity of DNA. In contrast, a complex that binds exclusively in the DNA grooves typically causes less pronounced (positive or negative) or no changes in DNA solution viscosity [40,41].

Cannon–Ubbelohde viscometer maintained at a constant temperature of 32.0 ± 0.1°C in a thermostat was used to measure the relative viscosity of DNA (200 µM) solutions in the presence of complexes **RPFcA 1-4** (with [Complex]/[DNA] ratio of 0, 0.04, 0.08, 0.12, 0.16, 0.20 and 0.24) in Tris-HCl buffer (pH 7.2). Digital stopwatch with least count of 0.01 s. was used for flow time measurement with accuracy of ± 0.1 s. The flow time of each sample was measured three times and an average flow time was calculated. Data are presented as $(\eta/\eta_0)^{1/3}$ *versus* [complex]/[DNA], where η is the viscosity of DNA in the presence of complex and η_0 is the viscosity of DNA alone. Viscosity values were calculated from the observed flow time of DNA-containing solutions (t) corrected for that of the buffer alone (t_0), $\eta = (t–t_0)/t_0$ [42].

5.2.4 Results and discussion:

5.2.4.1 Inh series:

The K_b (intrinsic binding constant) values (*Table 5.2*) obtained from the plot of [DNA]/(ε_A-ε_f) *versus* [DNA] (*Fig. 5.4 A,B,C)* using equation **(5.1)** are in the range of 1.7 - 5.7 x 10^3 M^{-1} for **Inh 1-4**, 1.7 - 8.8 x 10^3 M^{-1} for **RPInh 1-4** and 1.6 - 6.1 x 10^3 M^{-1} for **RAInh 1-4** suggesting moderate binding of the ligands and their complexes to CT-DNA. An observed hypochromism along with a bathochromic shift is indicative of intercalative mode of binding to the DNA. Of the ruthenium phenanthroline complexes **RPInh-2** shows the highest K_b value (8.8 x 10^3 M^{-1}); similarly **RAInh-2** shows the highest K_b value (6.1 x 10^3 M^{-1}) among ruthenium arene complexes. An overall comparison of the K_b values show that the Ru-phenanthroline complexes are relatively better DNA binders compared to Ru-arene complexes

Table 5.2: *DNA binding constants of* ***Inh 1-4***, ***RPInh 1-4*** *and* ***RAInh 1-4***.

Compound	*DNA binding constants*		
	K_b M^{-1}	K_{SV} M^{-1}	*λ shift*
Inh-1	5.7 x 10^3	1.6 x 10^3	-
Inh-2	4.3 x 10^3	1.8 x 10^3	-
Inh-3	1.7 x 10^3	1.5 x 10^3	-
Inh-4	2.0 x 10^3	1.0 x 10^3	-
RPInh-1	3.2 x 10^3	0.8 x 10^4	-
RPInh-2	8.8 x 10^3	4.1 x 10^4	-
RPInh-3	5.5 x 10^3	1.9 x 10^4	2 nm
RPInh-4	1.7 x 10^3	1.8 x 10^4	-
RAInh-1	2.9 x 10^3	3.7 x 10^3	2 nm
RAInh-2	6.1 x 10^3	6.7 x 10^3	3 nm
RAInh-3	4.3 x 10^3	5.3 x 10^3	3 nm
RAInh-4	1.6 x 10^3	3.8 x 10^3	2 nm

Competitive EB binding studies show quenching of DNA–EB fluorescence on titration with the ligands and complexes suggesting that the compounds displace EB from the DNA–EB complex and interact with DNA via intercalative mode. The Stern–Volmer quenching plots of DNA–EB (*Fig. 5.6 A,B,C*) illustrate that the quenching of EB bound to DNA by the compounds is in good agreement (R = 0.93-0.99) with the linear Stern–Volmer equation **(5.2)**. The K_{SV} values of the compounds given in *Table 5.2* show that they have good affinity for DNA with values in the range of 1.0 – 1.8 x 10^3 M^{-1} for **Inh 1-4**, 0.8 – 4.1 x 10^4 M^{-1} for **RPInh 1-4** and 3.7 - 6.7 x 10^3 M^{-1} for **RAInh 1-4**. It can be well noted that the ruthenium phenanthroline complexes show 10 fold better displacement efficacies of EB from DNA-EB complex than the ruthenium arene. This observation is in line with the K_b values obtained from UV absorption studies. The planarity of **RPInh 1-4** complexes

owing to the two 1,10-phenanthroline ligands coordinated to the ruthenium centre helps in intercalative stacking making them better intercalators compared to their arene analogues. The K_{SV} values show that **RPInh-2** and **RAInh-2** show maximum quenching efficiency (K_b values are also supportive of this fact) among the phenanthroline and arene analogues respectively which may be attributed to possible hydrogen bonding between the –OH group of the ligand and a nucleic acid base.

5.2.4.2 Ferrocene series:

The absorption bands of **FcA 1-4** and **RAFcA 1-4** complexes showed hypochormism and bathochromism whereas **RPFcA 1-4** complexes exhibited hypochromism but with negligible red shift. Though the DNA intercalators show larger bathochromic shift and hypochromism of the spectral bands, the intercalative mode of binding of the complexes with DNA cannot be ruled out completely [43]. The magnitude of binding strength to CT-DNA determined through the calculation of binding constants K_b (obtained from plots in *Fig. 5.4 D,E,F*) have been tabulated in *Table 5.3.* K_b values for the ligands **FcA 1-4** are in the range of 1.3 – 6.7 x 10^4 M^{-1} indicative of strong binding of the ligands with **FcA-1** showing the highest value. The binding values of ruthenium phenanthroline complexes (2.5 x 10^5 – 5.3 x 10^6 M^{-1}) showed 10-100 fold higher binding efficacy compared to the ligands while ruthenium arene complexes showed relatively poor binding to DNA with binding values in the range of 2.1 – 3.9 x 10^3 M^{-1}. In general, **RPFcA 1-4** complexes exhibit much stronger binding interactions than **RAFcA 1-4** complexes due to (i) intercalation facilitated by the presence of the phenanthroline ligands by insertion of the complex into the adjacent base pairs of DNA and (ii) groove binding of the ferrocenyl moiety. Complex **RPFcA-1** with a

Table 5.3: *DNA binding constants of* ***FcA 1-4****,* ***RPFcA 1-4*** *and* ***RAFcA 1-4****.*

Compound	*DNA binding constants*		
	K_b M^{-1}	K_{SV} M^{-1}	*λ shift*
FcA-1	6.7 x 10^4	1.8 x 10^3	2 nm
FcA-2	2.3 x 10^4	1.2 x 10^3	1 nm
FcA-3	1.4 x 10^4	1.1 x 10^3	3 nm
FcA-4	1.3 x 10^4	1.3 x 10^3	3 nm
RPFcA-1	5.3 x 10^6	8.3 x 10^3	-
RPFcA-2	3.8 x 10^5	7.3 x 10^3	-
RPFcA-3	2.5 x 10^5	6.5 x 10^3	-
RPFcA-4	1.1 x 10^6	1.2 x 10^4	-
RAFcA-1	3.9 x 10^3	4.0 x 10^3	3 nm
RAFcA-2	2.1 x 10^3	3.3 x 10^3	5 nm
RAFcA-3	3.4 x 10^3	2.7 x 10^3	4 nm
RAFcA-4	3.5 x 10^3	4.7 x 10^3	4 nm

tyrosine substituted ferrocenyl moiety bound to the Ru(II) centre shows the highest binding efficacy due to additional hydrogen bonding interactions between –OH group of tyrosine and DNA nucleobases which are accessible both in major groove and minor groove and is also observed in case of the free ligand **FcA-1**. Complex **RPFcA-4** with a tryptophan substituted ferrocenyl moiety bound to Ru(II) centre shows a similar binding value as **RPFcA-1** which also may be due to additional hydrogen bonding interaction between –NH group of tryptophan and DNA nucleobases. Similar trend was observed also in corresponding ruthenium arene complexes.

The Stern–Volmer quenching plots (*Fig. 5.6 D,E,F*) illustrate that the quenching of EB bound to DNA by ferrocenyl mannich bases and their ruthenium complexes are in good agreement (R = 0.93-0.99) with the linear Stern–Volmer equation. The Stern-Volmer quenching constant K_{SV} values have been tabulated in *Table 5.3***.** Complexes **RPFcA-1** and **RPFcA-4** show higher quenching constant values of 8.3 x 10^3 M^{-1} and 1.2 x 10^4 M^{-1} respectively indicating their greater efficiency to replace EB and bind strongly with DNA which is also evident from their higher K_b values.

In order to further confirm the mode of binding of **RPFcA 1-4** to CT-DNA**,** viscosity measurements of DNA solutions were carried out in presence and absence of these complexes. The effects of the complexes and classical intercalator EB on the viscosities of CT-DNA solution are shown in *Fig. 5.7*. With increasing [complex]/[DNA] concentration ratios, the relative viscosities of CT-DNA increased gradually indicative of characteristic intercalative mode of binding which is in accordance with previous findings.

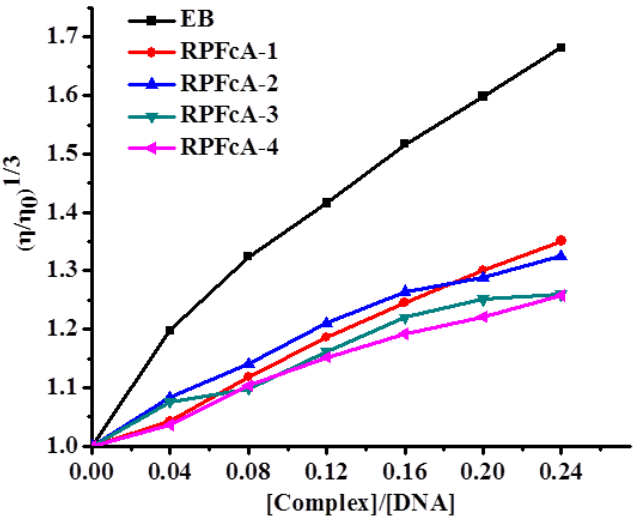

Fig. 5.7: *Effect of increasing amounts of the complexes **RPFcA 1-4** and Ethidium Bromide (**EB**) on the relative viscosity of CT-DNA (200µM) in Tris-HCl buffer at 32 (± 0.1) °C. [Complex]/[DNA] = 0, 0.04, 0.08, 0.12, 0.16, 0.20, 0.24.*

5.2.4.3 Stilbene series:

DNA binding constant K_b (*Table 5.4*) (*Fig. 5.4 M,N*) for **Stb 1-4** and **RAStb 1-4** were obtained in the range of 1.6 – 2.6 x 10^3 M^{-1} and 1.3 – 2.9 x 10^3 M^{-1} respectively from the decay of absorbance. It can be seen that **Stb-2** and **RAStb-2** show the highest binding values in both the respective series. The observed higher activity of these compounds may be attributed to the electron releasing methoxy group in the ligand making the interactions more facile. Moreover it has been seen in the literature that stilbene derivatives with methoxy substituents show excellent cytotoxicities against various cancer cell lines [44]. The K_{SV} values (obtained from plots in *Fig. 5.6 M,N*) also point towards the same conclusion as discussed above. Overall both the pyridyl stilbene ligands and their arene complexes show moderate binding towards DNA mostly through intercalation.

Table 5.4: *DNA binding constants of* ***Stb 1-4*** *and* ***RAStb 1-4****.*

Compound	*DNA binding constants*		
	K_b M^{-1}	K_{SV} M^{-1}	*λ shift*
Stb-1	1.6 x 10^3	2.5 x 10^3	-
Stb-2	2.6 x 10^3	3.8 x 10^3	1 nm
Stb-3	1.6 x 10^3	2.8 x 10^3	-
Stb-4	1.7 x 10^3	3.1 x 10^3	1 nm
RAStb-1	1.3 x 10^3	1.9 x 10^3	-
RAStb-2	2.9 x 10^3	3.9 x 10^3	-
RAStb-3	2.4 x 10^3	4.0 x 10^3	-
RAStb-4	1.4 x 10^3	3.6 x 10^3	-

5.2.4.4 Isatin series:

The $n \rightarrow \pi^*$ bands of **Isa 1-4** and their complexes **RPIsa 1-4** and **RAIsa 1-4** showed hypochormism with a slight red shift. The binding constants K_b (obtained from plots in *Fig. 5.4 G,H,I*) have been tabulated in *Table 5.5*. K_b values for the ligands **Isa 1-4** are in the range of 2.4 x 10^3 – 8.4 x 10^4 M^{-1} indicative of strong binding of the ligands with **Isa-1** showing the highest value. The complexes **RPIsa-1** and **2** ($\mathbf{K_b}$ = 1.1 x 10^5 and 3.5 x 10^4 M^{-1} respectively) showed 10 fold better DNA binding than their corresponding ligands while complexes **3** and **4** exhibited about same binding efficacy**. RAIsa 1-4** showed moderate binding to DNA with binding values in the range of 6.4 – 8.3 x 10^3 M^{-1}. In general, ruthenium phenanthroline complexes exhibit much stronger binding interactions than the corresponding ruthenium arene complexes owing to the phenanthroline ligands which facilitate intercalation.

The Stern–Volmer quenching plots (*Fig. 5.6 G,H,I*) illustrate that the quenching of EB bound to DNA by isatin hydrazones and their ruthenium complexes are in good agreement (R = 0.93-0.99) with the linear Stern–Volmer equation. The Stern-Volmer quenching constant K_{SV} values have been tabulated in *Table 5.5***.** An overall view of the quenching constants suggest that the **RPIsa 1-4** complexes show better quenching than the corresponding ligands as well as arene analogues indicating their greater efficiency to replace EB and bind strongly with DNA which is also evident from their higher K_b values.

Table 5.5: *DNA binding constants of* ***Isa 1-4***, ***RPIsa 1-4*** *and* ***RAIsa 1-4****.*

Compound	DNA binding constants		
	K_b M^{-1}	K_{SV} M^{-1}	λ shift
Isa-1	8.4×10^4	5.5×10^3	-
Isa-2	2.4×10^3	2.2×10^3	-
Isa-3	1.2×10^4	1.9×10^3	-
Isa-4	1.6×10^4	1.9×10^3	-
RPIsa-1	1.1×10^5	2.6×10^4	1 nm
RPIsa-2	3.5×10^4	3.9×10^4	2 nm
RPIsa-3	1.3×10^4	2.0×10^4	1 nm
RPIsa-4	1.7×10^4	2.0×10^4	1 nm
RAIsa-1	8.2×10^3	5.9×10^3	-
RAIsa-2	6.5×10^3	6.1×10^3	-
RAIsa-3	8.3×10^3	4.6×10^3	-
RAIsa-4	6.4×10^3	9.3×10^3	-

Table 5.6: *DNA binding constants of* ***Flq 1-3***, ***RPFlq 1-3*** *and* ***RAFlq 1-3****.*

Compound	DNA binding constants		
	K_b M^{-1}	K_{SV} M^{-1}	λ shift
Flq-1	4.7×10^3	7.2×10^3	-
Flq-2	7.8×10^3	7.5×10^3	-
Flq-3	7.2×10^3	6.3×10^3	-
RPFlq-1	6.1×10^3	2.6×10^4	1 nm
RPFlq-2	1.0×10^4	3.9×10^3	2 nm
RPFlq-3	7.5×10^3	2.0×10^4	2 nm
RAFlq-1	0.8×10^3	4.2×10^3	-
RAFlq-2	1.8×10^3	4.3×10^3	-
RAFlq-3	1.7×10^3	4.1×10^3	-

5.2.4.5 Fluoroquinolone series:

The binding constant K_b values (*Table 5.6*) as calculated using the Mehan's equation **(5.1)** and plots in *Fig. 5.4 J,K,L* for **Flq 1-3** and their complexes **RPFlq 1-3** are in the range of 6.1 x 10^3- 1.0 x 10^4 M^{-1} and those of **RAFlq 1-3** are in the range of 0.8 x 10^3- 4.7 x 10^3 M^{-1}. The K_b values of the complexes suggest that the phenanthroline complexes are better DNA binders compared to the arene complexes. Competitive binding studies with EB follow the same pattern as electronic absorption studies for interaction with DNA. The stern-volmer

quenching constants K_{SV} (obtained from plots in *Fig. 5.6 J,K,L*) show that **RPFlq 1-3** complexes are better quenchers of DNA-EB fluorescence than **RAFlq 1-3**. Levofloxacin containing Ru-phenanthroline complex (**RPFlq-2**) shows best DNA binding ability amongst all the complexes.

5.3 Drug-BSA interactions:

5.3.1 Serum Albumin: an important biomolecule:

Albumin is the most abundant protein in the blood plasma of all vertebrates with the concentration in human serum being 35–50 mg/ml and a molecular weight of 66.5 kDa. Albumin is stable in the pH range of 4–9, soluble in 40% ethanol, and can be heated at 60°C for up to 10 hours without deleterious effects. These properties, as well as preferential uptake in tumor and inflamed tissue, ready availability, biodegradability, and lack of toxicity and immunogenicity make serum albumin an ideal candidate for drug delivery [45].

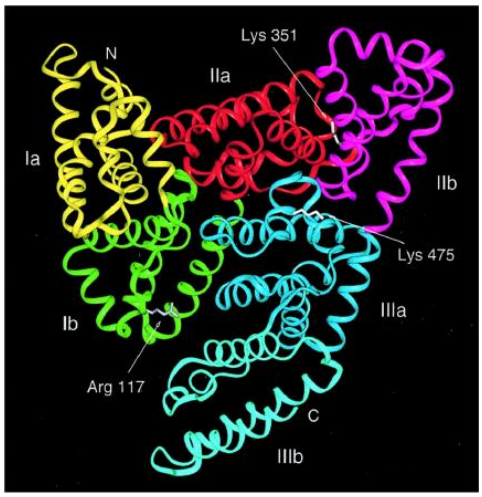

Fig. 5.8: *Structure of human serum albumin consisting of three domains, each grouped into subdomains A and B*

❖ **Structure and function:**

Human serum albumin (HSA) is composed of three homologous domains, numbered I, II, and III [46]. Each domain is grouped into subdomains A and B that possess common structural motifs. The two principal regions responsible for ligand-binding to HSA are known as Sudlow's Site I and II, located in subdomain IIA and IIIA (*Fig. 5.8*), respectively [47,48].

Albumin is able to bind various endogenous molecules, including long-chain fatty acids, steroids, L-tryptophan, etc. Moreover, albumin is also involved in transporting ions in the circulation, including copper, zinc, calcium, etc. Additionally, this vital protein is able to bind exogenous compounds and drugs, such as warfarin, ibuprofen, chlorpromazine and naproxen, with the affinity of their binding significantly affecting their activity and half-life [47, 49, 50].

❖ **Distribution**

Interestingly, albumin is predominately present in the extravascular space (~242 g) rather than the intravascular space (~118 g). In fact, the protein is prevalent in extracellular locations such as skin, gut, muscle, other fluids (i.e., cerebrospinal, pleural,

etc.) and secretions (e.g., sweat, tears and milk). However, very low concentrations of albumin are present intracellularly. Albumin returns from the extravascular space to the circulation *via* the lymphatic system, making ~28 "trips" in and out of the lymphatic system during its lifetime [47,50].

❖ **Accumulation of albumin in the tumor interstitium:**

Solid tumors commonly possess an immature, highly permeable vasculature that is acted upon by vascular permeability enhancing factors. However, despite this there is generally insufficient lymphatic drainage. This subsequently results in an accumulation of macro- molecules (>40 kDa) within the tumor interstitium, and this is known as the enhanced permeation and retention effect EPR (*Fig. 5.9*) [51-53]. The retention of albumin in tumors has since been observed in various experimental solid tumors (e.g., sarcoma, ovarian carcinoma, Novikof hepatoma, etc.) using radio labeled- or dye-complexed serum albumin [54].

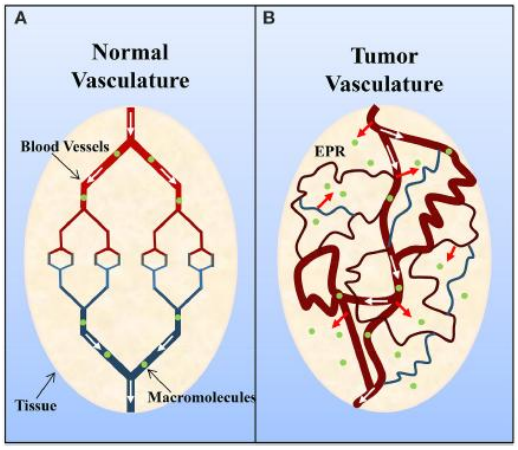

Fig. 5.9: *Schematic representation on (A) normal and (B) tumor vasculature. Normal tissue is composed of mature, organized blood vessels, while tumor tissue consists of immature, leaky and tortuous vessels.*

Considering the enhanced permeation and retention effect and the accumulation of albumin in the tumor interstitium, the development of albumin as a drug carrier is increasingly important to consider in terms of the targeted delivery of cancer therapy. Various drug delivery systems with albumin have been developed including albumin nanoparticles, drug albumin conjugates, albumin-binding drug derivatives and prodrugs [55,56]. The development and market approval of the paclitaxel- loaded albumin nanoparticle, *nab*-paclitaxel or Abraxane® [57,58], was a major breakthrough in the field of albumin carrier development.

Moreover, albumin-binding as a general strategy for improving the pharmacokinetics of drugs is also being assessed. Traditionally, the binding of a drug to albumin is believed to reduce the level of free drug available to exert its therapeutic activity [59,60]. However, studies have also demonstrated mechanisms by which albumin acts to effectively improve therapeutic use or reduce rapid clearance. For instance, the experimental anti-cancer thiosemicarbazone, namely di- 2-pyridylketone4,4-dimethyl-3-thiosemicarbazone (Dp44mT) [61], has been shown to be internalized by cancer cells *via*

a putative carrier/receptor. Interestingly, the uptake, toxicity and apoptotic activity of Dp44mT is greatly enhanced in the presence of HSA [62,63].

❖ **Outlook:**

Albumin is a versatile and captivating protein. Recent applications of serum albumin (human and bovine) have demonstrated some advantages as a natural and therefore biocompatible and biodegradable carrier for drugs [64,65,66]. The albumin-based drug delivery system has increased the diseased tissue/normal tissue drug concentration ratio. The search and characterization of albumin-binding drugs, particularly in cancer cells, is of considerable interest in light of the development of albumin as an effective drug carrier to target tumors. Albumin-binding may provide an advantage when generating tumor targeting agents and this requires further intense investigation.

5.3.2 Materials and instrumentation:

The BSA (Bovine Serum Albumin) binding studies were solely carried out in tris buffer (containing 15 mM tri-sodium citrate and 150 mM NaCl at pH 7.0 prepared in double distilled water). BSA stock solution was prepared in double distilled water with a concentration of 10^{-4} M. The stock solutions of all the compounds under study were prepared in neat DMSO with a stock concentration of 10^{-3} M. BSA was purchased from Hi-media, Mumbai, India.

Fluorescence spectra were recorded in tris buffer solution at concentrations of 10^{-6} M on JASCO FP-6300 fluorescence spectrophotometer.

The data generated from the titration experiments were analyzed and plotted with the help of the software OriginPro 8.

5.3.3 Experimental :

Bovine serum albumin (BSA) is extensively studied, due to its structural homology with human serum albumin (HSA). HSA contains 585 amino acid residues with only one tryptophan located at position 214, while BSA has two tryptophans at positions 134 and 212 along the chain (*Fig. 5.10*). BSA solutions exhibit a strong fluorescence emission with a peak at 343 nm, due to the tryptophan residues, when excited at 296 nm.

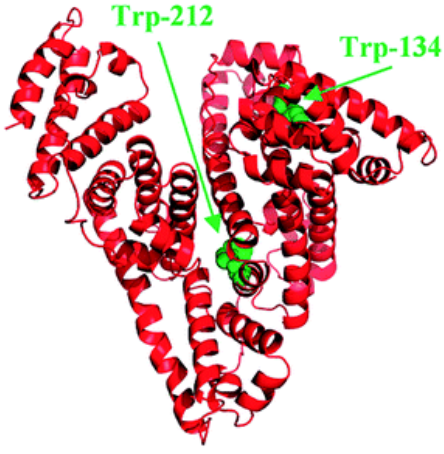

Fig. 5.10: *Structure of bovine serum albumin showing the two tryptophan residues.*

The interaction of compounds with BSA has been studied from tryptophan emission-quenching experiments. The changes in the

emission spectra of tryptophan in BSA are primarily due to change in protein conformation, subunit association, substrate binding or denaturation [67,68]. Addition of a compound to a solution of BSA results in a decrease of the fluorescence intensity because of their binding to BSA which may change the protein secondary structure leading to changes in the tryptophan environment of BSA.

The protein-binding study for the ruthenium complexes was performed by tryptophan fluorescence quenching experiments using bovine serum albumin (BSA, 3-16 μM) in buffer. The quenching of emission intensity of the tryptophan residues of BSA at 343 nm was monitored in the presence of increasing concentrations of complexes as quenchers. Fluorescence spectra were recorded from 300 to 500 nm at an excitation wavelength of 296 nm. The titration curve so generated has been representatively shown in *Fig. 5.11*.

The Stern–Volmer equation **(5.2)** (discussed in sec. *5.2.3.2*) may be used in order to study the interaction of a quencher with serum albumins.

$$\mathbf{Io/I = 1 + K_{SV}[Q]} \qquad \mathbf{(5.2)}$$

where Io is the initial tryptophan fluorescence intensity of BSA, I the tryptophan fluorescence intensity of BSA after the addition of the quencher and $\boldsymbol{K_{SV}}$ the dynamic quenching constant, The dynamic quenching constant ($\boldsymbol{K_{SV}}\,M^{-1}$) can be obtained from the slope of the plot Io/I *versus* [Q]. The $\boldsymbol{K_{SV}}$ plots for all the synthesized ligands and their corresponding Ru(II) complexes have been shown in *Fig. 5.12.* The $\boldsymbol{K_{SV}}$ values obtained from these plots have been tabulated and discussed in section *5.3.4.*

Quenching of emission spectra may be owing to a variety of molecular interactions including excited-sate reactions through collisional quenching, energy transfer, ground state complex formation and molecular rearrangements. The different mechanisms of quenching are usually classified as:

- Static quenching (the formation of a complex between quencher and fluorophore)
- Dynamic quenching (a collisional process).

The type of quenching mainly operating in the systems can be speculated from the nature of the Stern–Volmer plots. Linear Stern–Volmer plots (*Fig. 5.12*) represent a single quenching mechanism, either static or dynamic although which mechanism is operative cannot be speculated. Sometimes a nonlinear Stern–Volmer plot with an upward curvature, concave towards the y-axis at high [Q], may result if both static and dynamic quenching processes operate simultaneously in an interacting system (*Fig. 5.12, O and P*).

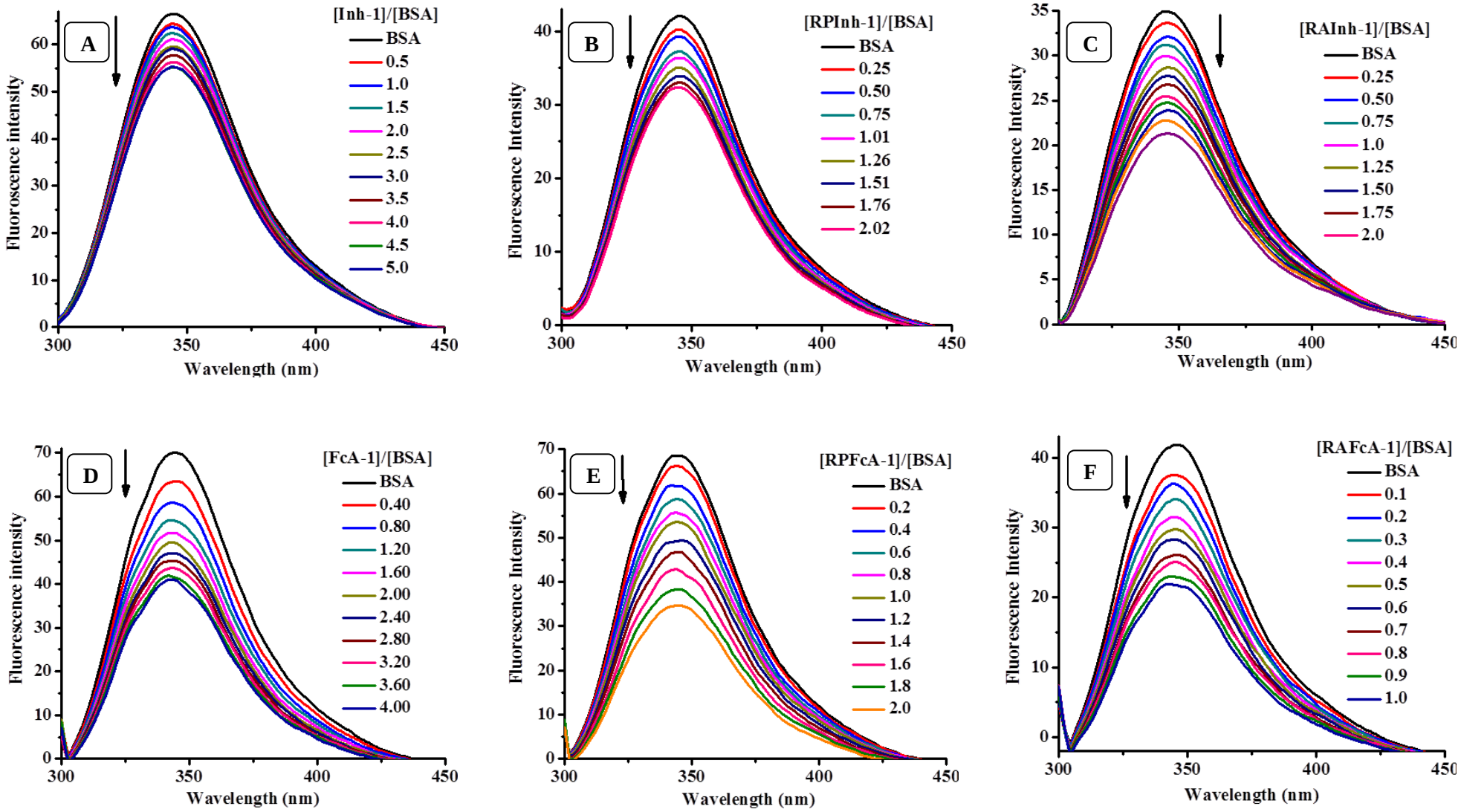

Fig. 5.11: *Fluorescence emission spectra of BSA at increasing concentrations of (A)* ***Inh-1*** *(B)* ***RPInh-1*** *(C)* ***RAInh-1*** *(D)* ***FcA-1*** *(E)* ***RPFcA-1*** *(F)* ***RAFcA-1****, the arrow shows decrease in intensity (quenching of BSA fluorescence) upon increasing concentration of the complex.*

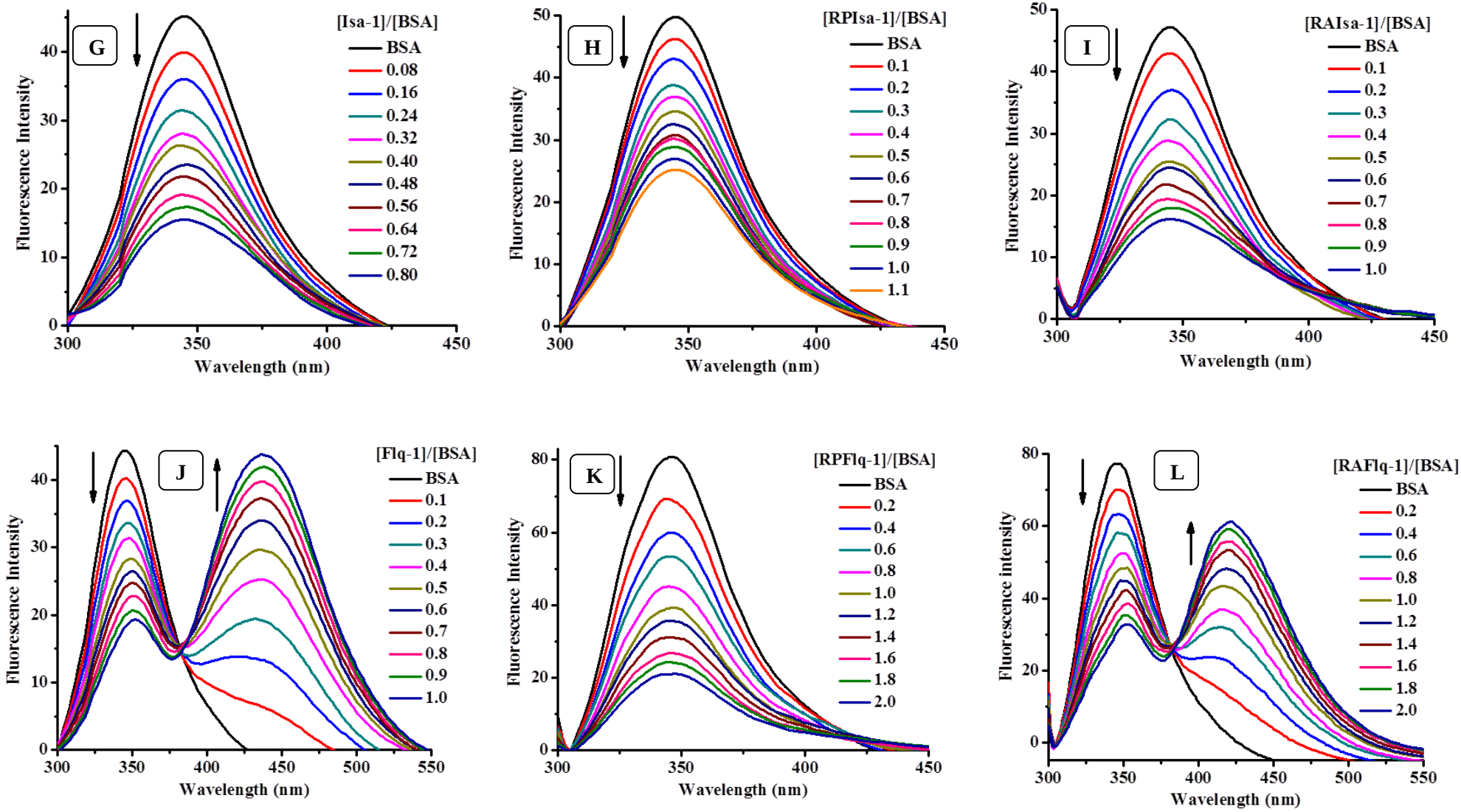

Fig. 5.11(Cont...): *Fluorescence emission spectra of BSA at increasing concentrations of (G)* ***Isa-1*** *(H)* ***RPIsa-1*** *(I)* ***RAIsa-1*** *(J)* ***RAFlq-1*** *(K)* ***RPFlq 1-3*** *(L)* ***RAFlq-1****, the arrow shows decrease in intensity (quenching of BSA fluorescence) upon increasing concentration of the complex.*

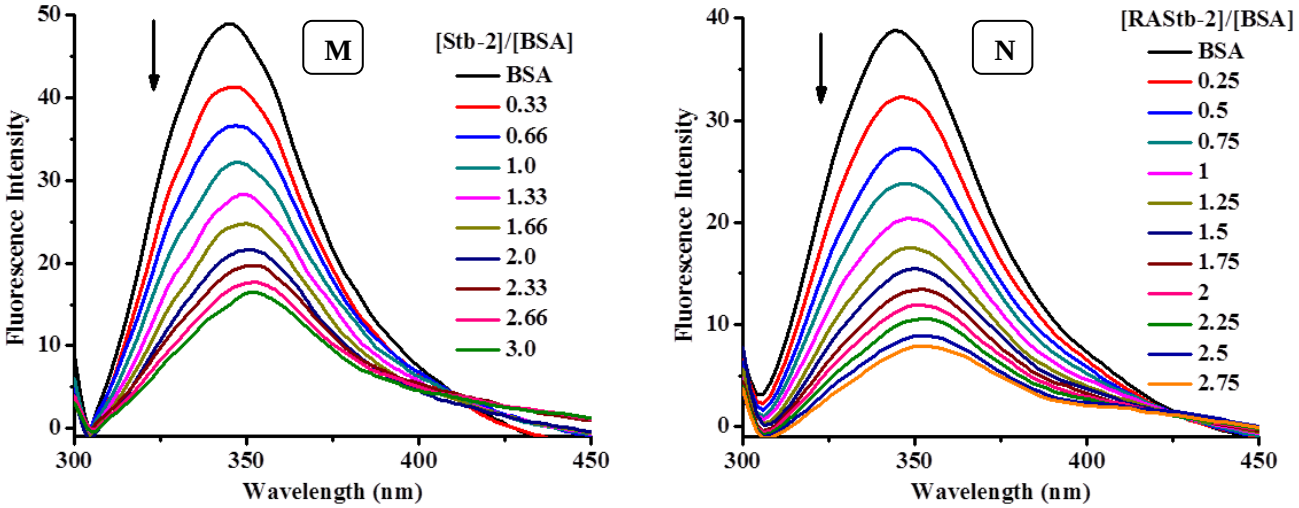

Fig. 5.11(Cont...): *Fluorescence emission spectra of BSA at increasing concentrations of (M)* ***Stb-2*** *(N)* ***RAStb-2****, the arrow shows decrease in intensity (quenching of BSA fluorescence) upon increasing concentration of the complex.*

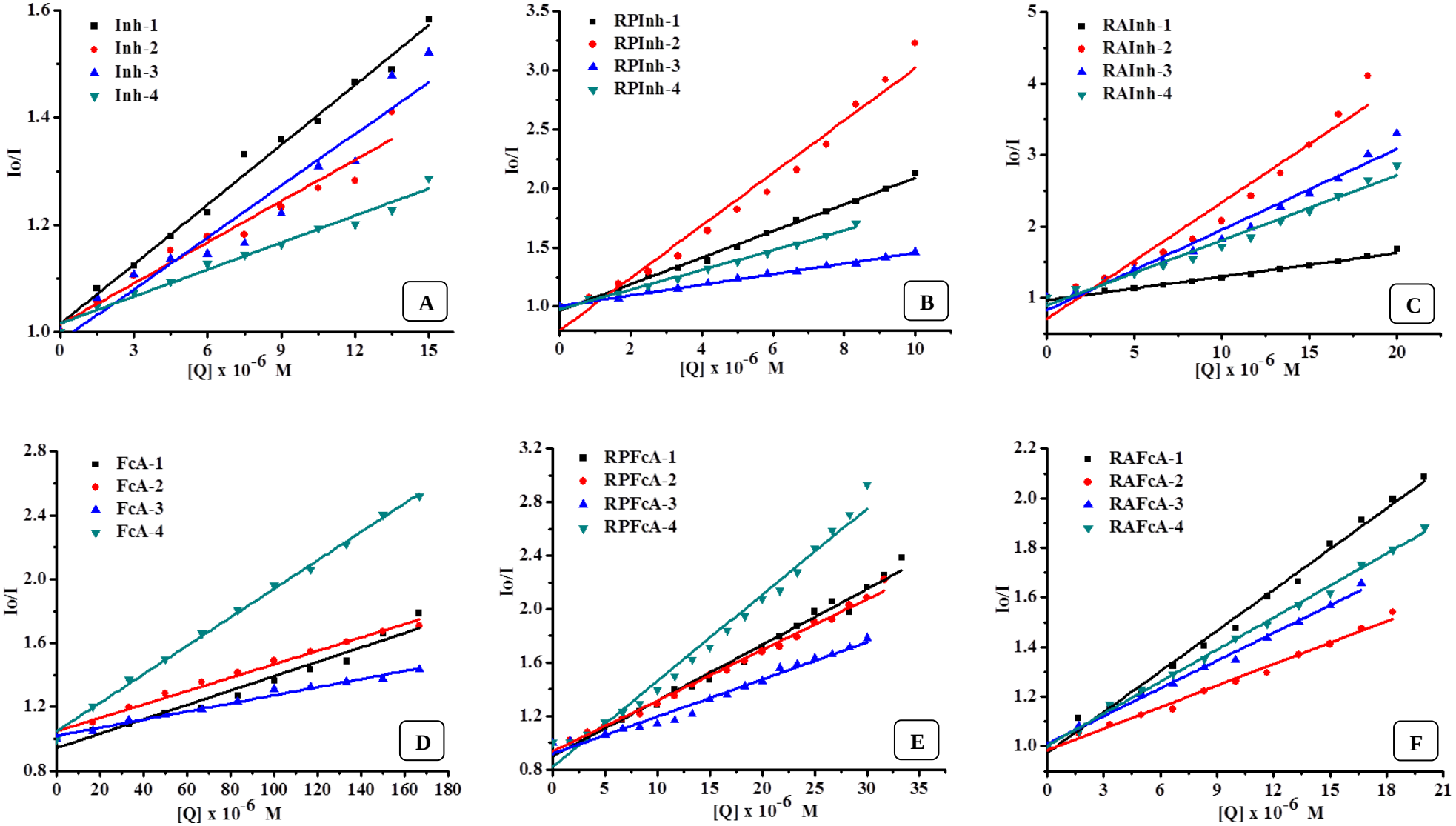

Fig. 5.12: *Stern-Volmer quenching plot Io/I versus [Q] of BSA for (A)* ***Inh 1-4*** *(B)* ***RPInh 1-4*** *(C)* ***RAInh 1-4*** *(D)* ***FcA 1-4*** *(E)* ***RPFcA 1-4*** *(F)* ***RAFcA 1-4***

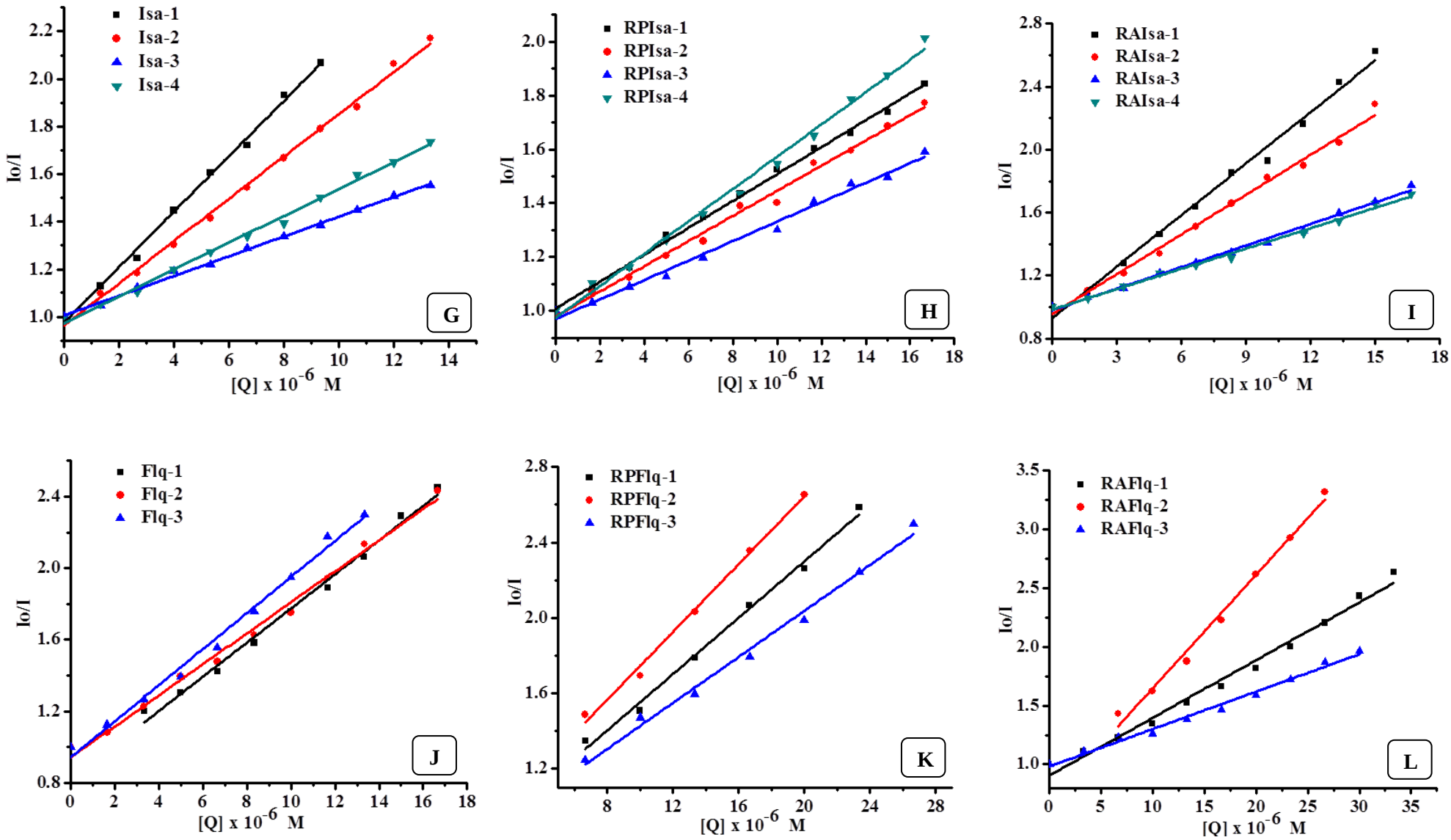

Fig. 5.12 (Cont...): *Stern-Volmer quenching plot Io/I versus [Q] of BSA for (G)* ***Isa 1-4*** *(H)* ***RPIsa 1-4*** *(I)* ***RAIsa-1*** *(J)* ***Flq 1-3*** *(K)* ***RPFlq 1-3*** *(L)* ***RAFlq 1-3***

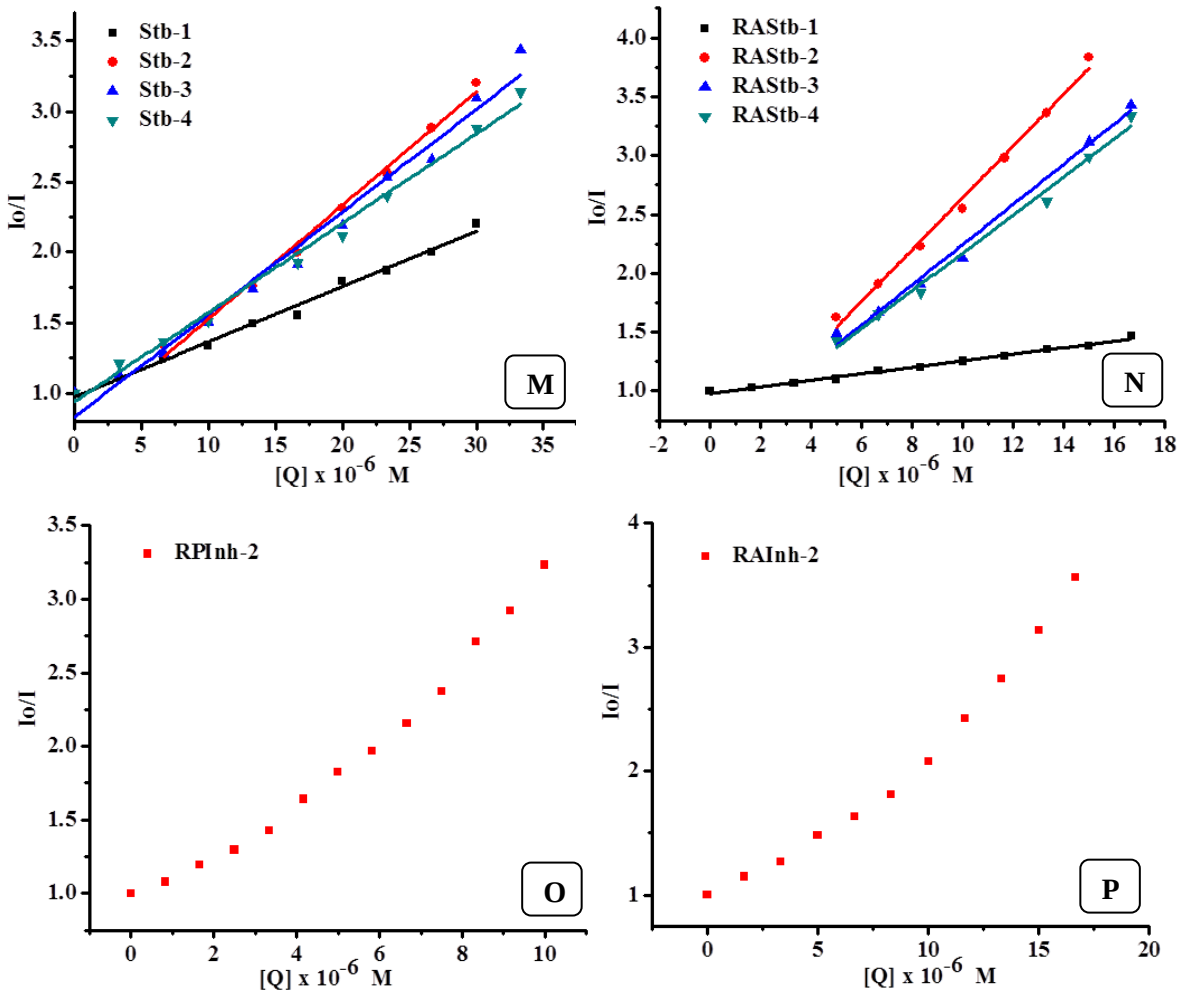

Fig. 5.12 (Cont...): *Stern-Volmer quenching plot Io/I versus [Q] of BSA for (M)* ***Stb 1-4*** *(N)* ***RAStb 1-4*** *(O)* ***RPInh-2*** *showing the non-linear (upward curved) SV plot (P)* ***RAInh-2*** *showing the non-linear (upward curved) SV plot*

When small molecules are bound independently to a set of equivalent sites on a macromolecule, the equilibrium between free and bound molecules is given by double-logarithm equation **(5.3)** [69]. This equation has been employed in order to determine the binding constant (***Ka***) and the number of binding sites (***n***) for complexe – BSA interaction.

$$\log (I_o\text{-}I)/I = \log K_a + n \log [Q] \qquad (5.3)$$

where Io and I are the fluorescence intensities in the absence and the presence of quencher, and [Q] is the concentration of quencher (ruthenium complexes). The plot of log [(Io-I)/I] *versus* log [Q] for all the systems is linear (*Fig. 5.13*) and the values of ***Ka*** and ***n*** have been obtained from the intercept and slope, respectively which have been tabulated and discussed in section *5.3.4*.

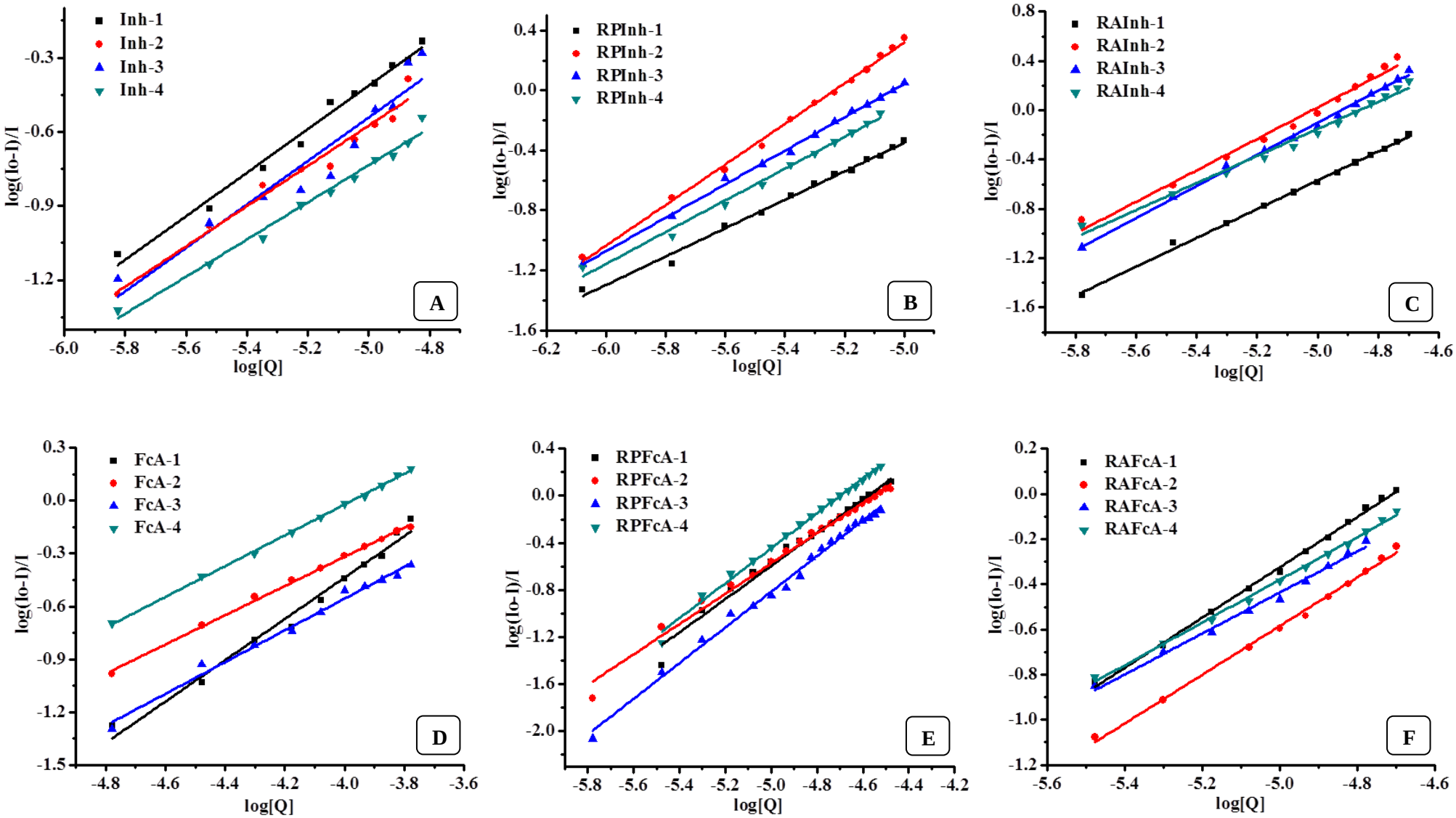

Fig. 5.13: *Double logarithmic plot for the quenching of BSA fluorescence by (A)* ***Inh 1-4*** *(B)* ***RPInh 1-4*** *(C)* ***RAInh 1-4*** *(D)* ***FcA 1-4*** *(E)* ***RPFcA 1-4*** *(F)* ***RAFcA 1-4.***

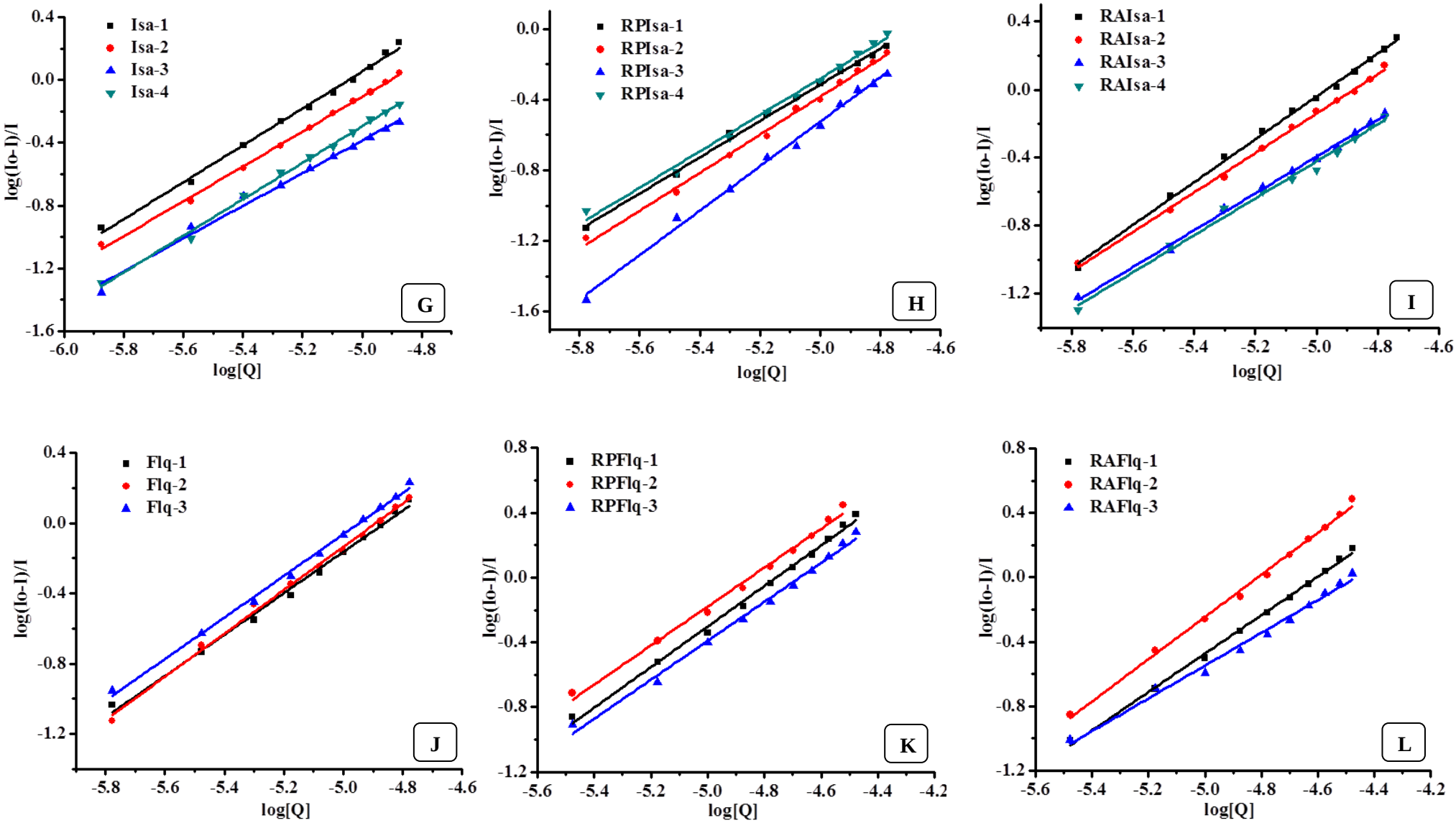

Fig. 5.13 (Cont...): *Double logarithmic plot for the quenching of BSA fluorescence by (G)* ***Isa 1-4*** *(H)* ***RPIsa 1-4*** *(I)* ***RAIsa 1-4*** *(J)* ***Flq 1-3*** *(K)* ***RPFlq 1-3*** *(L)* ***RAFlq 1-3***

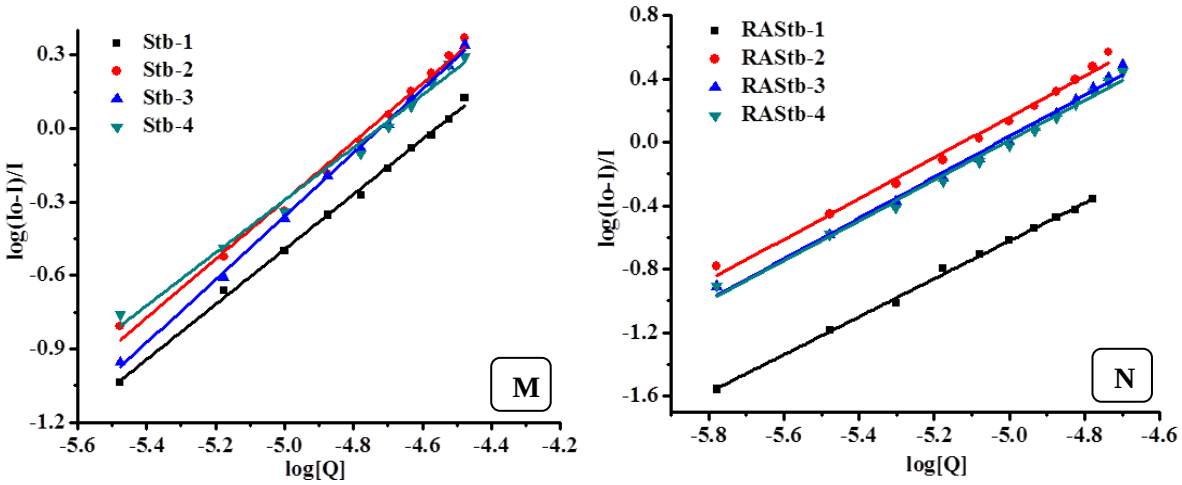

Fig. 5.13 (Cont...): *Double logarithmic plot for the quenching of BSA fluorescence by (M)* ***Stb 1-4*** *(N)* ***RAStb 1-4***

5.3.4 Results and discussion:

5.3.4.1 Inh series:

The binding interactions of the compounds under study with BSA led to quenching of its fluorescence. The Stern–Volmer plots (*Fig. 5.12 A,B,C*) show that the curves have fine linear relationships (r = 0.99) according to the Stern–Volmer quenching equation **(5.2)** indicative of a single quenching process in the system**.** The Stern-Volmer quenching constants K_{SV} (*Table 5.7*) calculated using equation **(5.2)** show that the ligands **Inh 1-4** show 10 folds more quenching on complexation with the metal. The Stern-Volmer quenching plot of **RPInh-2** (*Fig. 5.12 O*) as well as **RAInh-2** (*Fig. 5.12 P*) shows an exceptional upward curve indicating the presence of dual quenching processes which is also evident from highest K_{SV} values among their respective series.

Quantitative binding to BSA was

Table 5.7: *BSA binding constants of* ***Inh 1-4***, ***RPInh 1-4*** *and* ***RAInh 1-4***.

Compound	BSA binding constants		
	$K_a\ M^{-1}$	$K_{SV}\ M^{-1}$	n
Inh-1	9.8×10^3	3.7×10^4	0.9
Inh-2	3.1×10^3	2.6×10^4	0.8
Inh-3	7.2×10^3	3.2×10^4	0.9
Inh-4	1.1×10^3	1.7×10^4	0.7
RPInh-1	2.4×10^4	0.4×10^5	0.9
RPInh-2	1.2×10^6	2.2×10^5	2.2
RPInh-3	4.2×10^5	1.1×10^5	1.1
RPInh-4	1.5×10^5	0.8×10^5	1.1
RAInh-1	0.2×10^6	0.3×10^5	1.2
RAInh-2	2.6×10^6	1.6×10^5	1.3
RAInh-3	2.2×10^6	1.1×10^5	1.3
RAInh-4	0.2×10^6	0.9×10^5	1.1

achieved using double logarithmic plot. The plots of log [(Io-I)/I] *versus* log [Q] for the present system are linear (*Fig. 5.13 A,B,C*) and the values of ***Ka*** and ***n*** have been tabulated in *Table 5.7.* The ***Ka*** values confirm that ligands show much better (100-1000 fold) binding efficacies after complexation with ruthenium(II). In case of BSA binding it has been found that **RAInh 1-4** complexes showed 10-100 fold better binding propensities to BSA compared to **RPInh 1-4** owing to the more hydrophobic nature of the arene complexes making them suitable to interact with the hydrophobic pockets of the protein.

The *n* values for all the complexes average out to be 1 which suggests that there is one binding site available on the protein. Moreover the linear nature of the double logarithm plots of the complexes indicates that only one of the tryptophan residues on BSA protein is interacting with the compounds.

5.3.4.2 Ferrocene series:

The values of the Stern–Volmer quenching constant for ligands **FcA 1-4** and their complexes interacting with BSA as calculated by Stern-Volmer quenching equation **(5.2)** and the corresponding Stern-Volmer plots (*Fig. 5.12 D,E,F*) are cited in *Table 5.8* which suggest good binding propensity of the complexes with BSA. The double logarithmic plots for the ligands and their ruthenium complexes are linear (*Fig. 5.13 D,E,F*). The association binding constant K_a and the number of binding sites per albumin ***n*** obtained from equation **(5.3)** have been provided in *Table 5.8.* It can be observed that **RPFcA 1-4** show stronger protein binding efficiency ($2.8 – 9.6 \times 10^6$ M^{-1}) than the ligands and their arene complexes which falls out as an exception compared to other series studied in this thesis.

Table 5.8: *BSA binding constants of* ***FcA 1-4****,* ***RPFcA 1-4*** *and* ***RAFcA 1-4****.*

Compound	***BSA binding constants***		
	K_a M^{-1}	K_{SV} M^{-1}	***n***
FcA-1	1.8×10^3	4.5×10^3	0.9
FcA-2	1.0×10^3	4.2×10^3	0.8
FcA-3	1.1×10^3	2.5×10^3	0.9
FcA-4	3.0×10^3	8.9×10^3	0.9
RPFcA-1	2.8×10^6	4.1×10^4	1.4
RPFcA-2	7.3×10^6	3.8×10^4	1.3
RPFcA-3	5.8×10^6	2.8×10^4	1.5
RPFcA-4	9.6×10^6	6.4×10^4	1.5
RAFcA-1	1.7×10^5	5.4×10^4	1.1
RAFcA-2	6.5×10^4	2.8×10^4	1.1
RAFcA-3	1.2×10^6	3.7×10^4	0.9
RAFcA-4	2.3×10^4	4.3×10^4	0.9

5.3.4.3 Stilbene series:

The K_{SV} (*Fig. 5.12 M,N*) and K_a (*Fig. 5.13 M,N*) for interaction of the pyridyl stilbenes and their mixed ligand arene ruthenium complexes with BSA given in *Table 5.9* suggest good binding efficacies. The association binding constant K_a indicate that **RAStb 1-4** interact with BSA, 100-1000 folds stronger ($K_a \sim 10^5$-$10^6 M^{-1}$) than with DNA ($K_b \sim 10^3 M^{-1}$). **Stb-2** and its complex **RAStb-2** with a methoxy group showed overall good interactions with BSA for the same reason as discussed in *sec 5.2.4.3*.

Table 5.9: *BSA binding constants of* ***Stb 1-4*** *and* ***RAStb 1-4****.*

Compound	*BSA binding constants*		
	$K_a\ M^{-1}$	$K_{SV}\ M^{-1}$	*n*
Stb-1	1.3×10^5	3.9×10^4	1.0
Stb-2	4.8×10^5	8.1×10^4	1.2
Stb-3	1.3×10^5	1.7×10^4	1.3
Stb-4	1.2×10^5	6.3×10^4	1.1
RAStb-1	2.3×10^5	2.7×10^4	1.2
RAStb-2	3.9×10^6	2.2×10^5	1.3
RAStb-3	3.1×10^6	1.7×10^5	1.3
RAStb-4	2.1×10^6	1.6×10^5	1.3

Table 5.10: *BSA binding constants of* ***Isa 1-4****,* ***RPIsa 1-4*** *and* ***RAIsa 1-4****.*

Compound	*BSA binding constants*		
	$K_a\ M^{-1}$	$K_{SV}\ M^{-1}$	*n*
Isa-1	8.7×10^5	1.2×10^5	1.2
Isa-2	2.8×10^5	8.9×10^4	1.1
Isa-3	6.5×10^4	4.2×10^4	1.0
Isa-4	3.3×10^5	5.6×10^4	1.2
RPIsa-1	6.5×10^5	5.0×10^4	1.0
RPIsa-2	9.7×10^4	4.6×10^4	1.1
RPIsa-3	5.6×10^4	3.6×10^4	1.2
RPIsa-4	7.2×10^4	5.9×10^4	1.0
RAIsa-1	1.8×10^6	1.1×10^5	1.2
RAIsa-2	4.6×10^5	8.4×10^4	1.1
RAIsa-3	1.1×10^5	4.4×10^4	1.1
RAIsa-4	1.1×10^5	4.3×10^4	1.1

5.3.4.4 Isatin series:

The values of the Stern–Volmer quenching constant for ligands **Isa 1-4** and their complexes interacting with BSA obtained from Stern-Volmer plots (*Fig. 5.12 G,H,I*) are cited in *Table 5.10* which suggest good binding propensity with BSA. The double logarithmic plots for the ligands and their ruthenium complexes are linear (*Fig. 5.13 G,H,I*). The association binding constant K_a and the number of binding sites per albumin ***n*** have been provided in *Table 5.10*. The arene analogues **RAIsa 1-4** show stronger protein binding efficiency ($1.1 \times 10^5 - 1.8 \times 10^6\ M^{-1}$) than the ligands and their phenanthroline analogues. This observation is in line with those of other arene complexes discussed in this chapter.

5.3.4.5 Fluoroquinolone series:

The stern volmer quenching constants K_{SV} obtained from stern volmer plots (*Fig. 5.12 J,K,L*) for interaction of the fluoroquinolone complexes with BSA given in *Table 5.11* suggest good binding intensities with the protein. The double logarithmic plot (*Fig. 5.13 J,K,L*) for all the complexes have been found to be linear. The association binding constant so calculated indicate that the arenes **RAFlq 1-3** interact with the protein 10 folds better than the phenanthroline complexes **RPFlq 1-3**. Levofloxacin containing phenanthroline (**RPFlq-2**) and arene (**RAFlq-2**) complexes show highest BSA binding interactions amongst all the **Flq** complexes. In *Fig. 5.11 J and L* the new peak observed at 438 nm and 420 nm respectively is owing to the intrinsic fluorescence of the compounds which also exhibits hyperchromism with increased concentration of the compound as expected.

Table 5.11: *BSA binding constants of* ***Flq 1-3***, ***RPFlq 1-3*** *and* ***RAFlq 1-3***.

Compound	***BSA binding constants***		
	$K_a\ M^{-1}$	$K_{SV}\ M^{-1}$	***n***
Flq-1	5.3×10^4	6.5×10^4	1.1
Flq-2	1.1×10^5	8.6×10^4	1.2
Flq-3	2.2×10^4	1.0×10^4	1.1
RPFlq-1	9.1×10^4	7.4×10^4	1.2
RPFlq-2	6.8×10^5	9.0×10^4	1.2
RPFlq-3	4.2×10^4	6.1×10^4	1.2
RAFlq-1	3.2×10^5	4.9×10^4	1.2
RAFlq-2	2.1×10^6	9.6×10^4	1.3
RAFlq-3	3.5×10^5	3.2×10^4	1.0

In-Cellulo assays

In-cellulo studies also comes under the banner of *in-vitro* studies with the only distinction that these studies are carried out within a cellular environment. Cell-based assays are often used for screening of compounds to determine if the test molecules have effects on cell proliferation or show direct cytotoxic effects that eventually lead to cell death. Cell-based assays also are widely used for measuring receptor binding and a variety of signal transduction events that may involve the expression of genetic reporters, trafficking of cellular components, or monitoring organelle function. Regardless of the type of cell-based assay being used, it is important to know how many viable cells are remaining at the end of the experiment. There are a variety of assay methods exploiting different cellular properties for different targets (summarized in *Table 5.12*).

Table 5.12: *Summary of different assays being prominently used to assess different cellular targets owing to the common cellular properties which has been used in the current study.*

Cellular properties/targets	***Assays***
Enzymatic property (viability)	MTT assay
<u>Membrane integrity</u> • Cell membrane integrity • Mitochondrial membrane integrity • Membrane phospholipid phosphatidylserine translocation (apoptosis)	<u>Dye exclusion test</u> • AO/EB stain • Rhodamine 123 stain • Annexin V FITC assay
ROS (reactive oxygen species) generation	DCFDA stain
DNA condensation	DAPI stain
Apoptosis	Gene expression studies

5.4 Cytotoxicity on A549 (human lung cancer) and MCF7 (human breast cancer) cell lines:

5.4.1 Concept and principle of MTT assay:

This is a colorimetric assay that measures the reduction of yellow 3-(4,5-dimethythiazol- 2-yl)-2,5-diphenyl tetrazolium bromide (MTT) into an insoluble, coloured (dark purple) formazan product within the cell (*Fig. 5.14*). The cells are then solubilised with an organic solvent (e.g. DMSO) and the released, solubilised formazan reagent with an absorbance maximum near 570 nm is measured spectrophotometrically. Since reduction of MTT can only occur in metabolically active cells the level of activity is a measure of the viability of the cells. Viable cells with active metabolism convert MTT into formazan product but when cells die, they lose the ability to convert MTT into formazan, thus color formation serves as a useful and convenient marker of only the viable cells. The exact cellular mechanism of MTT reduction into formazan is not well understood. Speculation in the early literature involving specific mitochondrial enzymes has led to the assumption that MTT is measuring mitochondrial activity, the reduction being caused by mitochondrial succinate dehydrogenase, but most likely involves reaction with NADH or similar reducing molecules that transfer electrons to MTT [70,71,72].

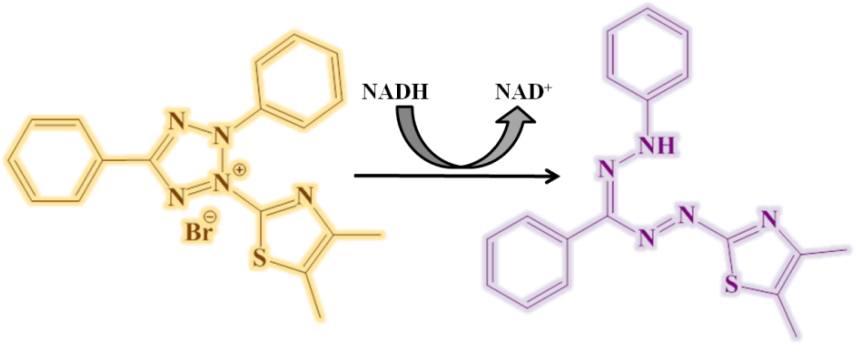

MTT **Formazan**

Fig. 5.14: *structure of MTT and colored formazan product.*

5.4.2 Materials and instrumentation:

The cell lines were cultured in Dulbecco's Modified Eagle Medium (DMEM), while Phosphate Buffer Saline (PBS) was used for washing purpose. The stock solutions of compounds (1 mg/ml) were prepared by first dissolving in minimum volume of DMSO (50µl) and then diluting the concentrated DMSO solution with DMEM media to 1 ml. Further dilutions from the stock solution were made using DMEM for subsequent dosing. Both DMEM and PBS were purchased from Hi-Media. The MTT dye was purchased from SRL (Sisco research laboratory, Mumbai, India.). DMSO used to prepare stock

solution as well as to dissolve formazan crystals was of analytical grade and purchased from Merck. 96-well culture plates were purchased from Tarson India Pvt. Ltd. The cell lines were procured from National Centre for Cell Science (NCCS), Pune, India.

The spectrophotometric detection of culture plates was done by Biotek-ELX universal ELISA reader (Bio-Tek instruments, Inc., Winooski, VT). The data so obtained were converted into percentage viability and were analyzed and plotted with the help of the software Graphpad Prism 3 using one-way ANOVA as the statistical tool.

5.4.3 Experimental:

The MTT reduction assay was the first homogeneous cell viability assay developed for a 96-well format [73]. The MTT tetrazolium assay technology has been widely adopted and remains popular in academic labs as evidenced by thousands of published articles.

In the present study two different cancer cell lines have been targeted for two different series of ruthenium complexes. All ruthenium(II) phenanthroline complexes have been checked for their cytotoxicities on A549 (human lung cancer) cell line while ruthenium(II) arene complexes on MCF7 (human breast cancer) cell line.

According to the standard assay, the cancer cells (A549 and MCF7) with a cell density of 5.0×10^3 cells $well^{-1}$ were placed in 96-well culture plates (Tarson India Pvt. Ltd.) and grown overnight at 37°C in a 5% CO_2 incubator. Compounds to be tested were then added to the wells to achieve a final concentrations as per the doses fixed (the final dosing was fixed per compound as per the results of subsequent trials). Control wells were prepared by addition of culture medium without the compounds. The plates were incubated at 37°C in a 5% CO_2 incubator for 48 h. Upon completion of incubation, MTT dye solution (prepared using serum free culture medium) was added to each well to a final concentration of 0.5 mg/ml. After 4 h of incubation with MTT, the culture media was discarded and the wells were washed with Phosphate Buffer Saline, followed by addition of DMSO to dissolve the formazan crystals so formed and subsequent incubation for 30 min. The optical density of each well was measured spectrophotometrically at 490 nm using Biotek-ELX universal ELISA reader (Bio-Tek instruments, Inc., Winooski, VT). The IC_{50} values were determined by plotting the percentage viability *versus* concentration (*Fig. 5.15*) and reading off the concentration at which 50% of cells remained viable relative to the control. Each experiment was repeated at least three times to obtain mean values.

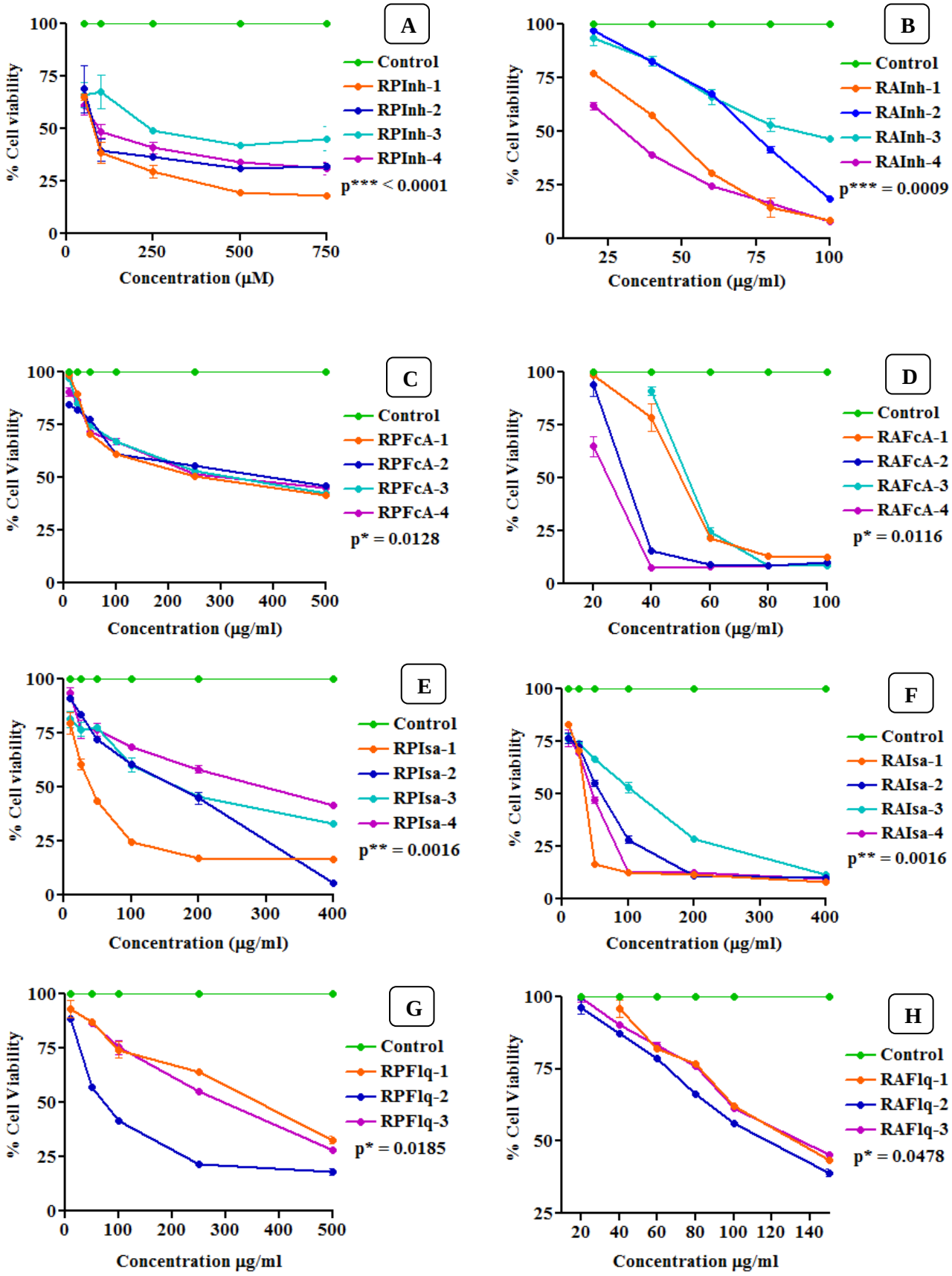
A
% Cell viability
Concentration (µM)
Control
RPInh-1
RPInh-2
RPInh-3
RPInh-4
p*** < 0.0001
B
% Cell viability
Concentration (µg/ml)
Control
RAInh-1
RAInh-2
RAInh-3
RAInh-4
p*** = 0.0009
C
% Cell Viability
Concentration (µg/ml)
Control
RPFcA-1
RPFcA-2
RPFcA-3
RPFcA-4
p* = 0.0128
D
% Cell Viability
Concentration (µg/ml)
Control
RAFcA-1
RAFcA-2
RAFcA-3
RAFcA-4
p* = 0.0116
E
% Cell viability
Concentration (µg/ml)
Control
RPIsa-1
RPIsa-2
RPIsa-3
RPIsa-4
p** = 0.0016
F
% Cell viability
Concentration (µg/ml)
Control
RAIsa-1
RAIsa-2
RAIsa-3
RAIsa-4
p** = 0.0016
G
% Cell Viability
Concentration µg/ml
Control
RPFlq-1
RPFlq-2
RPFlq-3
p* = 0.0185
H
% Cell Viability
Concentration µg/ml
Control
RAFlq-1
RAFlq-2
RAFlq-3
p* = 0.0478

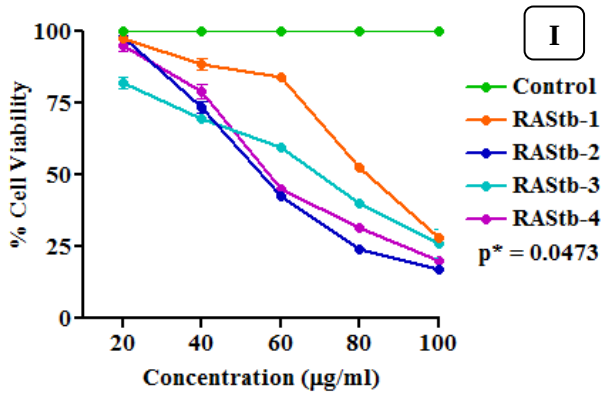

Fig. 5.15: *% Cell viability verses concentration plots of (A)* ***RPInh 1-4*** *(C)* ***RPFcA 1-4*** *(E)* ***RPIsa 1-4*** *(G)* ***RPFlq 1-3*** *on A549 human lung cancer cell lines and (B)* ***RAInh 1-4*** *(D)* ***RAFcA 1-4*** *(F)* ***RAIsa 1-4*** *(H)* ***RAFlq 1-3*** *(I)* ***RAStb 1-4*** *on MCF7 human breast cancer cell lines. Each point is the mean ± standard error obtained from three independent experiments.*

5.4.4 Results and discussion:

In-vitro cytotoxicity tests of ruthenium(II)phenanthroline complexes were performed on the human lung cancer cell line (A549) and those of ruthenium(II)arene complexes were performed on human breast cancer cell line (MCF7). The selection of these two cell lines are purely based on their higher occurrence in human population worldwide which is of prime concern.

The cell viabilities (%) were obtained with continuous exposure of the cells to the said compounds for 48 h. The cytotoxicities of the complexes were found to be dose dependent, that is, the cell viability decreased with increasing concentrations (*Fig. 5.15*). The IC_{50} values of the complexes have been tabulated in *Table 5.13*.

Although the synthesized ruthenium complexes are found to be less active compared to *cis* platin (IC_{50} ~ 15-39 µM), they are much more active on cancer cells as compared to NAMI-A whose IC_{50} values have been found to be in the range of 550-750 µM for various cancer cell lines on treatment for 48 h [74;75] and those of RAPTA-C >1600 µM on treatment for 72 h [76]. The *in-vitro* anticancer activity of the compounds need not be consistent with their DNA/BSA-binding abilities. The different order of biomolecular binding affinity and the *in-vitro* anticancer activity means multiple targets and multiple mechanisms coexisted in the anticancer process of the compounds. DNA/serum albumin binding need not be the only target and mechanism for cytotoxicity. Moreover target mechanisms of the compounds may vary vividly whilst in a cellular environment.

Table 5.13: *IC_{50} values of complexes obtained from MTT assay on A549 and MCF7 cell lines. Values have been expressed in* ***µg/ml*** *and* ***µM*** *concentrations. Reported values of cisplatin and known ruthenium complexes NAMI-A and RAPTA have been provided for reference.*

Compound	***IC_{50} (A549)***		***Compound***	***IC_{50} (MCF7)***	
	(µg/ml)	***(µM)***		***(µg/ml)***	***(µM)***
RPInh-1	61.2	78	**RAInh-1**	45.7	92.4
RPInh-2	65.6	82	**RAInh-2**	73.5	143.8
RPInh-3	198.6	239	**RAInh-3**	88.0	162.6
RPInh-4	76.6	94	**RAInh-4**	29.5	56.2
RPFcA-1	250	266	**RAFcA-1**	49	75.5
RPFcA-2	390	422	**RAFcA-2**	30	47.3
RPFcA-3	300	337	**RAFcA-3**	52	86.6
RPFcA-4	275	286	**RAFcA-4**	25	37.1
RPIsa-1	38.4	46.5	**RAIsa-1**	32.8	61.3
RPIsa-2	166.5	201.5	**RAIsa-2**	58.2	108.5
RPIsa-3	168	219.8	**RAIsa-3**	111.5	235.2
RPIsa-4	182.6	234	**RAIsa-4**	46.5	94.9
RPFlq-1	361	394	**RAFlq-1**	130.5	209
RPFlq-2	66	71.5	**RAFlq-2**	117	185
RPFlq-3	275	308	**RAFlq-3**	134	222
-	-	-	**RAStb-1**	82	168.2
-	-	-	**RAStb-2**	54.7	105.7
-	-	-	**RAStb-3**	70	127.6
-	-	-	**RAStb-4**	56.5	111.7
Cisplatin[75]	-	36	-	-	39.3
NAMI-A[75]	-	-	-	-	750.4
RAPTA-C[76]		1029			>1600

5.5 Cell staining assays to indicate apoptosis:

5.5.1 Introduction to various cell stains and their theory:

Since apoptosis occurs via a complex signaling cascade that is tightly regulated at multiple points, there are many opportunities to evaluate the activity of the proteins involved. As the activators, effectors and regulators of this cascade continue to be elucidated, a large number of apoptosis assays are devised to detect and count apoptotic cells. However, many features of apoptosis and necrosis can overlap, and it is therefore crucial to employ two or more distinct assays to confirm that cell death is occurring via apoptosis. One assay may detect early (initiation) apoptotic events and a different assay may target a later (execution) event. The second assay, used to confirm apoptosis, is generally based on a different principle.

5.5.1.1 Induction of Apoptosis (Evaluation by Fluorescent Double Staining with AO/EB):

DNA-binding dyes AO (Acridine Orange) and EB (Ethidium Bromide) were used for the morphological detection of apoptotic and necrotic cells. AO is taken up by both viable and non-viable cells and intercalates in double stranded DNA emitting green fluorescence whereas, EB is taken up only by non-viable cells and emits red fluorescence. Also, the viable cells with green chromatin will have organized cellular architecture whereas the apoptotic cells (yellow or orange) will have condensed or fragmented chromatin. The necrotic cells have nuclei characteristics similar to a viable cell but will be stained orange to red [77;78]

5.5.1.2 Nuclear condensation (Evaluation by Fluorescent DAPI stain):

It is known that cells undergoing apoptosis display typical features, namely cell shrinkage, membrane blebbing, chromatin condensation and nuclear fragmentation. Dramatic changes occur within the nucleus during apoptotic death. It is commonly thought that the nuclear changes are due to activation of endogenous nuclease(s) which cleaves DNA into oligonucleosomal fragments. This is associated with the appearance of dense, crescent-shaped chromatin aggregates which line nuclear membrane. Later, the nucleolus disintegrates; nuclear membrane develops deep invaginations and, ultimately, the nucleus fragments into dense granular particles (apoptotic bodies). Chromatin condensation, nuclear shrinkage and formation of apoptotic bodies can easily be observed under fluorescence microscopy, after appropriate staining of nuclei with DNA-specific fluorochromes. 4, 6-Diamidino-2-phenylindole (DAPI) is a dye that can be used as a tool to visualise nuclear changes and assess apoptosis. It binds strongly and selectively to the minor groove of adenine-

thymine regions of DNA. When bound to double-stranded DNA, DAPI absorbs light at 340nm (ultraviolet light) and emits at 488nm (fluoresces blue). Bound DAPI has a fluorescence intensity approximately 20 fold higher than that of unbound DAPI. The fluorescence is also directly proportional to the amount of DNA present. This dye is partially cell-permeable. Once it overpasses cell membranes of normal cells, the blue fluorescence can be observed under fluorescence microscopy. As the apoptotic cell membrane is compromised, more DAPI enters the cell and stains a stronger blue colour. In case of normal cells, round nucleus is stained uniformly and its margin is clear. But, in case of apoptotic cells, the margin of nucleus is abnormal and the condensed chromosome is easily stained. Thus apoptotic cells can be evaluated from the strength of fluorescence and the conformation of nucleus by using this stain. The differing nuclear morphology of apoptotic cells such as chromosome condensation and fragmentation also helps in visual identification of apoptotic cells stained with DAPI. [79]

5.5.1.3 ROS Accumulation (Evaluation by Fluorescent DCFH-DA stain):

The two major sources of cellular ROS (Reactive Oxygen Species) are NADH dehydrogenase and superoxide dismutase that are integral parts of the mitochondrial electron transport chain. Though, low levels (or optimum levels) of ROS are important to drive the signaling pathways, excessive ROS production (cellular or external) overwhelms the cellular antioxidant capacity. This causes macromolecular damage (by reacting with DNA, proteins and lipids) and disruption of thiol redox circuits leading to apoptosis or necrosis. It is well-known that apoptosis can be triggered by increased intracellular ROS levels [80], and there is strong evidence that ROS are also involved in the induction of autophagy [81]. The 5-(and-6)-chloromethyl-2′,7′-dichlorodihydrofluorescin diacetate (DCFH-DA) probe was chosen to assess the formation of oxidative stress by-products in cell cultures. Owing to its non-polar and non-ionic structure, DCFH-DA diffuses through the cell membranes. Once it reaches the cytoplasm, DCFH-DA is hydrolysed by intracellular esterases to non-fluorescent DCFH. In the presence of reactive oxygen species, DCFH is oxidised to fluorescent dichlorofluorescein (DCF). The DCFH-DA probe provides a fluorometer-based assay, which allows the evaluation of oxidative product formation [82,83,84].

5.5.1.4 Induction of Mitochondrial Dysfunction (Evaluation by Fluorescent Rh 123 stain):

Mitochondrial dysfunction is involved in both apoptotic and autophagic cell death. Mitochondria play important roles in apoptosis through the release of pro-apoptotic factors such as cytochrome c and apoptosis-inducing factor [85,86]. As a mechanism to maintain genomic integrity in the face of metabolic stress, drug treatment, or radiation, autophagy can selectively remove damaged mitochondria, which are major sites of genotoxic ROS production [87]. Thus, mitochondrial dysfunction was determined by measuring changes in the mitochondrial membrane potential (MMP, $\Delta\Psi m$). The rhodamine 123 (Rh 123) fluorescent probe was used as an indicator of cytotoxicity as well as for evaluating the effects of treatment on mitochondrial membrane potential [88,89]. The cationic fluorescent dye Rh 123 is specific for the localization of mitochondria in living cells [90]. It's cationic functionality have the ability to traverse the mitochondrial lipid membrane by using the negative potential gradient of the organelle as an electrostatic driving force which results in a 100-500 fold increase in accumulation of the dye in the mitochondria of live cells when the mitochondrial lipid membrane is intact [91]. Rh 123 stains mitochondria directly without passage through endocytic vesicles and lysosomes according to the well-established premise that diffusion of this dye is directly proportional to the degree of polarisation of the membrane.

5.5.1.5 Annexin-V FITC/Propidium iodide dual stain (FACS-Flow cytometric analysis):

Apoptosis is characterized by specific morphological features, including loss of plasma membrane asymmetry and attachment, plasma membrane blebbing, condensation of the cytoplasm and nucleus, and internucleosomal cleavage of DNA. Loss of plasma membrane asymmetry is one of the earliest features of apoptosis. In apoptotic cells, the membrane phospholipid phosphatidylserine (PS) is translocated from the inner to the outer leaflet of the plasma membrane, thereby exposing PS to the external cellular environment. Annexin-V is a 35–36 kDa Ca^{2+}-dependent phospholipid-binding protein with high affinity for PS, and binds to exposed apoptotic cell surface PS [92,93,94]. Annexin-V can be conjugated to fluorochromes while retaining its high affinity for PS and thus serves as a sensitive probe for flow cytometric analysis of cells undergoing apoptosis. This process is summarized in *Fig. 5.16.*

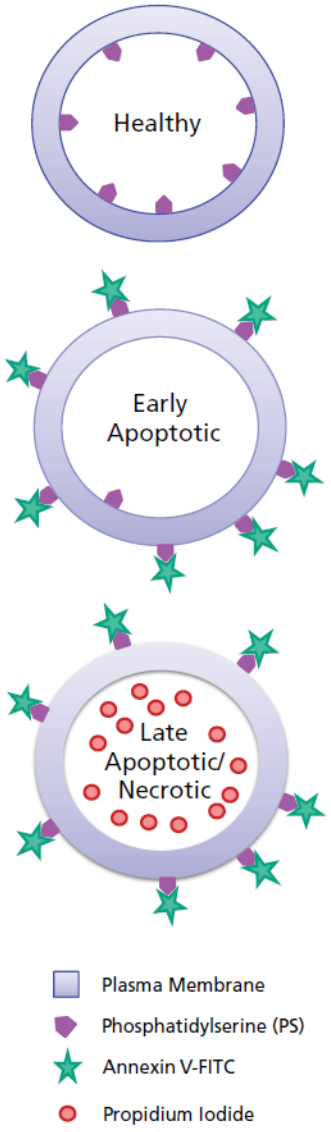

Fig. 5.16: *Diagram showing healthy and apoptotic cells with markers for detection of apoptosis.*

PS translocation precedes the loss of membrane integrity, which accompanies the later stages of cell death resulting from either apoptotic or necrotic processes. Therefore, staining with Annexin-V is typically used in conjunction with a vital dye such as propidium iodide (PI) for identification of early and late apoptotic cells. Viable cells with intact membranes exclude PI, whereas the membranes of dead and damaged cells are permeable to PI. Therefore, cells that are considered viable are both Annexin-V and PI negative, while cells that are in early apoptosis are Annexin-V positive and PI negative, and cells that are in late apoptosis or already dead are both Annexin-V and PI positive. This assay does not distinguish between cells that have undergone apoptotic death versus those that have died as a result of a necrotic pathway because they will also stain with both Annexin-V and PI. However, when apoptosis is measured over time, cells can often be tracked from Annexin-V and PI negative (viable, or no measurable apoptosis), to Annexin-V positive and PI negative (early apoptosis with intact membranes), and finally to Annexin-V and PI positive (end stage apoptosis and death). The presence of cells with these three phenotypes within a mixed cell population, or the "movement" of a synchronized cell population through these three stages, suggests apoptosis. In contrast, a single observation indicating that cells are both Annexin-V and PI positive, in and of itself, reveals less information about the process by which the cells underwent their demise.

5.5.2 Materials and instrumentation:

The cancer cells were cultured and treated with the Ru(II) complexes in Dulbecco's Modified Eagle Medium (DMEM), while Phosphate Buffer Saline (PBS) was used for washing purpose. The stock solutions of compounds (1 mg/ml) were prepared by first dissolving in minimum volume of DMSO (50µl) and then diluting the concentrated DMSO solution with DMEM media to 1 ml. Further dilutions from the stock solution were made using DMEM for subsequent dosing. Both DMEM and PBS were purchased from Hi-Media. All the stains used in this study were purchased from Sigma Aldrich, USA. Dead cell apoptosis kit with Annexin-V FITC and PI, purchased from Invitrogen, California, USA, was used for flow cytometry. 12 well and 96-well culture plates were

purchased from Tarson India Pvt. Ltd. The cell line was procured from National Centre for Cell Science, Pune, India (NCCS).

5.5.3 Experimental:

*5.5.3.1 Ru(II) complexes induced Apoptosis (AO/EB dual staining)***:**

A549 cells were grown in triplicates using a 12 well tissue culture plate and allowed to acclimatize overnight. Next day, cells were treated with the **RPInh 1-4** complexes at a single concentration (IC_{50} value obtained from MTT assay). After 48 hours of incubation, cells were stained with acridine orange (AO) and ethidium bromide (EB) dyes for 5 min in dark and immediately washed with PBS three times. Cells were re-suspended in PBS, observed and photographed on Floid cell imaging station (Life Technologies, USA) [95].

5.5.3.2 Nuclear condensation (DAPI stain):

A549 cells were grown in 96 well tissue culture plate and were treated and incubated with a single concentration (IC_{50} value obtained from MTT assay) of **RPInh 1-4** for 48 hours in CO_2 incubator at 37 ºC with 5 % CO_2. Next day, cells were washed with PBS twice for 10 min at room temperature. Cells were then stained with DAPI (0.6 μg/ml in PBS), incubated for 5 min, and washed three times with PBS for 5 min to remove unbound and excess stain. Chromatin fluorescence was observed and photographed on Floid cell imaging station (Life Technologies, USA) [96].

5.5.3.3 Intracellular oxidative stress (DCFH-DA stain):

To investigate the effect of the complexes on ROS (Reactive Oxygen Species) production in A549 cells, DCFH-DA was used as a probe for the presence of hydroxyl radical. Well grown A549 cells in tissue culture 96 well plate were incubated in presence of a single concentration (IC_{50} value obtained from MTT assay) of **RPInh 1-4** in a CO_2 incubator at 37 ºC with 5 % CO_2. After the removal of media from wells, cells were incubated with 2.5 μM/ml of DCFH-DA for 10 minutes. The cells were then thoroughly washed 3 times with PBS and photographed on Floid cell imaging station (Life Technologies, USA) [97].

5.5.3.4 Mitochondrial dysfunction (Rh 123 stain):

To explore the effect of complexes on the mitochondrial membrane potential ($\Delta\Psi m$), the lipophilic cationic probe Rhodamine 123 was used. Rh 123 exhibits potential-dependent accumulation in mitochondria, as indicated by the fluorescence

excitation at 505 nm and emission at 525 nm. After the treatment and incubation with a single concentration (IC_{50} value obtained from MTT assay) of **RPInh 1-4** for 48 hours in a CO_2 incubator at 37 ºC with 5 % CO_2, cells were rinsed with serum free medium, followed by the addition of Rh 123. The cells were again incubated with the dye at 37 °C for 20 min, washed with cold PBS and photographed using fluorescence microscope. The cells were then lysed using 0.5% triton X-100 and centrifuged at 2500 rpm, supernatant was collected and read using a spectrofluorimeter (Jasco FP-6300) [98].

5.5.3.5 Annexin V- PI dual staining (Facs):

Annexin-V FITC/PI dual staining assay was used to quantify apotosis, according to the manufacturer's protocol (Invitrogen, California, USA). A549 and MCF7 cells were incubated in presence of ruthenium(II) phenanthroline complexes and ruthenium(II) arene complexes respectively at their IC_{50} values for 48 hours. The cells from each well were then centrifuged, washed with PBS and suspended in 100 µl buffer. 5 µl of Annexin-V FITC conjugate and 10 µl of propidium iodide solution were added to each cell suspension and incubated for 10 min at room temperature in hte dark. The samples were analyzed on flow cytometer (MoFlo^{TM} Cytomation, Modular Flow Cytometer) using Cell quest software.

5.5.4 Results and discussion:

5.5.4.1 Induction of apoptosis (AO/EB dual stain):

The confocal images of A549 cells treated with **RPFcA 1-4** show that the live cells are stained with AO and hence emit green fluorescence (*Fig. 5.17 A*) whereas the cells treated with **RPFcA 1-4** bore yellow-orange nucleus indicating early apoptosis (*Fig. 5.17 B*). Moreover distinct nuclear fragmentation can also be seen within the treated cells, appearance of blebs and the presence of apoptotic bodies makes it evident that the mode of cell death is apoptosis.

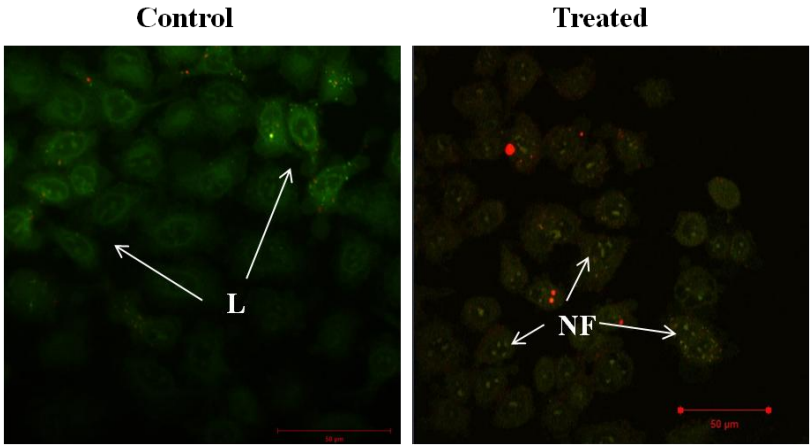

Fig. 5.17: *Confocal images of A549 cells treated with (250µg/ml)* ***RPFcA-1*** *for 16 h followed by dual staining with AO/EB. Here "**L**" stands for Live cells and "**NF**" stands for Nuclear Fragmentation. Also in the treated cells, cell blebbing is distinctly visible which is a characteristic of apoptosis.*

In another case, A549 cells treated with **RPInh 1-4** showed a large population of cells that were orange in colour (*Fig. 5.18 B*) as compared to the control cells that showed a prominent green colour (*Fig. 5.18 A*). Also, majority of the treated cells appeared to be rounded and shrunken. These characteristics indicate that the treatment was able to induce apoptotic death of A549 cells.

5.5.4.2 Nuclear condensation (DAPI stain):

The morphological assessment of nuclei using a nucleophilic dye DAPI was performed in untreated and **RPInh 1-4** treated A549 cells. The treated cells show increased blue fluorescence due to higher penetration of DAPI into the nucleus. These observations reveal that a large population of the treated cells show nuclear condensation and associated nuclear anomalies (*Fig. 5.18 D*) [99]. These observations provide further evidence on nuclear dysfunction induced by the Ru(II) complexes in A549 cells.

5.5.4.3 ROS accumulation (DCFH-DA stain):

In the present study, the control cells showed mild fluorescence but the A549 cells treated with **RPInh 1-4** showed a prominent fluorescence indicating excessive ROS generation (*Fig. 5.18 F*). This is because the schiff base derivative of INH produces carbon, nitrogen or oxygen centred free radicals on interaction with catalase-peroxidases in the cell, thus resulting in prominent fluorescence in the treated cells [100].

5.5.4.4 Mitochondrial dysfunction (Rh 123 stain):

The treated A549 cells showed prominent decrement in mitochondrial membrane potential (*Fig. 5.18 H inset*) indicated by very less accumulation of the dye, compared to control cells (*Fig. 5.18 G inset*). These facts indicate at a possible role of the Ru(II) complexes in inducing mitochondrial dysfunction leading to apoptosis.

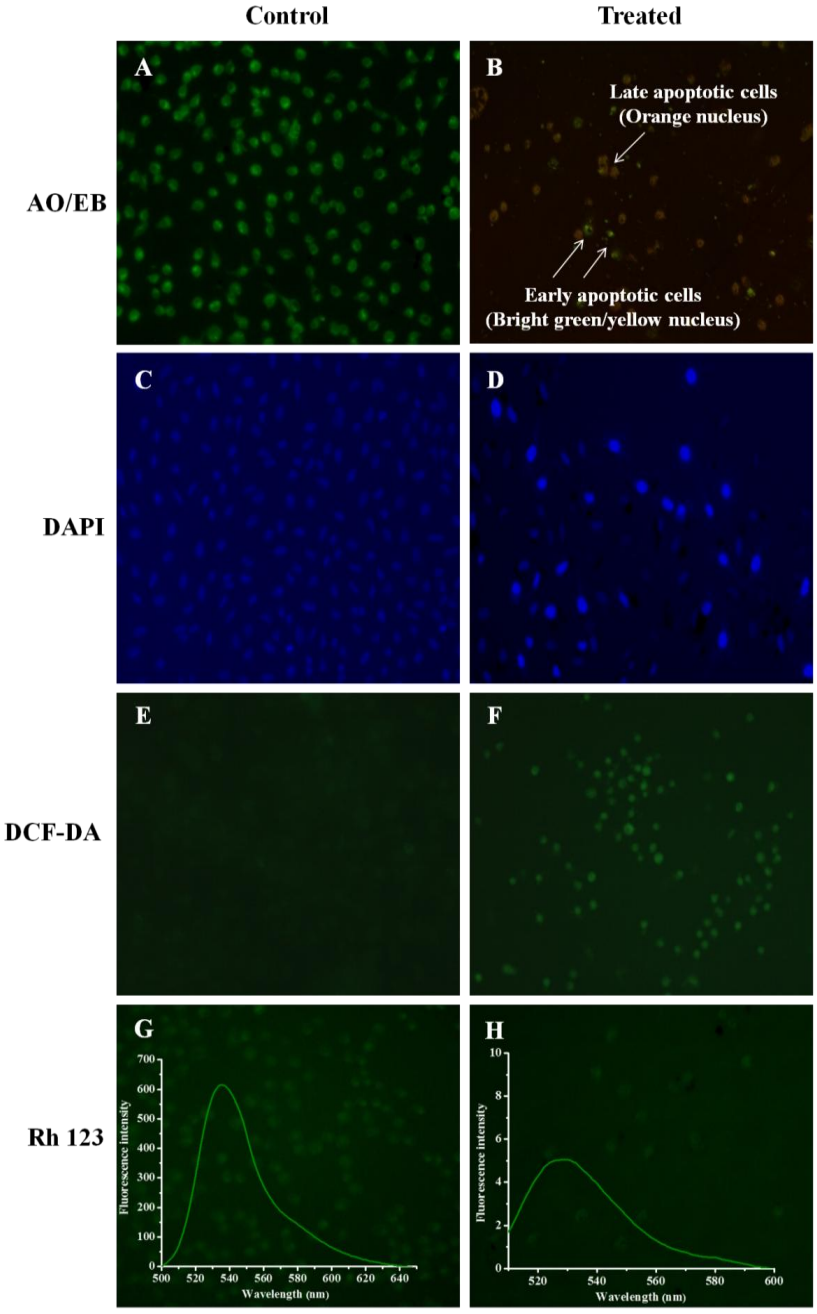

Fig. 5.18: *Images of A549 cells observed under fluorescence microscope:* ***(A)*** *control cells and* ***(B)*** *treated cells stained with AO/EB****;*** ***(C)*** *control cells and* ***(D)*** *treated cells stained with DAPI;* ***(E)*** *control cells and* ***(F)*** *treated cells stained with DCF-DA;* ***(G)*** *control and* ***(H)*** *treated A549 cells stained with Rh 123 after incubation at 37 °C and 5 % CO_2 for 48 h with 100µM* ***RPInh-1****.* ***Insets:*** *Fluorescence emission plot of Rh 123 in* ***(G)*** *control and* ***(H)*** *treated A549 cells after incubation at 37 °C and 5 % CO_2 for 48 h with 100µM* ***RPInh-1*** *excited at a wavelength of 511 nm.*

5.5.4.5 Annexin V- PI dual staining (Flow cytometry):

An apoptosis study using flow cytometer was carried out to distinguish different cell types such as viable cells, early apoptotic / pro apoptotic cells, and late apoptotic cells. The measurement of annexin V-propidium iodide dual stain as an indicator for apoptosis has been performed along with a dye exclusion test to establish the integrity of the cell membrane. Annexin V, a calcium-dependent phospholipid binding protein with high affinity for phosphatidylserine, binds to the phosphatidylserine that has migrated outside the cell membrane on the onset of apoptosis whereas propidium iodide (PI), a viability stain which binds to the nucleus once the membrane has broken down, is used as an indicator of membrane structural integrity. A549 cells were incubated with the synthesized ruthenium(II) phenanthroline complexes (representative complex of each series showing the best cytotoxicity in MTT assay) for 48 h at IC_{50}, similarly MCF7 cells were incubated with the synthesized ruthenium(II) arene complexes, followed by staining with annexin V and PI. Data was collected by a flow cytometer. The results are shown in *Fig. 5.19 (A)* and *(B)* respectively for A549 and MCF7 cell lines. It can be seen that viable cells did not bind to annexin V or PI (lower-left quadrant), early apoptotic cells are bound to annexin V but excluded PI (lower-right quadrant), and late apoptotic cells were positive for both annexin V and PI (upper-right quadrant). The upper-left quadrant contains dead cells. The results indicate that the control cells contain 3.3 % apoptotic A549 cells (upper-right quadrant) and 2.7 % apoptotic MCF7 cells. Among the ruthenium phenanthroline complexes, **RPFcA-1** showed the highest percentage of A549 apoptotic cells (40.8%). In case of ruthenium arene complexes **RAInh-4** showed the highest number of MCF7 apoptotic cells (20.9 %). These results indicate that the mixed ligand ruthenium(II) complexes synthesized and studied are capable of inducing apoptosis of A549 and MCF7 cells.

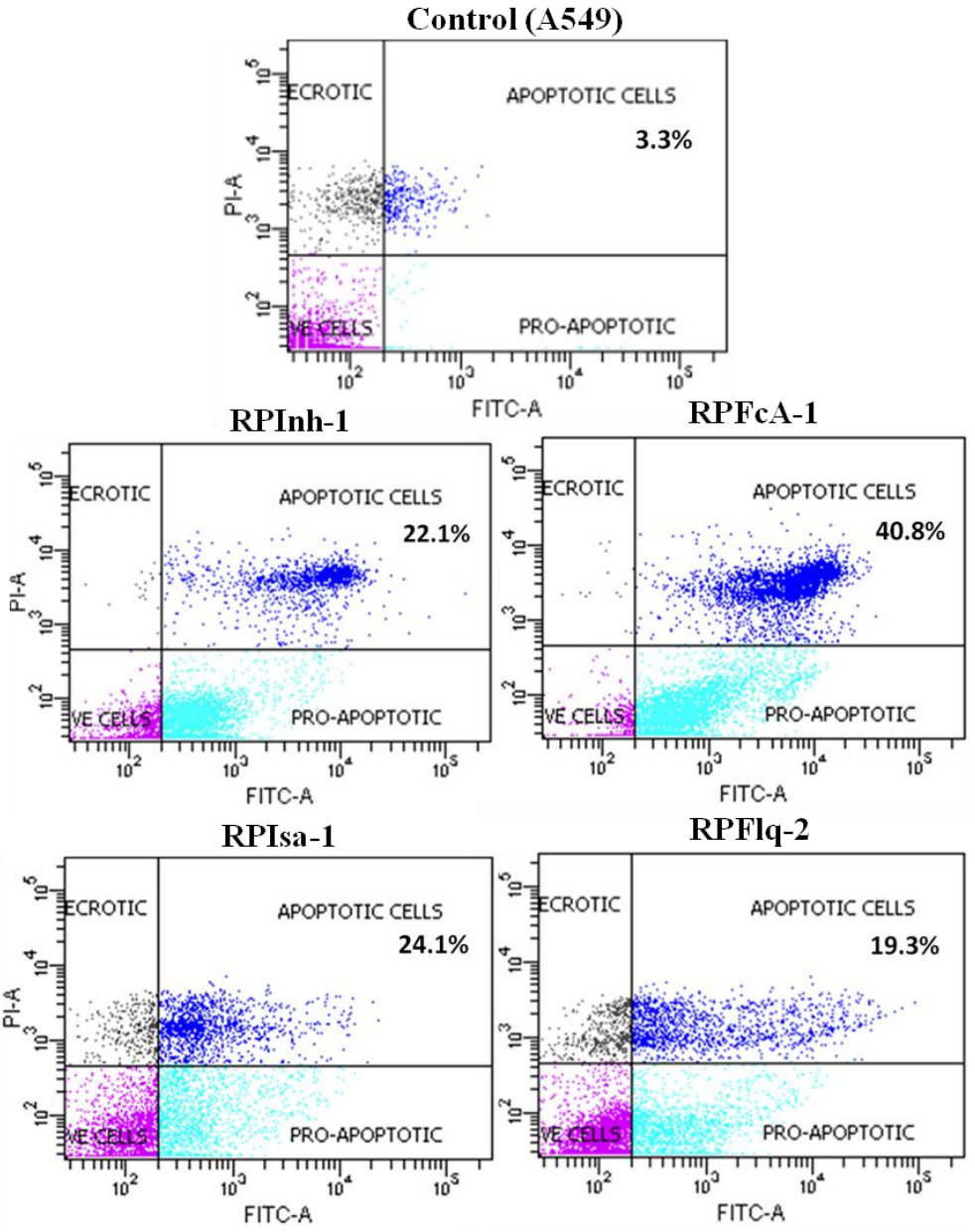

Fig. 5.19 (A): *Annexin V staining shows induction of apoptosis of A549 cells treated with* ***[Ru(phen)$_2$L]ClO$_4$*** *complexes. The percent of apoptotic cells were detected by analysing Annexin V and PI binding with the help of flow cytometry. Viable cells did not bind to Annexin V or PI (lower left quadrant), early apoptotic cells bound to Annexin V but excluded PI (lower right quadrant), and late apoptotic cells were both annexin V- and PI-positive (upper right quadrant), the upper left quadrant contains the dead cells.*

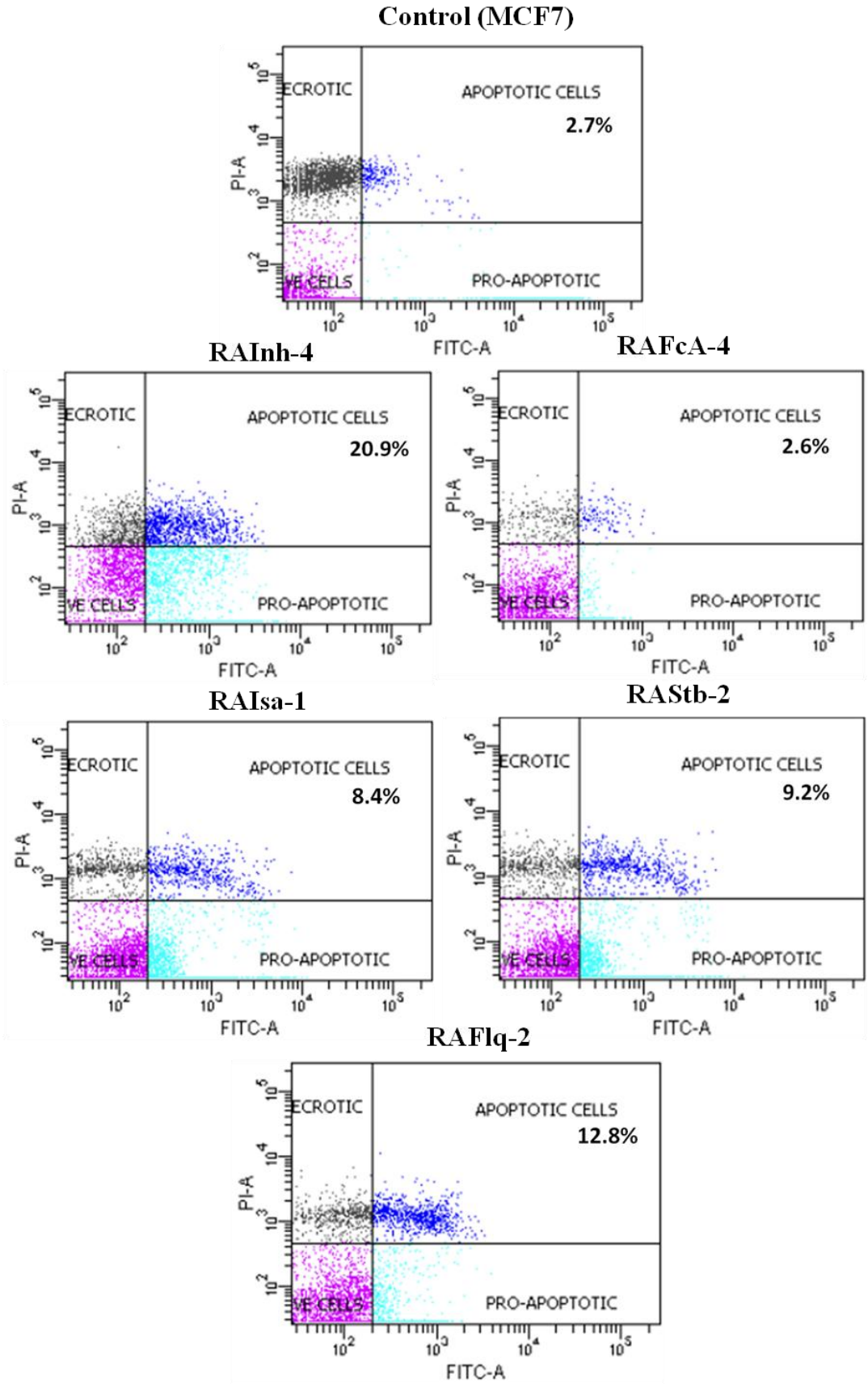

Fig. 5.19 (B): *Annexin V staining shows induction of apoptosis of MCF7 cells treated with* ***[Ru(p-cym)(L)Cl]*** *complexes. The percent of apoptotic cells were detected by analysing Annexin V and PI binding with the help of flow cytometry. Viable cells did not bind to Annexin V or PI (lower left quadrant), early apoptotic cells bound to Annexin V but excluded PI (lower right quadrant), and late apoptotic cells were both annexin V- and PI-positive (upper right quadrant), the upper left quadrant contains the dead cells.*

5.6 Gene expression studies:

5.6.1 Gene targeted investigation towards apoptosis:

❖ **The core apoptotic machinery:**

Apoptotic cell death is triggered by intracellular cues such as DNA damage and osmotic stress, and extracellular cues including growth factor withdrawal, matrix detachment, and direct cytokine-mediated killing. Two central pathways are involved in the process of apoptotic cell death, one involving the activation of the caspase proteases (Extrinsic pathway) and a second, mitochondrial, pathway (Intrinsic pathway) (*Fig. 5.20*). A common feature of this machinery and of the signaling pathways that impinge on this machinery is that at nearly every level, the action of pro-apoptotic molecules is opposed by sets of inhibitors [101].

❖ **The mitochondrial (Intrinsic) pathway : Bcl-2 gene family**

Mitochondrial pathway to apoptosis is the likely province of the Bcl-2 family of proteins. The anti-apoptotic protein Bcl-2, originally cloned as an oncogene from the t(14:18) breakpoint found in low-grade lymphomas, is the founding member of a large family that consists of pro-apoptotic factors such as Bax, Bak, Bcl-XS, and Bad, and anti-apoptotic factors such as Bcl-2, Bcl-XL, and Bcl-W. In response to apoptotic signals, pro-apoptotic Bcl-2 family members translocate to and alter the permeability of the mitochondrial membrane. These proteins are thought to either form channels in the outer mitochondrial membrane or to alter the activity of existing channels, leading to changes in the mitochondrial membrane potential, cytochrome *c* release, and the production of reactive oxygen species. Anti-apoptotic members of the Bcl-2 family (such as Bcl-2 itself) reside in the outer mitochondrial membrane and counter these effects. Certain of the pro-apoptotic family members, including Bcl-XS, Bid, and Bad, may act by binding and antagonizing the anti-apoptotic members of the family, rather than by any direct effects on mitochondrial permeability.

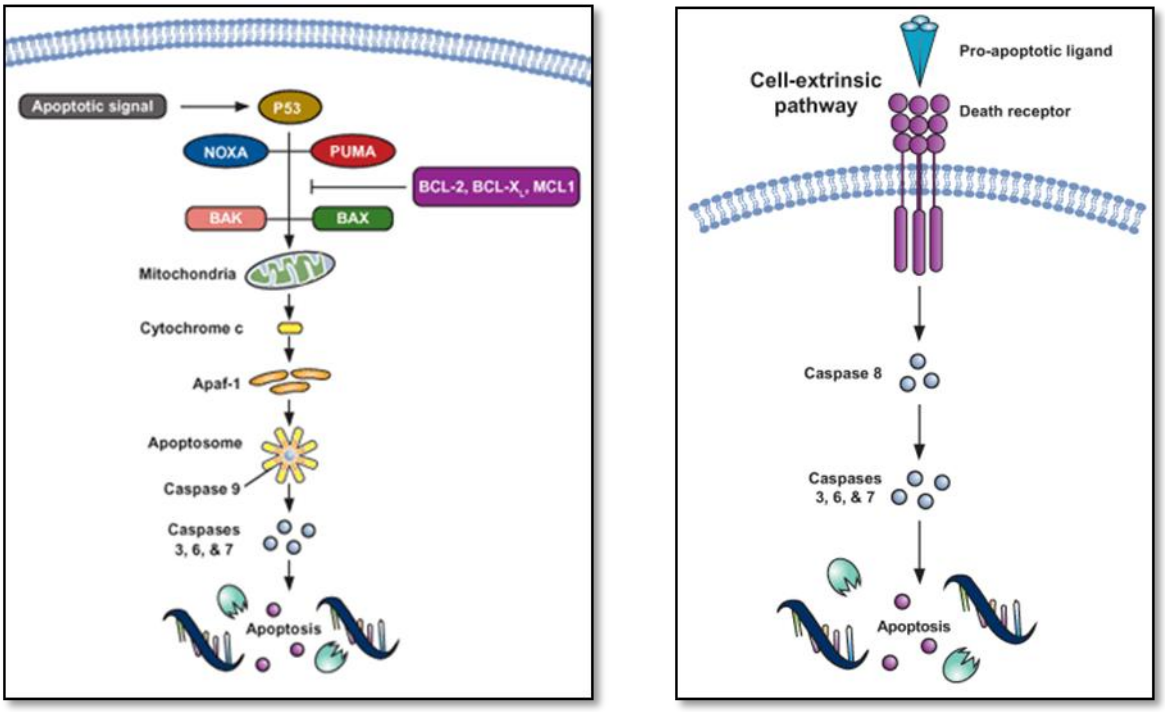

Intrinsic pathway (mitochondrial pathway) ***Extrinsic pathway (Caspase cascade)***

Fig. 5.20: *The schematic diagram of the intrinsic and extrinsic pathways in apoptotic mechanism.*

Here more light has been thrown on the mitochondrial pathway; however the mitochondrial and caspase apoptotic pathways are intimately connected. For example, caspase 8 cleaves the Bcl-2 family member known as Bid to produce truncated Bid (tBid). In turn, tBid, in cooperation with Bad, can induce cytochrome *c* release, causing the caspase adaptor Apaf-1 to activate caspases 9 and 3. This interconnection leads to signal amplification involving a caspase-

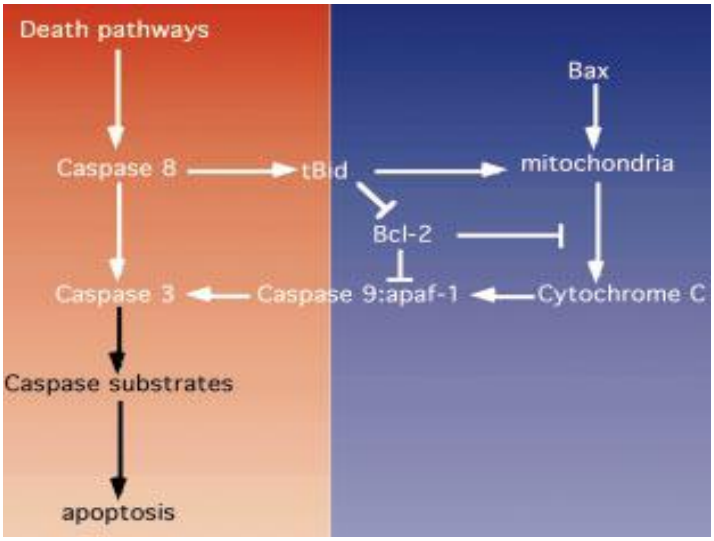

Fig. 5.21: *The core apoptotic machinery. The core apoptotic machinery comprises the caspases, members of the Bcl-2 family, and Apaf-1. Caspase 3 and other effector caspases carry out the process of cellular destruction that accompanies apoptotic signals. Effector caspases are cleaved and activated by initiator caspases, such as caspases 8 and 9. Caspase 8 is a target of activation by death signaling pathways. Bcl-2 family members regulate both mitochondrial damage and caspase activation. Certain anti-apoptotic proteins can directly inhibit caspase 9 activation by Apaf-1, and in turn are antagonized by pro-apoptotic Bcl-2 family members such as tBid. The cleavage of Bid to tBid by caspase 8 and the inhibition of caspase 9 by Bcl-2 family members are examples of interconnections between the caspase pathway and the mitochondrial pathway of apoptosis.*

mitochondrial loop (*Fig. 5.21*). In addition, Bcl-XL binds and inactivates Apaf-1, whereas pro-apoptotic members can displace Bcl-XL from Apaf-1, allowing Apaf-1 to activate caspase 9. Thus, these Bcl-2 family members can directly influence the caspase pathway [102].

❖ **Apoptosis Defect and Cancer:**

Defects in programmed cell death (apoptosis) mechanisms play important roles in tumor pathogenesis, allowing neoplastic cells to survive over intended life spans, subverting the need for exogenous survival factors and providing protection from oxidative stress and hypoxia as the tumor mass expands. That gives time for accumulation of genetic alterations that deregulate cell proliferation, interfere with differentiation, promote angiogenesis, and increase invasiveness during tumor progression [103]. Apoptosis defects are now considered an important complement of proto-oncogene activation, as many deregulated oncoproteins that drive cell division also trigger apoptosis (e.g., Myc, E1a, and Cyclin-D1) [104]. On the other hand, the noncancerous cells have a DNA repair machinery. Defects in DNA repair and/or chromosome segregation normally trigger cell suicide as a defense mechanism for eradicating genetically unstable cells and thus such suicide mechanism's defects permit survival of genetically unstable cells, providing opportunities for selection of progressively aggressive clones and may promote tumorigenesis [105].

There are varieties of molecular mechanisms that tumor cells use to suppress apoptosis. Tumor cells can acquire resistance to apoptosis by the expression of anti-apoptotic proteins such as Bcl-2 or by the down-regulation or mutation of pro-apoptotic proteins such as BAX. Since the expression of both Bcl-2 and BAX is regulated by the p53 tumor suppressor gene [106], some forms of human B-cell lymphoma have Bcl-2 over expression. That example represents the first and strongest lines of evidence that failure of cell death contributes to cancer [107].

Cancer-associated defects in apoptosis play a role in treatment resistance with conventional therapies like chemotherapy and radiotherapy, increasing the threshold for cell death and thereby requiring higher doses for tumor killing agents [108]. Thus, deregulated or defective apoptosis regulation is a fundamental aspect of the tumor biology. Successful eradication of cancer cells by nonsurgical means is ultimately approached via induction of apoptosis. Therefore, all the cancer drug designers try either to activate the inactivated apoptotic mechanism or rectify a defective one. Hence, all cytotoxic anticancer therapies currently in clinical use, when they work, induce apoptosis of malignant cells. Hence, deeper understanding of the molecular mechanisms of apoptosis and its defective status opens the gate for a new class of targeted therapeutics.

❖ **Drug targets in the core apoptotic machinery:**

A number of genes that encode components of the apoptotic machinery are directly targeted by activating or inactivating genetic lesions in cancer. These genetic changes, which may inform future drug development programs, presumably highlight proteins or pathways upon which the tumor is critically dependent. Several of the genes have been identified only recently, so the frequency and extent of lesions at these loci are not well known. However, Bcl-2, which was originally cloned by its association with a chromosomal translocation common among follicular B-cell lymphomas, is over expressed in a number of malignancies.

5.6.2 Materials, instrumentation and experimental:

Expression of apoptosis related genes, Bax (pro-apoptotic) and Bcl-2 (anti-apoptotic) were studied using Real Time PCR (RT-PCR) wherein GAPDH was used as a control. The studies were carried out on A549 and MCF7 cell lines. The IC_{50} values from MTT assay was taken as dosage for the treatment. Total RNA was isolated using TRIzol reagent (Invitrogen, California, USA). cDNA was synthesized by reverse transcription of 1 μg of total RNA using iScript cDNA Synthesis kit (BIORAD, California, USA). PCR was carried out using SYBR Green Master Mix kit (Invitrogen, California, USA) according to manufacturer's instruction. Cycler conditions were as follows: Initial denaturation at 95°C for 3 min further it was followed by 35 reaction cycles (30 sec at 94°C, 30 sec at 55°C and 30 sec at 72°C) and final cycle at 72°C for 10 min. Statistical analysis was done by using One way ANOVA. Primers used for this study are listed in *Table 5.14*.

Table 5.14: *Primers used for gene expression study*

List of genes	*Details*	*Length of amplicon*
GAPDH	Accession number (NM_002046) Forward primer (Template: 113-132) 5′-GCTCTCTGCTCCTCCTGTTC-3′ Reverse primer (Template: 366-385) 5′-CAGTTCCGACTCTTGCCCT -3′	273bp
Bcl-2	Accession number (NM_000633) Forward primer (Template: 959-978) 5′-GTCATGTGTGTGGAGAGCGT-3′ Reverse primer (Template: 1083-1102) 5′-GGAAACACCTTGACATGCCG -3′	144bp
BAX	Accession number (NM_001291428) Forward primer (Template: 138-157) 5′-GGCCCTTTTGCTTCAGGGTT -3′ Reverse primer (Template: 341-360) 5′-AGAAAAAGGCTCACCGTCGA-3′	223bp

5.6.3 Results and discussion:

Expression levels of pro-apoptotic (Bax) and anti-apoptotic (Bcl-2) genes were assessed on A549 (Human Lung Carcinoma) and MCF7 (Human breast carcinoma) by a 48 h exposure of ruthenium(II)phenanthroline and ruthenium(II)arene complexes respectively to the cancer cells. One complex of each series with the lowest IC_{50} value has been selected for the gene expression studies. Results (*Fig. 5.22*) revealed that in both the cases expression of Bax notably increased after treatment with the complexes suggesting that they possibly have capacity to trigger apoptotic pathway and cause death of cancer cells. Alternatively expression levels of Bcl-2 in both the cancer cells treated with the respective complexes were significantly low further suggesting higher vulnerability for trigger of apoptosis. These results provide valuable evidence on the role of Ru(II) complexes in triggering apoptosis in cancer cells and indicate towards the merits of Ru(II) metal complexes as potent anticancer agents.

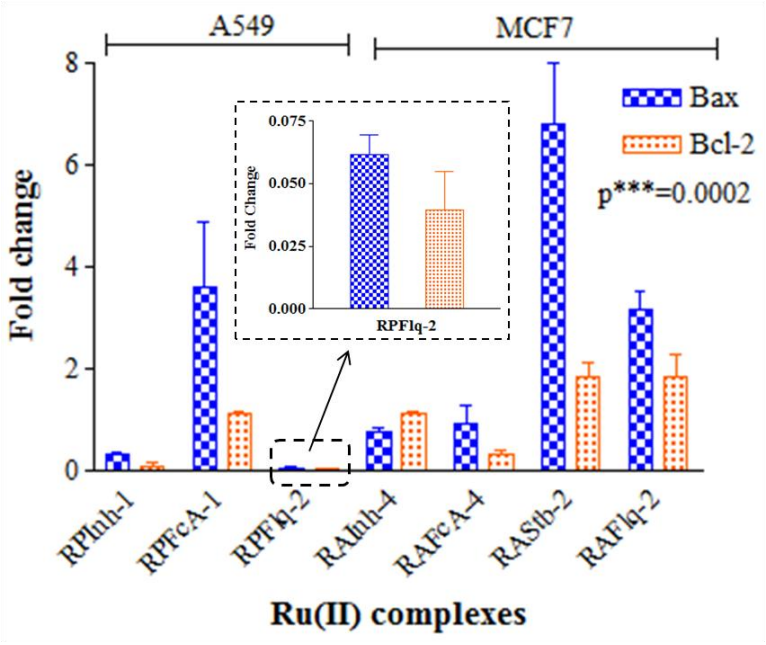

Fig. 5.22: *Expression levels of pro-apoptotic gene (Bax) and anti-apoptotic gene (Bcl-2) were studied using quantitative real time PCR. The CT values were determined and transformed into fold change in expression. Statistical analysis was done using One way Anova, for n=2, p<0.0002***.*

5.7 Summary:

All the compounds synthesized and presented in this thesis have been stepwise evaluated for their bioactivity. First the compounds have been checked for their interactions with DNA and serum albumin which are the most commonly sought after biomolecular targets for anticancer activity. The results so obtained prompted to go for *in cellulo* studies. MTT assay gave an idea regarding the general cytotoxicity of the test compounds. This was followed by various facs analysis and various staining techniques which confirmed that the mode of cell death was apoptosis. Of the various mechanisms taking place during apoptosis, we studied the apoptotic gene expression in presence of the compounds and it was found that the test compounds led to enhancement of Bax (pro-apoptotic gene) as compared to Bcl2 (anti-apoptotic gene) leading to increased apoptosis in the treated cells.

5.8 References:

[1] Ten statistical highlights in global public health. World Health Statistics 2007. Geneva: World Health Organization, **2007**.

[2] Robert Koch Institute, *Federal Health Reporting, Cancer in Germany 2003-2004*, **2008**, 6th eds., p. 18.

[3] Schwartsmann, G.; Winograd, B.; Pinedo H. M. *Radiother. Oncol.*, **1988**, *12*, 301.

[4] Narang, A. S.; Desai, S. D.; Lu, Y.; Mahato, R. I. (eds.), *Pharmaceutical Perspectives of Cancer Therapeutics*, **2009**, 49.

[5] Institute, National Cancer. Targeted Cancer Therapies, **2008**. http://www.cancer.gov/cancertopics/factsheet/Therapy/targeted.

[6] Rosenberg, B.; Vancamp, L.; Trosko, J. E.; Mansour, V. H. *Nature*, **1969**, *222*, 385.

[7] Jakupec, M. A.; Galanski, M.; Arion, V. B.; Hartinger, C. G.; Keppler, B. K. *Dalton Trans.* **2008**, *2*, 183.

[8] Dyson, P. J.; Sava, G. *Dalton Trans.*, **2006**, 1929.

[9] Wang, D.; Lippard, S. J. *Nat. Rev. Drug Discovery*, **2005**, *4*, 307.

[10] Lippert, B. *Verlag Helvetica Chimica Acta*: Zurich, Switzerland, **1999**.

[11] Pineto, H. M.; Schornagel, J. H. (Eds.), *Platinum and Other Metal Coordination Compounds in Cancer Chemotherapy*, Plenum, New York, **1996**.

[12] Buolamwini, J. K. *Curr. Opin. Chem. Biol.*, **1999**, *3*, 500.

[13] Lockshin, R. A.; Williams, C.M. *J. Insect Physiol.*, **1965,** *11*(2), 123.

[14] Cotter, T. G. *Nat. Rev. Cancer*, **2009**, *9*(7), 501.

[15] Kerr, J. F.; Wyllie, A. H.; Currie, A. R. *Br. J. Cancer*, **1972**, *26*(4), 239.

[16] Fischer, U.; Klaus, S. O. *Pharmacol. Rev.* **2005**, *57*, 187.

[17] Neidle, S. *Nucleic Acid Structure and Recognition*, Oxford University Press, Oxford, UK, **2002**.

[18] Kastan, M. B.; Bartek, J. *Nature*, **2004**, *432*, 316.

[19] Clarke, M. J.; Zhu, F.; Frasca, D. R. *Chem. Rev.*, **1999**, *99*, 2511.

[20] Zhang, C. X.; Lippard, S. J. *Curr. Opin. Chem. Biol*., **2003**, *7*, 481.

[21] Bruijnincx, P. C. A.; Sadler, P. J. *Curr. Opin. Chem. Biol*., **2008**, *12*, 197.

[22] Metcalfe, C.; Thomas, J. A. *Chem. Soc. Rev*., **2003**, *32*, 215.

[23] Paul, A.; Bhattacharya, S. *Curr. Sci*., **2012**, *102*(2), 25 January.

[24] Foley, F. M.; Keene, F. R.; Collins, J. G. *J. Chem. Soc., Dalton Trans.*, **2001**, 2968.

[25] Marmur, J. *J. Mol. Biol*., **1961**, *3*, 208.

[26] Reichmann, M.F.; Rice, S.A.; Thomas, C.A.; Doty, P. *J. Am. Chem. Soc*., **1954**, *76*, 3047.

[27] Son, G.; Yeo, J.; Kim, M.; Kim, S.; Holmen, A.; Akerman, B.; Norden, B. *J. Amer. Chem. Soc.*, **1998**, *120*, 6451.

[28] Xiao, Y.N.; Zhan, C.X. *J. Appl. Polym. Sci*., **2002**, *84*, 887.

[29] Sohrabi, N. *J. Pharm. Sci. & Res.*, **2015**, *7*(8), 533.

[30] Tabassum, S.; Asbahy, W. M.; Afzal, M.; Arjmand, F. *J. of Luminescence*, **2012**, *132*, 3058.

[31] Pyle, A. M.; Rehmann, J. P.; Meshoyrer, R.; Kumar, C. V.; Turro, N. J.; Barton, J. K. *J. Am. Chem. Soc.*, **1989**, *111*, 3051.

[32] Dimitrakopoulou, A.; Dendrinou-Samara, C.; Pantazaki, A. A.; Alexiou, M.; Nordlander, E.; Kessissoglou, D. P. *J. Inorg. Biochem*., **2008**, *102*, 618.

[33] Zhao, G.; Lin, H.; Zhu, S.; Sun, H., Chen, Y. *J. Inorg. Biochem.*, **1998**, *70*, 219.

[34] Dhar, S.; Nethaji, M.; Chakravarty, A. R. *J. Inorg. Biochem*., **2005**, *99*, 805.

[35] Baguley, B. C.; Falkenhaug, E. M. *Nucleic Acids Res.*, **1978**, *5*, 161.

[36] Boger, D.L.; Fink, B. E.; Brunette, S. R.; Tse, W. C.; Hedrick, M. P. *J. Am. Chem. Soc.*, **2001**, *123*, 5878.

[37] Pasternack, R. F.; Cacca, M.; Keogh, B.; Stephenson, T. A.; Williams, A. P.; Gibbs, F. J. *J. Am. Chem. Soc.*, **1991**, *113*, 6835.

[38] Lakowicz, J. R.; Weber, G. *Biochemistry*, **1973**, *12*, 4161.

[39] Satyanarayana, S.; Dabrowiak, J. C.; Chaires, J. B. *Biochemistry*, **1993**, *32*, 2573.

[40] Suh, D.; Chaires, J. B. *Bioorg. Med. Chem.*, **1995**, *3*, 723.

[41] Kelly, J. M.; Tossi, A. B.; McConnell, D. J. *Nucleic Acids Res.*, **1985**, *13*, 6017.

[42] Patel, M. N.; Patel, C. R.; Joshi, H. N.; Thakor, K. P. *Spectrochim. Acta Part A*, **2014**, *127*, 261.

[43] Rahimnejad, M.; Jahanshahi, M.; Najafpour, G. D. *Afr. J. Biotechnol*., **2006**, *5*(20), 1918.

[44] Lee, S. K. et al. *Arch. Pharm.Res.* **2003**, *26*, 253.

[45] Dongmei, Z.; Xiuhua, Z.; Yuangang, Z.; Jialei, L.; Yu, Z.; Ru, J.; Zhonghua, Z. *Int. J. Nanomed.*, **2010**, *5*, 669.

[46] He, X. M.; Carter, D. C. *Nature*, **1992**, *358*, 209.

[47] Peters, T. *All About Albumin: Biochemistry, Genetics and Medical Applications.* San Diego, CA: Academic Press Limited; **1996**.

[48] Sudlow, G.; Birkett, D. J.; Wade, D. N. *Mol. Pharmacol.*, **1976**, *12*, 1052.

[49] Kragh-Hansen, U. *Pharmacol. Rev.* **1981**, *33*, 17.

[50] Evans, T. W. *Aliment. Pharmacol. Ther.*, **2002**, *16*(Suppl.5), 6.

[51] Carmeliet, P.; Jain, R. K. *Nature*, **2000**, *407*, 249.

[52] Maeda, H.; Wu, J.; Sawa, T.; Matsumura, Y.; Hori, K. *J. Controlled Release,* **2000**, *65*, 271.

[53] Greish, K . *J. Drug Target.*, **2007**, *15*, 457.

[54] Angelica, M. M.; Danuta, S. K.; Des, R. R. *Frontiers in Physiology, Integrative Physiology,* **2014**, *5*(Article 299), 1.

[55] Kratz, F. *J. Controlled Release,* **2008**, *132*, 171.

[56] Kratz, F. *Int. J. Clin. Pharmacol. Ther.* **2010**, *48*, 453.

[57] Green, M. R.; Manikhas, G. M.; Orlov, S.; Afanasyev, B.; Makhson, A. M. Abraxane®, *Ann Oncol*., **2006**, *17*(8), 1263.

[58] Miele, E.; Spinelli, G. P.; Miele, E.; Tomao, F.; Tomao, S. *Int J Nanomedicine*., **2009**, *4*, 99.

[59] Lancon, A.; Delmas, D.; Osman, H.; Thenot, J. P.; Jannin, B.; Latruffe, N. *Biochem. Biophys. Res. Comm.,* **2004**, *316*, 1132.

[60] Vuignier, K.; Schappler, J.; Veuthey, J. L.; Carrupt, P. A.; Martel, S. *Anal. Bioanal. Chem.*, **2010**, *398*, 53.

[61] Merlot, A. M.; Kalinowski, D. S.; Richardson, D. R. *Antioxid. Redox Signal.* **2013 a**, *18*, 973.

[62] Merlot, A. M.; Pantarat, N.; Menezes, S. V.; Sahni, S.; Richardson, D. R.; Kalinowski, D. S. *Mol. Pharmacol.*, **2013 b**, *84*, 911.

[63] Merlot, A. M.; Richardson, D. R. *Vitam. Miner.*, **2014**, *3*, 125.

[64] Temming, K.; Meyer, D. L.; Zabinski, R. et al. *Bioconjug Chem*., **2006**, *17*(6), 1385.

[65] Temming, K.; Meyer, D. L.; Zabinski, R. et al. *Mol Pharm*., **2007**, *4*(5), 686.

[66] Lakowicz, J. R. *Principles of Fluorescence Spectroscopy,* 2nd Ed., Plenum Press, New York, **1999**.

[67] Wang, Y.; Zhang, H.; Zhang, G.; Tao, W.; Tang, S. *J. Luminescence*, **2007**, *126*, 211.

[68] Ahmad, B.; Parveen, S.; Khan, R. H. *Biomacromolecules,* **2006**, *7*, 1350.

[69] Goswami, T. K.; Chakravarthi, B. V. S. K.; Roy, M.; Karande, A. A.; Chakravarty, A. R. *Inorg. Chem.*, **2011**, *50*, 8452.

[70] Berridge, M. V.; Tan, A. S. *Arch. Biochem. Biophys.*, **1993**, *303*(2), 474.

[71] Berridge, M.; Tan, A.; McCoy, K.; Wang, R. *Biochemica,* **1996**, *4*, 14.

[72] Marshall, N. J.; Goodwin, C. J.; Holt, S. *J. Growth Regul.*, **1995**, *5*(2), 69.

[73] Mosmann, T. *J. Immunol. Meth.*, **1983**, *65*, 55.

[74] Petra H.; Bock K.; Atil B.; Hoda M. A.; Korner W.; Bartel C.; Jungwirth U.; Keppler B. K.; Michael M.; Berger W.; Gunda K. *J. Biol. Inorg. Chem.* 2010, 15, 737.

[75] Tan C.; Hu S.; Liu J.; Liangnian J. *Eur. J. Med. Chem.* 2011, 46, 1555.

[76] Wee, H. A.; Elisa, D.; Claudine, S.; Rosario, S.; Lucienne, J.; Dyson, P. J. *Inorg. Chem.*, **2006**, *45*, 9006.

[77] Renvoize, C.; Biola, A.; Pallardy, M.; Breard, J. *Cell Biol. Toxicol.,* **1998**, *14*, 111.

[78] Ribble, D.; Goldstein, N. B.; Norris, D. A.; Yiqun, G. *BMC Biotechnology,* **2005**, *5*, 12.

[79] Gorman, A.; McCarthy, J.; Finucane, D.; Reville, W.; Cotter, T. Morphological assessement of apoptosis. In: *Techniques in Apoptosis. A user's guide*. TG Cotter and SJ Martin eds, Portland Press, New York, **1994,** pp. 1-20.

[80] Ozben, T. *J. Pharm. Sci.,* **2007**, *96*, 2181.

[81] Scherz-Shouval, R.; Elazar, Z. *Trends Cell Biol.,* **2007**, *17*, 422.

[82] LeBel, C. P.; Ischiropoulos, H.; Bondy, S. C. *Chem. Res. Toxicol.,* **1992**, *5*, 227–231.

[83] Rosenkranz, A. R.; Schmaldienst, S.; Stuhlmeier, K. M.; Chen, W.; Knapp, W.; Zlabinger, G. J. *J. Immunol. Methods,* **1992**, *156*, 39.

[84] Zhu, H.; Bannenberg, G. L.; Moldeus, P.; Shertzer, H. G. *Arch. Toxicol.,* **1994**, *68*, 582.

[85] Hotchkiss, R. S.; Strasser, A.; McDunn, J. E.; Swanson, P. E. *N. Engl. J. Med.,* **2009**, *361*, 1570.

[86] Wang, C. X.; Youle, R. J. *Annu. Rev. Genet.,* **2009**, *43*, 95.

[87] Kim, I.; Rodriguez Enriquez, S.; Lemasters, J. J. *Arch. Biochem. Biophys*., **2007**, *462*, 245.

[88] Rahn, C.A.; Bombick, D. W.; Doolittle, D. J. *Fundam. Appl. Toxicol.,* **1991**, *16*(3), 435.

[89] Palmeira, C.M.; Moreno, A. J. M.; Madeira, V. M. C.; Wallace, K. B. *J. Pharmacol. Toxicol. Methods*, **1996**, *35*, 35.

[90] Johnson, L.V.; Walsh, M. L.; Chen, L. B. *Proc. Natl. Acad. Sci. U.S.A.*, **1980**, *77*, 990.

[91] Hoye, A. T.; Davoren, J. E.; Wipf, P.; Fink, M. P.; Kagan, V. E. *Acc. Chem. Res.,* **2008**, *41*, 87.

[92] Casciola-Rosen, L.; Rosen, A.; Petri, M.; Schlissel, M. *Proc. Natl. Acad. Sci. U.S.A.*, **1996**, *93*, 1624.

[93] van Engeland, M.; Ramaekers, F. C.; Schutte, B.; Reutelingsperger, C. P. *Cytometry*., **1996**, *24*, 131.

[94] Vermes, I.; Haanen, C.; Steffens-Nakken, H.; Reutelingsperger, C. P. *J. Immunol. Methods*., **1995**, *184*, 39.

[95] Arunkumar, A.; Vijayababu, M. R.; Kanagaraj, P.; Balasubramanian, K.; Aruldhas. M. M.; Arunakaran, J. *Biol. Pharm. Bull.,* **2005**, *28*, 740.

[96] Darzynkiewicz, Z.; Bruno, S.; Bino, G. D.; Gorczyca, W.; Hotz, M. A.; Lassota, P.; Traganos, F. *Cytometry,* **1992**, *13*, 795.

[97] Degli, E. M. *Methods in cell biology,* academic press, **2001**, pp 75–96.

[98] Pereira, C. F.; Oliveira, C. R *Neurosci. Res.,* **2000**, *37*, 227.

[99] Darzynkiewicz, Z.; Bruno, S.; Del Bino, G.; Gorczyca, W.; Hotz, M. A.; Lassota, P.; Traganos, F. *Cytometry*, **1992**, *13*, 795.

[100] Benfang, L.; Chih-Jen, W.; Shiao-Chun, Tu. *J. Biol. Chem.*, **2000**, *275*(28), 2520.

[101] Pan, G. et al. *Science.* **1997**, *277*, 815.

[102] William, R. S,; David, E. F. *J. Clin. Invest*., **1999**, *104*(12), 1655.

[103] Reed, J. C.; Jurgensmeier, J. M.; Matsuyama, S. *Biochim. Biophys. Acta*, **1998**, *1366*(1-2), 127.

[104] Green, D. R.; Evan, G. I. *Cancer Cell*, **2002**, *1*(1), 19.

[105] Ionov, Y.; Yamamoto, H.; Krajewski, S.; Reed, J. C.; Perucho, M. *Proc. Natl. Acad. Sci. U.S.A.*, **2000**, *97*(20), 10872.

[106] Miyashita, T.; Krajewski, S.; Krajewska, M. et al., *Oncogene*, **1994**, *9*(6), 1799.

[107] Vaux, D. L. *Springer Seminars in Immunopathology*, **1998**, *19*(3), 271.

[108] Makin, G.; Hickman, J. A. *Cell Tissue Res.*, **2000**, *301*(1), 143.